

SPATIO-TEMPORAL EVOLUTION OF DIESEL SPRAYS USING HIGH SPEED OPTICAL DIAGNOSTICS

A thesis submitted for the degree of Doctor of Philosophy

by
Radboud Pos

College of Engineering, Design and Physical Sciences
Brunel University London
October 2016

Abstract

Decades of research on compression ignition engines have led to a highly efficient combustion cycle in contemporary diesel engines. Nonetheless, the combustion process is being studied perpetually to meet both current and future emission regulations. One of the most influential parameters that impacts the combustion quality, is the fuel spray evolution during injection, and subsequent fuel–air mixture formation inside the engine cylinder. The spray evolution has been investigated to a high level of detail, and the highly complex processes of mixture formation and combustion are well-documented for diesel engines. Most of these investigations are limited to studying either research-grade injectors, or brand new production injectors. Injectors in real-world diesel engines, i.e. normal passenger cars and trucks that are used on a daily basis, are however subject to deposit formation at the tip of the injector nozzle. These deposits have the potential of altering the internal nozzle flow and fuel spray pattern, which in turn degrades combustion quality and increases engine emissions.

In the work presented in this thesis the spray evolution of production injectors has been studied over a wide range of injector conditions. Common rail light-duty injectors with a usage history of up to 90 000 miles were acquired from the UK commuter car parc, and several brand new injectors were studied for comparison purposes. It is shown that the spray pattern of the injected fuel changes over the lifetime of the injector. For used injectors a reduced penetration rate was observed in the transient regime of fuel injection, during needle lift. The reduced penetration rate was often accompanied by anomalous radial expansions. Although the magnitude of the effects varied from injector to injector, the highest mileage injectors tended to produce the strongest spray deviations. For several high-mileage injectors the end of injection appeared retarded with respect to new injectors. Expulsions of liquid ligaments and droplets after the end of injection were observed from all injectors, irrespective of the mileage of the injector.

Contents

Abstract	2
Contents	3
List of Figures	6
List of Tables	9
Acknowledgements	10
Publications	12
List of Acronyms	13
1 Introduction	14
1.1 Diesel combustion	15
1.2 The research treated in this thesis	16
1.3 Thesis outline	17
2 Background on diesel sprays and deposits	20
2.1 The evolution of diesel sprays	21
2.1.1 Start of injection	28
2.1.2 Transient regime	29
2.1.3 Stable regime	33
2.1.4 End of injection and post-injection	35
2.1.5 Combined characterization of fuel sprays	38
2.2 Injector deposits	40
2.3 Spray degradation from fouled injectors	45
3 Characterising sprays by injecting high pressure diesel into water	48

3.1	Experimental set-up	49
3.1.1	Fuel pump and common rail	51
3.1.2	Injector driver and injectors	51
3.1.3	High speed camera	52
3.1.4	High power LED	52
3.1.5	Control and timing	53
3.1.6	Initial measurement parameters	55
3.2	Measurement results	56
3.2.1	Spray anomalies	56
3.2.2	Comparison of a new and end of life injector	59
3.3	Analysis of recorded sprays and anomalies	63
3.3.1	Pre-analysis manipulations	63
3.3.2	Variations in the start of injection	68
3.3.3	Fuel spray cone angle determination	71
3.3.4	First occurrence of radial expanding anomalies	73
3.3.5	Variations in the end of injection	76
3.4	Discussion of the results	77
3.4.1	Injectors	77
3.4.2	Liquid backpressure medium	78
3.4.3	Numerical data	78
3.5	Conclusion	80
4	Characterising sprays from used injectors in a high-pressure constant volume chamber	83
4.1	Experimental set-up	84
4.1.1	Fuel pump and common rail	85
4.1.2	Injector driver and injectors	85
4.1.3	High speed cameras	90
4.1.4	Illumination source	92
4.1.5	Control and Timing	92
4.1.6	The constant volume chamber	93
4.2	Measurements	96
4.2.1	SIM16 measurements (series 1)	96
4.2.2	Fastcam SA-X2 measurements (series 2)	101
4.3	Spray analysis	109
4.3.1	Start of injection penetration rate	110

4.3.2	Transient regime	113
4.3.3	Stable spray regime	124
4.3.4	End of injection	129
4.3.5	Post-injection expulsions	131
4.4	Discussion	136
4.5	Conclusion	140
5	Discussion of results	142
5.1	Qualitative comparison of spray evolutions	142
5.2	Fuel spray cone angle and penetration	147
5.2.1	Fuel spray cone angles	147
5.2.2	Spray penetration	149
5.3	Deposit rich injectors	151
6	Conclusions	152
7	Directions for future work	154
	Bibliography	156

List of Figures

2.1.1	The four breakup regimes of liquid jets	23
2.1.2	Different stages of an atomizing spray, injecting into a high temperature environment	24
2.1.3	Schematic of an evolving diesel spray with combustion sites	26
2.1.4	Mushroom-shaped anomaly at the start of fuel injection	29
2.1.5	Model comparison of spray penetration at the start of injection	32
2.1.6	Spray tip widening in the early injection regime	33
2.1.7	Imaging of the liquid core inside an atomized spray	34
2.1.8	Expulsion of ligaments and droplets post-injection	35
2.1.9	Liquid length recession after the end of injection	36
2.1.10	Dependence of flame lift-off length on mechanical parameters	37
2.1.11	Gas ingestion into the nozzle after injection	38
2.1.12	Qualitative description of injection and combustion process	40
2.2.1	Impact of fuel zinc concentration on engine torque	42
2.2.2	Impact of zinc doping on rated power and fuel injection rate	43
2.2.3	DW-10 nozzle coking test with zinc doped biofuels	44
2.2.4	Internal injector deposits on an injector needle	44
2.3.1	Impact of deposits on fuel spray penetration and dispersion	46
2.3.2	NOx and PM emissions of clean and fouled injectors	47
3.1.1	Schematic of the set-up used for measurements in a high density ambient environment	50
3.1.2	Graphical representation of pulse/trigger timing	54
3.2.1	Examples of typical injection events	57
3.2.2	Fuel injection into a liquid medium from different injectors	58
3.2.3	Transient anomalies recorded from an end of life injector	60
3.2.4	Variation in the time of occurrence of anomalies	61
3.2.5	Transient expansions in a low-density ambient environment	62

3.3.1	Correction for specular reflections in recorded images	66
3.3.2	Manual determination of a binarization threshold	67
3.3.3	Start of injection repeatability for a new and used injector . . .	69
3.3.4	Analysis of inconsistency in the start of injection	70
3.3.5	Spray cone angle determination for a single spray	72
3.3.6	Spray cone angle evolution when a transient radial anomaly occurs	72
3.3.7	Evolution of averaged fuel spray cone angle from a new injector	72
3.3.8	Evolution of averaged fuel spray cone angle from a used injector	74
3.3.9	Start of occurrence of radially expanding anomalies	74
3.3.10	Average spray cone angle after correcting data for radial bulges	75
3.3.11	Reproducibility of the time at which fuel injection ended	76
4.1.1	Schematic of the CVC set-up	87
4.1.2	SEM and optical image of a used nozzle	89
4.1.3	Alterations to the set-up for imaging with the SIM16 system. .	91
4.1.4	Image of the constant volume chamber	94
4.2.1	Example recording of the SIM16 system	97
4.2.2	Impact of intensifiers on noise levels	98
4.2.3	Spray shape constancy at the start of injection	99
4.2.4	Comparison of spray penetrations for new and used injectors .	100
4.2.5	Onset of a radial anomaly	101
4.2.6	Example recording of the FASTCAM system	102
4.2.7	Comparison of image quality of both camera systems	103
4.2.8	Spray evolution of a new and a used injector	105
4.2.9	Spray anomalies near the end of the transient needle-lift regime	106
4.2.10	Anomalous expansions versus the quasi steady-state spray shape	107
4.2.11	Expulsion of ligaments and droplets post-injection	108
4.3.1	Spray tip penetration at the start of injection	111
4.3.2	Improvement of spray penetration from a deposit rich injector after prolonged use in an inert environment	113
4.3.3	Discrimination of different anomalies at the start of injection .	115
4.3.4	Evolution of anomalies shortly after the start of injection . . .	117
4.3.5	Spray cone angle evolution at the early start of injection	118
4.3.6	Average spray width of an emerging fuel spray	120
4.3.7	Occurrence of late radial anomalies	123
4.3.8	Fuel spray shape in the stable regime	126

4.3.9	Variation in the fuel spray cone angle in the stable regime . . .	127
4.3.10	Overview of spray cone angles in the stable regime	128
4.3.11	Transient spray behaviour at the end of injection	129
4.3.12	Variation in the fuel spray width at the end of injection	130
4.3.13	Post-injection expulsions	131
4.3.14	Image manipulations to quantify post-injection expulsions . . .	133
4.3.15	Analysis results for ejected ligaments and droplets #1	135
4.3.16	Analysis results for ejected ligaments and droplets #2	136
5.1.1	Qualitative overview of observed injection stages	143
5.1.2	Comparison of observed penetration reductions to literature . .	145
5.1.3	Persistence of off-axis anomalies	146
5.2.1	Comparison of spray penetrations to literature	150

List of Tables

3.1	Overview of materials used in this investigation	51
3.2	Experimental parameters applied for measurements conducted in a liquid backpressure medium	55
3.3	Numerical results from the high ambient density investigation .	80
4.1	Overview of materials used in the CVC set-up	86
4.2	Specifications of investigated nozzles	88
4.3	Injection and recording conditions	91
4.4	Overview of observed spray anomalies and injection regimes . .	137
4.5	Numerical results determined from measurements in the CVC .	139
5.1	Comparison of spray cone angles in this work to literature . . .	148

Acknowledgements

First and foremost I would like to thank my supervisor Lionel Ganippa wholeheartedly for having given me the opportunity to do the study presented in this thesis. Without his help and guidance, this work would not have been possible. He helped me whenever research went slow by pointing me into the right direction, while encouraging me to find my own way when the research went smooth. Thank you for the trust you placed in me and the support you provided me with.

I would also like to thank Thanos Megaritis, my second supervisor, for the discussions the three of us had during different phases of the project. In the initial phase of designing and building the pressure chamber his input was invaluable.

Without the funding received from SHELL Global Solutions UK, this project would have been impossible, and I am very grateful for this opportunity offered by SHELL. In addition, discussions with several experts from SHELL provided valuable input on different aspects of the research. Roger Cracknell, who served as the point of contact within SHELL, helped in shaping the research and provided valuable insights into the relevance for industry. Discussions with Robert Wardle on several observed transient characteristics led to new ideas for subsequent investigations, and Ian Moore provided most of the used injectors investigated in this study, including the servicing history of these injectors.

I greatly acknowledge the help provided by Madan Avulapati in modifying the constant volume chamber in the second half of the research. Things went a lot faster with the extra pair of hands available. In addition, the discussions we had on several of the observed anomalies in combination with the characteristics of the experimental set-up provided a solid background for subsequent analysis. The measurements we jointly conducted during the project provided sufficient data and understanding for several co-authored publications, and it was an honour to have worked with you.

Oscar de la Garza provided the internal nozzle geometries of several injectors, which proved to be essential for quantification of spray and injector characteristics. He is greatly acknowledged for his help in this, and I would additionally like to thank him for the joint work we conducted during his fellowship at Brunel.

Most of the bits and pieces required for this investigation were provided by different technical departments, with associated technicians, of the *College of Engineering, Design and Physical Sciences*. Without all the tailor-made mechanical, electrical, and electronic parts used in this research, the quality of the set-up would not have been nearly as good as it is. In random order: Thank you Peter, Ken, Costas, Clive, William, Andy, Greg, Eamon, and Chris.

In the initial investigation treated in Chapter 3 a high speed camera system was borrowed from the EIP Loan Pool of the Engineering and Physical Sciences Research Council (EPSRC). For the subsequent investigations treated in Chapter 4, an ultra-high frame rate camera system was once again borrowed from the EPSRC. These two camera systems provided good insights in the capabilities of the experimental set-ups, and helped me determine in an early phase of both experiments in which direction to continue the research. The EPSRC is thanked for providing me with these camera systems in the early phase of the research.

Finally, I would like to thank my little family for brightening up my life during the Ph.D. studentship. Kira provided infinite support and understanding during the whole process, and her positive attitude and optimism helped me put things into perspective whenever research progress was suboptimal. Jasper's excitement about anything and everything taught me to enjoy even the simplest things in life.

Publications

Journal papers

R. Pos, R. Cracknell and L. Ganippa. Transient Characteristics of Diesel Sprays from a Deposit Rich Injector. *Fuel* **153**, 183–191 (2015)

R. Pos, R. Wardle, R. Cracknell and L. Ganippa. Spatio-temporal Evolution of Diesel Sprays at the Early Start of Injection. *Applied Energy*, *under review*

R. Pos, M. Avulapati, R. Wardle, R. Cracknell, T. Megaritis and L. Ganippa. Combustion of ligaments and droplets expelled after the end of injection in a multi-hole diesel injector. *Fuel* **197**, 459–466 (2017)

Conference proceedings

R. Pos and L. Ganippa. Comparison of Spray Characteristics From Different Nozzles and Fuels in a Non-reactive Medium. *FISITA World Automotive Congress*, 2–6 June 2014, Maastricht (The Netherlands)

R. Pos, R. Cracknell and L. Ganippa. Characteristics of High Pressure Diesel Sprays at the End of Injection. *IMEchE Internal Combustion Engines Conference*, 2–3 December 2015, London, ISBN:978-0-9572374-6-9

R. Cracknell, R. Wardle, R. Pos and L. Ganippa. Effect of Diesel Injector Tip Deposits on Transient Spray Behaviour, *Internationaler Motorenkongress*, 23–24 February 2016, Baden-Baden (Germany), ISBN:978-3-658-12917-0

M. Avulapati, R. Pos, A. Megaritis, J. Xia and L. Ganippa. Characteristics of High Pressure Ethanol Spray Flames in Diesel Engine-like Environment using Optical Diagnostics, *ILASS-Asia*, 6–9 November 2016, Chennai (India)

List of Acronyms

BMEP	Brake mean effective pressure
CVC	Constant volume chamber
CW	Continuous wave
DI	Direct injection
EGR	Exhaust gas recirculation
EOI	End of injection
EOL	End of life
EPSRC	Engineering and Physical Sciences Research Council
ERA	Early radial anomaly
FLOL	Flame lift-off length
HSDI	High speed direct injection
IID	Internal injector deposit
LED	Light Emitting Diode
LII	LASER induced incandescence
LRA	Late radial anomaly
PM	Particulate matter
RME	Rapeseed Methyl Ester
SEM	Scanning Electron Microscopy
SOI	Start of injection
TDC	Top dead centre
UBHC	Unburned hydrocarbons
VCO	Valve covered orifice
X-RAY PCI	X-Ray Phase Contrast Imaging

Chapter 1

Introduction

*In 50 years every street in London will be
buried under nine feet of [horse] manure.
–The Times, 1894*

For large cities, the necessity of transport of goods and the environmental pollution resulting from the transport has been an intricate problem for well over a century. In order to sustain the inhabitants, a continuous transport of food and goods into, and a continuous transport of waste and garbage out of the city is essential. By virtue of the widespread incorporation of the internal combustion engine in transport at the beginning of the 20th century, the above-mentioned catastrophe predicted by The Times at the end of the 19th century has been averted. Although the internal combustion engine could be considered an environmental saviour for the 19th century pollution problems, at the start of the 21st century the widespread use of combustion engines is considered to be at least partly responsible for several world-wide problems including climate change and (locally) air pollution and smog. As there are no readily available plug-in alternatives to the combustion engine¹, reduction of the environmental impact of combustion engines is attempted through legislating emission, fuel economy, and fuel composition. The ever increasingly stringent emission requirements forces car manufacturers and fuel companies to perpetually conduct research in order to improve engine efficiency and fuel

¹This is an extremely complicated problem to which there is no simple solution readily available, and which stretches beyond the transport sector. The author considers electrical vehicles a promising future alternative to light-duty combustion engines. However the electric power required to charge electric vehicles must be generated, and replacing internal combustion engines with electric ones will merely shift the emission problem.

economy of internal combustion engines, and to synthesize ‘cleaner’ fuels. In this ever-growing field of research all aspects of the internal combustion engine have been, and are being, re-investigated and evaluated to further reduce emissions in order to satisfy future regulations.

The work presented in this thesis elaborates on one aspect within this tremendous research field of combustion engines and their emissions. It offers an insight into a possible cause for the formation of in-cylinder soot and NO_x by closely considering the lifetime fuel spray characteristics of diesel injectors. This investigation should therefore be considered as a research aimed at furthering existing knowledge on in-cylinder processes responsible for soot and NO_x formation, especially for engines running high-mileage (i.e. old) injectors.

1.1 Diesel combustion

The operation of the diesel engine, the workhorse of both heavy goods and long distance transport, is based on the compression-ignition principle inside an engine cylinder. By compression of air inside an engine cylinder, as a result of a piston moving towards the top dead centre (TDC), the temperature of the compressed air is increased to several hundreds of degree Celsius. Once the piston reaches the appropriate position, and the air is compressed to the required pressure and temperature, a small amount of fuel is injected into the cylinder by a high-pressure fuel injector. The injected fuel will atomize as a result of the high injection pressure and subsequently evaporate and ignite due to the high temperature inside the cylinder, all occurring in a very short time span. This combustion of (diesel) fuel leads to a further increase of the pressure inside the cylinder, performing work as the piston is pushed downwards. The complete internal combustion process, briefly mentioned here, is assumed to be known and understood by the reader, and any reader not familiar with the working of internal combustion engines is advised to read *Internal Combustion Engine Fundamentals* by J.B. Heywood [1], providing an excellent introduction to the workings of internal combustion engines in general.

The crucial part of such a compression ignition combustion cycle lies in the timing and control of the fuel injection process. When injector and cylinder are working in perfect tandem, the injected fuel will mix and evaporate in the compressed air, resulting in a fuel-air mixture and combustion utilizing most (ideally all) available air while fully burning all injected fuel. Combustion will

be complete, pressure gain and available work will have been maximized, and ideally the only combustion products would be CO_2 and H_2O . In reality, lack of an adequate amount of air entrainment locally into the fuel spray can result in incomplete combustion of the injected fuel, which can lead to (excessive) soot formation and NO_x formation. Other negative effects of bad injector-cylinder-engine matching may include liquid fuel impinging on the cylinder wall, excess unused air providing unnecessary ‘dead volume’, and combustion might occur too early (or too late) in the cycle. Due to decades of research, injectors and cylinders have been co-designed to provide an as-good-as-technically-feasible fuel–air mixture through optimizing fuel spray formation and evolution during injection, utilizing as much of the available air as possible. Despite major leaps made past decades, the combustion of diesel fuel inside a cylinder is still not perfect, and some formation of incomplete combustion products in the engine cylinder still occurs. Unburned fuel residuals, soot and particulates, can form deposits inside the engine cylinder, and when these deposits form at or in the tip of the fuel injector they might lead to a further degradation of the combustion quality by negatively affecting the fuel injection process. In addition, prolonged use of injectors can lead to wear, most notably cavitation damage in the tip of the nozzle, which can further alter the fuel injection process, reducing combustion efficiency. Research on the fuel spray evolution, its effect on combustion quality, and the impact deposits have on both fuel spray and combustion, is treated in more detail in Chapter 2.

1.2 The research treated in this thesis

The experiments and research done at Brunel University London, and as reported on in this thesis, was conducted to *investigate the impact of injector age (mileage) on the diesel fuel spray evolution, by optically studying fuel sprays from different production injectors*. To this end optical, time-resolved, images were recorded of fuel injections from different injectors. By comparison of fuel sprays from new injectors to those from used injectors that were acquired from real world diesel vehicles at different mileages, the effect of injector age (mileage) on the evolution of the fuel spray was determined. Unique aspects of this research, compared to other research on spray evolution from used or deposit rich injectors, are:

- Time-resolved injections were recorded to a sufficient detail to follow short-lived transients occurring at the very early start and at the end of injection.
- Injectors analysed in this research originated from vehicle engines from the ‘UK public commuter fleet’, i.e. the injectors were standard production injectors. The injectors were worn – and fouled – through normal on-road daily use of passenger cars instead of being purpose-fouled for/by the research community. As such the injectors investigated in this research, and the conditions they are in, are necessarily realistic.
- The total injector pool of 20 injectors contained new injectors, injectors that had done 30.000 miles, 60.000 miles, 90.000 miles, and end of life (EOL) injectors, providing an extensive range of injector conditions.

It is hoped that understanding the effect injector wear and deposits have on the fuel spray evolution will allow either a redesign of injectors or development of fuel additives, leading to the mitigation of fuel spray degradation. By maintaining optimal spray characteristics throughout the engine’s life, combustion will remain optimal and the total life-cycle emission of a diesel engine can be expected to be reduced accordingly.

1.3 Thesis outline

The current chapter, which provided an introduction on the research subject, is followed by Chapter 2, treating the current state of knowledge regarding fuel spray shape and evolution in Section 2.1. Section 2.2 provides several key aspects from research done on fouling of injectors and the impact on combustion quality and fuel economy. Section 2.3 ultimately provides an overview of research done to date on optically recording diesel sprays from deposit rich injectors.

In Chapter 3 an initial investigation is treated in which fuel injections were conducted into a liquid back-pressure environment. The initial investigation with a high ambient density was intended as a proof-of-principle to determine whether, and in what sense, injector age and the presence of deposits at the tip of an injector altered fuel sprays during injection. The investigation resulted in observations and recorded transient effects well beyond expectations. The investigation was subsequently expanded and provided sufficient data and

new insights to become a major part of this work altogether. Chapter 3 has the classical format of a report, consisting of an introduction followed by the treatment of the experimental set-up (3.1). The measurements section (3.2) shows a selection of the recorded injections, and is followed by a section on the analysis of the results (3.3). The discussion (3.4) and conclusion (3.5) summarize the observations and conclusions drawn based on the pilot project, and include a treatment on the main advantages and disadvantages of the method applied.

Chapter 4 uplifts the research piloted in Chapter 3 to a higher plane by replacing the liquid back-pressure medium with a compressed constant volume chamber (CVC) and several other improvements. The CVC allowed injection of diesel into a compressed, heated, and gaseous medium providing ambient densities comparable to those encountered in a engine cylinder. Under these (realistic) conditions, injectors were investigated with a higher level of detail than in Chapter 3. Chapter 4 has the same basic layout of Chapter 3, and refers to the corresponding sections in Chapter 3 where applicable, as part of the experimental set-up and analysis was identical for both experiments. A short discussion on the main characteristics and relevance of the results will be treated in Section 4.4. Conclusions and new insights are provided at the end of Chapter 4, in Section 4.5.

A more in-depth discussions of the results will be treated in Chapter 5, where a comparison to existing literature of the results from Chapter 4 will be provided. Comparison of spray shapes from clean, new, injectors to models available in literature will confirm the injectors and injection conditions applied in this research are consistent with what would be expected from fuel injectors inside engines.

General conclusions based on the research presented in this thesis, the highlights from Chapters 3 and 4, are treated in the Conclusions, Chapter 6. An outlook on further research to increase the knowledge of the impact of deposits on combustion is treated in Chapter 7. This Chapter will provide ideas for interesting follow-up studies to investigate some unexpected anomalies presented in this thesis. It will not treat a continuation of this specific research (i.e. the classic *outlook*), as research continuing along the line as discussed in this thesis has been picked up by other research groups. The author has noticed an increased interest in these aspects during the time the research was conducted. This is also reflected in Section 2.3, where one can see papers

published on similar subjects as treated in this thesis were published during the time this research was conducted, 2012 to 2016.

Chapter 2

Background on diesel sprays and deposits

Over the past decades the diesel fuel spray and its evolution have been researched extensively. The dynamics of spray formation and the dependence on injection parameters have been found to be very complex, and the details are still not fully understood. Main driving force behind these researches is the realization of improved engine efficiency and reduced emissions, that can be achieved by targeting sprays into the engine cylinder, thus improving mixing, ignition, and combustion, in diesel engines. The present chapter provides an overview of the current knowledge on diesel spray evolution and the impact of injector deposits.

Section 2.1 will discuss the framework of high pressure injection, atomization, fuel spray evolution, and ultimately combustion. The main goal of Section 2.1 is to provide sufficient background on injection characteristics to allow identification of spray changes treated in subsequent chapters, and estimate their impact on the combustion process.

Despite the available knowledge on the evolution of fuel sprays, and despite the improvements in emission reductions in diesel engines as seen in recent decades, the emission and combustion efficiency of a diesel engine slowly degrades throughout its lifetime. The most common culprits for efficiency degradation of real-world¹ engines, when considering the injection system, are the

¹The term ‘real-world’ is used several times in this work. ‘Real-world engines’ refers, in this thesis, to engines that are used according to the intended application, by the general population. I.e. a real-world vehicle engine should be an engine inside a normal vehicle, being used to drive that vehicle. Research-grade injectors or engines operated for the sole purpose of research are *not* considered ‘real-world engines’ in the context of this thesis.

formation of deposits and wear of injectors, most notably cavitation damage inside the nozzle. Section 2.2 provides the results of several recent investigations into combustion efficiency, fuel consumption, and the formation of deposits. Although these researches are primarily looking at external parameters only, i.e. degradation of fuel consumption or power output related to injector condition and the presence of deposits, it clearly shows that combustion quality in engines degrades over time. Vast amounts of data exist in literature, discussing the effects of different fuels and their quality on combustion efficiency and the coking of injector nozzles. Chemical analysis provides insights into the origin of most deposits. Several investigations are performed by artificially doping fuel with the right additive to enhance the deposit formation, and this provides opportunities to study deposits and efficiency loss. It is a well-established fact that deposits can have a severe impact on the diesel engine efficiency. A notable omission in this field of research is the lack of fuel spray investigations, and despite numerous studies on deposit formation and elimination, changes to the fuel spray structure as a result of deposits have not been studied.

The final section of this Chapter, Section 2.3, will treat recent investigations that were carried out *optically* to explore the impact of injector deposits on the fuel spray evolution, atomization and subsequent combustion. This is however still an emerging research field. The research treated in this thesis was also aimed at investigating the effect on fuel spray evolution from used and deposit rich injectors. At the start of the Ph.D. research in 2012, there was virtually no information available on this subject, and as will be shown in Section 2.3 the most relevant literature on this subject is dated around or after the start of this research project.

2.1 The evolution of diesel sprays

The compression ignition diesel engine relies, as the name indicates, on the ignition of fuel by compression of air inside a cylinder. By compression of trapped air inside a cylinder, the temperature and pressure of the gas rapidly increases to approximately 1000 K at about 5 MPa. The high temperature will allow fuel introduced into the cylinder to spontaneously ignite and combust, after evaporation and mixing. To ensure combustion occurs at the right time, fuel is introduced into the cylinder shortly before TDC in conventional diesel engines. Complete combustion of *all* fuel within the available time requires

rapid evaporation and proper mixing with available air inside the cylinder. Introducing fuel into the cylinder by high pressure injection through a (or several) small orifice(s) forces the liquid fuel to break up and atomize during injection, and this atomized stage provides a high surface-to-volume ratio of the liquid droplets, aiding rapid evaporation. By varying parameters such as injection pressure, nozzle geometry, and piston (bowl) shape, further control can be exerted on air entrainment, mixing and evaporation of the atomizing fuel jet. Optimizing fuel injection, fuel spray evolution, and subsequent fuel–air mixing, greatly improves the quality of combustion.

In this thesis, spray research is limited to consider only non-impinging liquid sprays which are injected into a quiescent, stationary, gaseous environment from a non-swirling nozzle. Under these conditions, the injected liquid breaks up into droplets of certain size and velocity, depending on the applied pressure difference. This breakup is classically divided into the following four regimes, depending on the injection pressure or liquid jet velocity.

- *Rayleigh regime* - Observed for a laminar liquid flow with a low velocity. The combination of surface tension and instabilities in the surface leads to the formation of long-wavelength surface waves. These waves amplify further downstream due to the interplay between surface tension and liquid inertia. Eventually the tip of the jet breaks up into ligaments, which subsequently break up into droplets. Droplet diameters are typically 1.5 to 2 times the orifice diameter.
- *First wind-induced regime* - Occurs for higher liquid velocities. Comparable to the Rayleigh regime, but the formation of surface instabilities is augmented by the liquid–gas interfacial forces. Breakup of the jet will start closer to the nozzle, and droplet diameters are on the order of the orifice diameter.
- *Second wind-induced regime* - At even higher injection velocities, short-wavelength instabilities quickly lead to breakup of the liquid stream. These instabilities will form small droplets at the surface of the liquid core, creating a conical expanding cloud of atomized droplets surrounding the liquid core. The origin of the short-wavelength instabilities lies in the liquid–gas interaction, and is caused by the large difference in velocities between the liquid jet and the ambient gas. Atomized droplet diameters are much smaller than the orifice diameter, and the expanding atomized

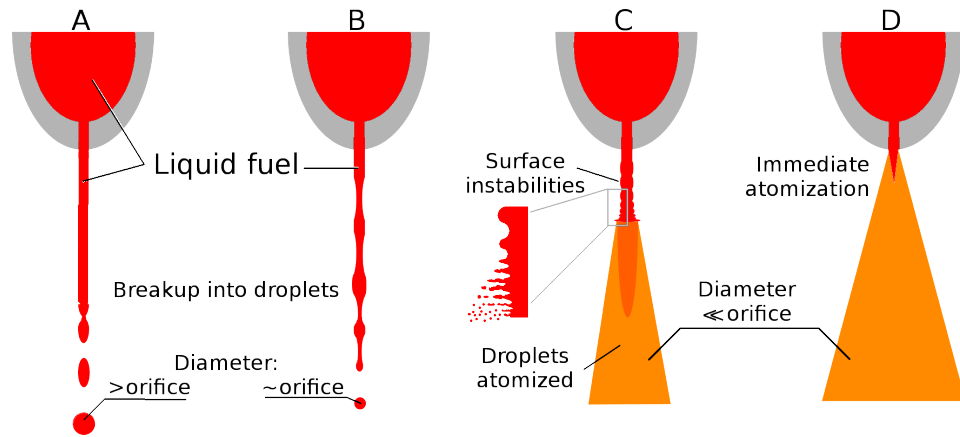


Figure 2.1.1: The four breakup regimes for liquid jets. (A) Low pressure injection in the Rayleigh regime. Breakup of the liquid jet leads to droplets with a diameter larger than the orifice diameter. (B) At an increased injection velocity the liquid – gas interaction leads to breakup into smaller droplets, on the order of the orifice diameter. (C) Higher injection pressures lead to the rapid growth of surface instabilities that break up into atomized droplets shortly after the liquid jet has left the orifice. (D) At the highest injection pressures atomization occurs at the orifice exit, the liquid core is tremendously reduced in length.

cloud entrains ambient gas as it moves further downstream of the jet.

- *Atomization regime* - For the highest injection velocities, the breakup and atomization occurs directly at the nozzle exit and an atomized cone surrounds the liquid core immediately upon exiting the orifice. The combination of turbulence in the liquid jet, cavitation, and liquid–gas interactions are responsible for the breakup starting directly at the nozzle exit. Droplets are atomized with diameters much smaller than the orifice diameter.

The four breakup regimes are depicted in the cartoon provided in Figure 2.1.1, and a more detailed description of the breakup process can be found in [2] or in any recent textbook on liquid atomization and sprays, for example [3]. Diesel engines operate in the fourth jet breakup regime, and atomization occurs at the nozzle exit. In the atomization regime both the surface-to-volume ratio of atomized droplets, and the mixing of the droplets with air, is maximized. This leads to a rapid evaporation and mixing of fuel with air, and will provide the fastest way of achieving a combustible mixture. In an engine, the thus prepared combustible mixture will spontaneously ignite as a result of the high in-cylinder temperature, and the subsequent increase in in-cylinder pressure allows the engine to perform work.

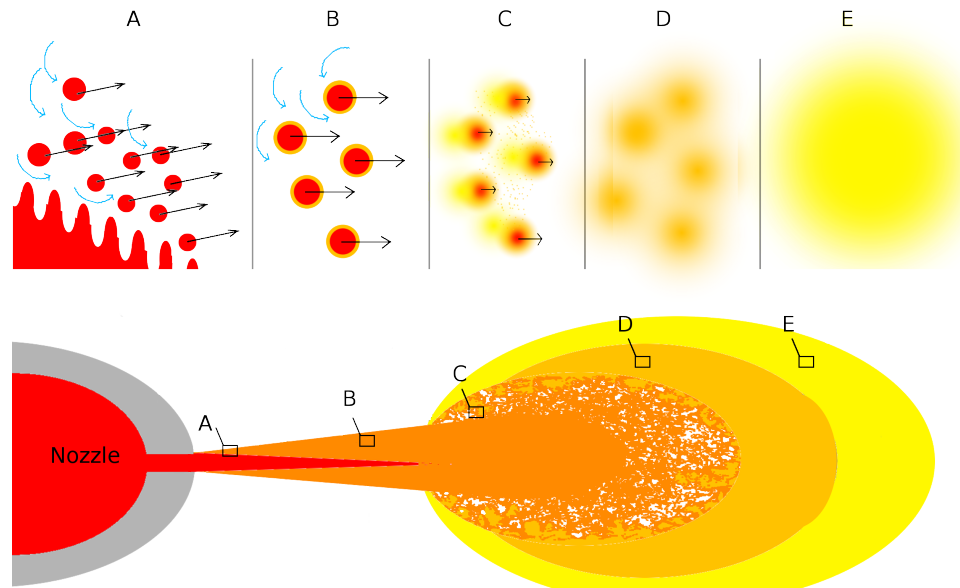


Figure 2.1.2: Different stages of the injected fuel when injecting into a high temperature environment, at a sufficient pressure to ensure atomization. Top row: (A) Upon high pressure injection the liquid fuel quickly atomizes near the nozzle exit, the atomized droplets have high momentum, primarily in the axial direction with a small radial component. Breakup of the liquid and forward velocity of atomized droplets entrain ambient gas into the atomized cloud. (B) Droplets evaporate in the high-temperature gas and initially keep a high forward momentum and continue air entrainment. (C) As droplets continue to evaporate momentum is lost and the fuel vapour fraction in the surrounding gas increases. (D) When the droplets have evaporated the mixture of ambient gas and fuel vapour is locally rich and may not be a fully homogeneous mixture. (E) All liquid fuel has evaporated and local mixing has resulted in a uniform mixture within combustible limits. Bottom row: The accompanying quasi steady-state shape of a non reacting diesel fuel spray.

The next step in understanding basic spray characteristics then looks at the effect of the high ambient temperature on the atomized spray. Not surprisingly the entrainment of high temperature ambient air into the atomized stream leads to droplet evaporation into the entrained air. The initially rich fuel-air mixture will continue to mix with entrained air whilst the atomized droplets continue to evaporate, until the fuel has fully evaporated and mixing has led to a uniform, homogeneous mixture. This process, which completes well within a few milliseconds is schematically depicted in Figure 2.1.2, top row. The atomized droplets undergo different stages of entrainment and evaporation processes, that occur at increasing distances downstream of the orifice due to the high initial velocity. This space-separated process of atomization, evaporation, and further mixing, will eventually result in a time-averaged quasi steady-state spray shape as depicted in the bottom row of Figure 2.1.2.

Autoignition occurs at the fuel–air interface closer to stoichiometry, and subsequent combustion of the fuel vapour will occur downstream of the spray where fuel and air have mixed to within combustible limits. The burning of the evaporated fuel on the outskirts of the spray in combination with the continuous supply of a fresh fuel–air mixture will eventually lead to the combustion spray attaining a quasi steady-state shape. The quasi steady-state spray flame will resemble the spray depicted in Figure 2.1.2, with a diffusion flame burning around the edges of the spray head. Conceptual models of diesel fuel sprays, their evolution, and the expected burn characteristics much as described up to this point, have been around for decades [4][5]. Experimental identification of underlying characteristics was not achievable until measurement techniques improved, roughly at the end of the twentieth century.

With the extensive application of novel techniques including LASER induced incandescence (LII) of soot, two-colour fluorescence, X-RAY transmission measurements, and infrared spectrometry in the last decade of the last century, a better insight was acquired regarding the detailed processes of mixing, combustion, and soot formation [6][7]. The ability to locate ignition sites and combustion, and to determine soot formation regions inside the spray, allowed the extension of the then-existing model to incorporate the (experimentally determined) combustion processes occurring inside the spray tip. These researches led to modification of the assumption, as made above, that all combustion occurred in a sheet surrounding the outer layer of the fuel spray. Most notably the observation of soot formation occurring inside the spray head indicated combustion occurred at least partly within the fuel-rich regions. The modified model for a combusting spray based on these experimental observations, and incorporating the location within the spray where both premixed and diffusion controlled combustion occurs, has been described in detail in [8] and has been widely accepted as the *de facto* standard for high temperature diesel combustion. Figure 2.1.3 provides a modified version of the spray in Figure 2.1.2, including the ignition and soot formation sites as described in [8]. Upon fuel injection and immediate onset of atomization, in the red and dark-orange coloured regions in Figure 2.1.3, air is entrained into the atomized spray. Evaporation of fuel droplets and further mixing with available air (mottled dark-orange) will eventually lead to a rich fuel–air mixture downstream of the spray (orange), which by further mixing with air will become sufficiently lean (yellow region) to allow complete combustion. Premixed combustion has

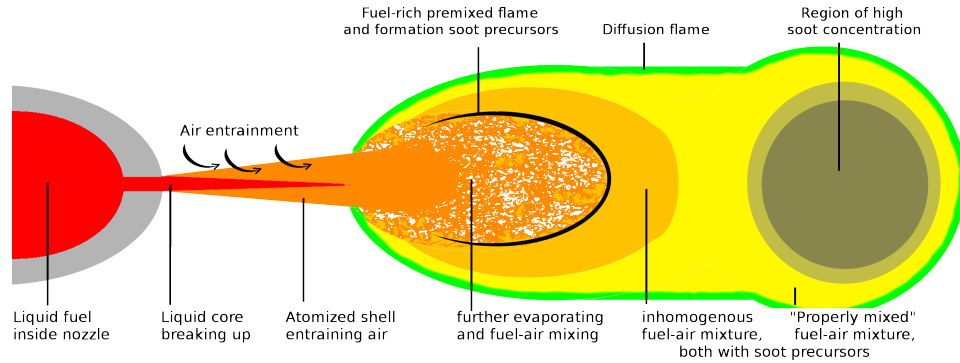


Figure 2.1.3: Schematic of a burning diesel spray with combustion sites for a high-temperature high speed direct injection (HSDI) engine, inspired by the work presented in [8].

been observed to occur in the fuel-rich mixing region indicated by the black crescent band in Figure 2.1.3, and soot precursors are formed in the wake of this premixed combustion. Diffusion controlled combustion occurs at the edge of the spray (green band), and soot has been observed to form in the grey-shaded region on the right in Figure 2.1.3. Soot formed in the grey region will further oxidise once it is transported to the diffusion-controlled burning envelope around the spray.

Mixing, evaporation, and combustion inside a diesel engine are strongly dependant on both injection and ambient conditions, and it should be understood the model provided in [8] and depicted in Figure 2.1.3, aims at describing combustion for high temperature, quiescent high speed direct injection (HSDI) engines only. A comparable conceptual model has been developed to describe diesel combustion under low temperature, exhaust gas recirculation (EGR)-diluted conditions, and a review on the subject is provided in [9]. Side by side comparison of both high and low temperature models, which is provided in [9], immediately shows the combustion processes are strongly dependant on engine operation conditions. For the present work, only the model described in [8] is relevant.

Up to this point only the stable, quasi steady-state spray shape has been discussed, the transient start and end of injection have not been considered. During the stable injection regime most fuel is injected and burned inside an engine, and this spray regime is arguably the most important part of the fuel injection process. Nonetheless, as measurement techniques advanced, and as emission regulations became more stringent, researchers were increasingly investigating the transient phases occurring at the start and end of injection.

Investigations that recorded spray atomization, including the early transient regime of spray build-up, observed temporal spray widening well before the start of the 21st century [10]. Early researches were however primarily aimed at furthering general knowledge on the overall spray build-up, and transient characteristics of spray formation were studied to identify limitations in existing models. Recent research is by contrast focussed *specifically* on these deviations and anomalies, not necessarily studying the impact of anomalies on global spray development. Over the past decades, the initial injection phase has been studied in high detail to acquire a better understanding of the primary spray break-up inside diesel engines [11], and numerous models are available to calculate break-up characteristics [12]. In addition, novel techniques incorporating X-Ray Phase Contrast Imaging (X-RAY PCI) and ballistic photon imaging, have allowed researchers to investigate the liquid core present inside the diesel spray [13][14]. This region is invisible to ‘classical’ optical techniques due to the high density of the atomized shell around the liquid core. The injection and combustion process, including the transient spray regimes, can be divided into the following four stages:

- *Early start of injection* - Time window starting directly at the start of injection (SOI), covering the very first bit of fuel leaving the nozzle. Small anomalies are observed, showing distinctly different behaviour from the transient phase in the next point. These anomalies are typically observed within the first 100 μ s after the start of injection (*aSOI*).
- *Transient regime* - Start of spray formation and transient build-up of the spray shape, lasting from the SOI up to the start of the quasi steady-state spray regime, roughly about 0.5 ms *aSOI*². Transient spray widening and asymmetric early development can be observed to occur in this regime. The needle is lifted inside the injector at a finite velocity, and part of the transient characteristics are expected to be the result of a changing internal nozzle flow caused by needle movement. After the needle has reached the fully open position, fuel flow will subsequently stabilize and lead to the quasi steady-state injection regime.
- *Stable or quasi steady-state regime* - Recently receiving more interest with

²The duration of the initial transient regime depends on injector mechanics and injection conditions. The indicated 0.5 ms was the typical time window in which transients associated with needle lift were observed for the injectors investigated in this work.

the novel possibilities to record the liquid core inside the spray. This is the most well-known phase of the diesel spray, and has been studied for several decades.

- *End of injection and post-injection*³ - Impact of terminating the injection on spray evolution and atomization. After the valve has closed, fuel residuals present in the SAC and/or orifices can be ejected post-injection, resulting in ligaments and droplets entering the cylinder. Recent studies with X-RAY systems on internal nozzle flow during and after the valve has closed, provide more insight in end of injection (EOI) flow behaviour.

Recent advances highlighting the current state of knowledge on these four regions are treated in the following subsections.

2.1.1 Start of injection

With the availability of modern high-resolution camera systems, long distance microscopes, and high power light sources, near-nozzle study of the very first start of injection has become feasible. Recording the SOI shows the build-up of the fuel spray is not a clean, instantaneous process. The SOI shows the presence of a spray tip anomaly moving at a relatively low velocity. This initial anomaly is rapidly overtaken and/or penetrated by subsequent injected fuel that leaves the orifice at a higher velocity, as has been observed in [15][16][17]. The evolution of the initial fuel mass, often shaped like a mushroom, has been recorded with unprecedented resolution in [18]. Although the origin of this very early anomalous spray start has not been researched extensively, the current consensus on the origin of the tiny pre-injection is that it results from fuel residuals present inside the orifice from an earlier injection. Where [15] shows the presence of an atomized jet appearing shortly before the main (liquid phase) injection starts, [16] includes images of a liquid mushroom head at SOI. The more recent paper [18] was able to measure, at different conditions, both the vapour state and the liquid state of this very early anomaly, along with the subsequent penetration of the mushroom cloud by the main fuel injection.

³In Chapter 4 this stage will be split into two separate stages to discriminate between different observations done in the present investigation.

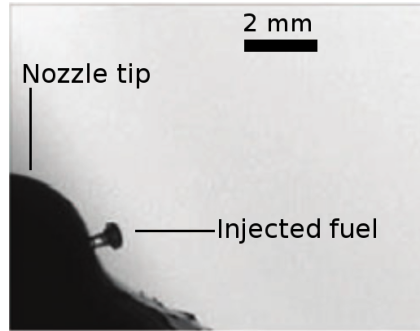


Figure 2.1.4: Mushroom-shaped anomalous SOI, assumed to be caused by residual fuel in the orifice being ejected by the inrush of liquid fuel at the SOI. Taken from [16]. The text and the scale displayed in the image were manually added by the present author.

Figure 2.1.4 provides an example of a mushroom shaped cloud, taken from [16]. In [18] the relevance of this anomaly for contemporary engines is discussed; If the anomaly is the result of fuel residuals in the orifice, this proves there *is* a fuel residual that remains inside the orifice after injection has ended. This residual fuel can lead to the formation of deposits inside the orifices, possibly altering internal flow and subsequent spray evolution.

2.1.2 Transient regime

In the transient regime, lasting from SOI until the diesel fuel spray has attained a quasi steady-state spray shape, the fuel spray tends to show several transient characteristics. The initial spray is wider than the quasi steady-state spray width, and the accompanying fuel spray cone angle changes during this transient period. The penetration rate of the tip of the atomized spray is high in the early build-up regime and the spray tip velocity decreases to zero near the end of the transient phase. In the stable regime the fuel spray cone angle is constant and minimized, and the spray tip velocity is zero as the spray has reached a steady-state. Empirical relations exist for the spray tip velocity in the transient regime, and the dependence on parameters such as injection pressure and ambient density can readily be found in literature [1][3]. Despite the available relations, a fundamental model for calculating-from-scratch the early spray evolution is not available. An early empirical relation between spray tip penetration at the start of injection and several physical parameters

determining spray evolution was formulated in [19] as

$$0 < t < t_b : \quad S = 0.39 \left(\frac{2\Delta P}{\rho_l} \right)^{0.5} t \quad (2.1)$$

$$t > t_b : \quad S = 2.95 \left(\frac{\Delta P}{\rho_a} \right)^{0.25} (Dt)^{0.5} \quad (2.2)$$

$$t_b = 28.65 \frac{\rho_l D}{(\rho_a \Delta P)^{0.5}} \quad (2.3)$$

where S indicates spray penetration, ΔP the pressure difference over the nozzle, $\rho_{l,a}$ equals the density of the fuel (l) or ambient environment (a), and D is the orifice diameter. t_b provides the break-up time, an empirically determined characteristic time at which the fuel spray penetration changes from being linearly dependant on time, having a constant velocity in Equation 2.1, to a square-root dependence in Equation 2.2. The empirical penetration relations provided in Equation 2.1 and 2.2 have been generalized for wider injection conditions in [20]. These generalized equations,

$$(2.1) \quad \Rightarrow \quad S = C_v \left(\frac{2\Delta P}{\rho_l} \right)^{0.5} t \quad (2.4)$$

$$(2.2) \quad \Rightarrow \quad S = \left(\frac{C_v \sqrt{2C_a}}{a \cdot \tan \frac{1}{2}\theta} \right)^{0.5} \left(\frac{\Delta P}{\rho_a} \right)^{0.25} (Dt)^{0.5} \quad (2.5)$$

provided similar dependencies on pressure and density as the model discussed in [19], with the empirical constants replaced by relations incorporating orifice parameters that depend on the detailed nozzle geometry. The effect of ambient density on spray dispersion and penetration was included in Equation 2.5 by application of the factor $a \cdot \tan \frac{1}{2}\theta$. The two coefficients C_v and C_a were introduced to correct fuel penetrations for losses in flow velocity (C_v) and reduction of effective orifice diameter (C_a), both directly related to the detailed flow behaviour inside the orifice. The velocity and area coefficients are in turn related through the discharge coefficient $C_d = C_a \cdot C_v$, which provides the ratio of actual fuel flow versus the theoretically maximum fuel flow, based on orifice geometry. Although C_d , C_a and C_v can be considered constant for most practical applications, the coefficients vary during injection, see for example [21]. A more recent study on the variation of the coefficients during injection from a multi-hole nozzle is provided in [22], and shows different orifices from a single SAC nozzle can have different discharge coefficients during a single injection.

Contemporary research is conducted on the early spray evolution stage, motivated in part by the need to develop an extended model to provide better predictions on spray evolution and the dependence of different parameters

involved [23][24]. In addition to the studies aimed at developing an extended model, studies are conducted to determine if existing models still suffice for modern diesel engines [25][26]. Investigations into the latter point is partially motivated by the increased technical possibilities to study transient behaviour of sprays. Higher precisions could be achieved and re-measurement of established spray stages might lead to new insights regarding underlying dependencies. For example, in [27] it was shown the spray tip penetration at SOI increased proportional to

$$S = \alpha \cdot t^{\frac{3}{2}} \quad (2.6)$$

where α was a numerical parameter determined by fitting the $\frac{3}{2}$ -power law to recorded penetration data. Based on Equation 2.4 the penetration was expected to provide a linear relation, the spray tip velocity being constant. Measurements in [27] were done in a non-reactive, inert environment. Later investigations under reactive conditions and with application of several different orifice configurations in [28], confirmed the $t^{\frac{3}{2}}$ provided better predictions than the classical, constant velocity model. In [28] the single fitting parameter α applied in [27] was replaced with an empirical relation of several injection parameters, leading to the following correlation for spray penetration at the very early start of injection.

$$0 < t < t_b : \quad S = \left(\frac{\rho_l}{\rho_a}\right)^{0.25} \left(\frac{\rho_a^{1/3} \Delta P}{12\rho_l}\right)^{0.5} t^{3/2} \quad (2.7)$$

A further investigation conducted under inert conditions, treated in [29], included measurement series from other groups to determine under which conditions experimental measurements of the spray tip velocity deviated from Equation 2.7. Here it became apparent the early spray penetration velocity can vary between different research groups, depending on the experimental conditions, and the data provided in [29] corresponded best to the relation provided by Equation 2.6 with accompanying determined values for α . The trends remained similar, in support of the $t^{\frac{3}{2}}$ dependency of penetration, but the pre-factor in Equation 2.7 apparently depended on the detailed experimental configuration.

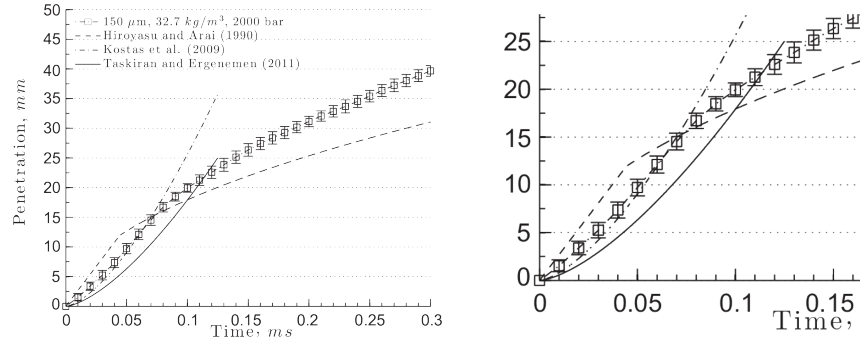


Figure 2.1.5: Penetration at SOI, as found in [29]. The three fit lines correspond to the classical linear spray tip penetration (Hiroyasu and Arai) and two models incorporating the $\frac{3}{2}$ -power law with different parameter estimates, from [27](Kostas et al.) and [28](Taskiran and Ergezenen). Right hand graph provides a magnified view of the lower left corner of the leftmost graph.

Figure 2.1.5, taken from [29], provides a graph where the (classical) linear velocity assumption alongside both results from [27] and [28] are plotted. Right graph in Figure 2.1.5 provides a magnified view of the early start of injection of the same graph. Despite the strong modification of the relations for the early spray tip penetration, changing from Equation 2.1 to Equation 2.7, the authors in [27], [28] and [29] noted the relation for the break-up time, Equation 2.3, provided sufficient accurate results in the new models. A more recent investigation on the spray tip penetration at the start of injection in [30], indicated better agreement between model and experiment can be achieved by replacing the break-up time in Equation 2.3 with the time of *peak tip velocity*, i.e. the time at which the spray tip velocity is highest.

Spray models used for calculation of the fuel spray cone angle initially only treated the stable regime, acknowledging (but not analyzing) the initial transient phase showed an increased width of the atomized spray [19]. In recent years the study of the transient phase through high speed imaging techniques have clearly shown that early spray widening occurs before the stable regime commences. Apart from the general observation that spray widening *occurs*, variations in spray widening, even under identical conditions, makes quantitative analysis impractical. Figure 2.1.6 provides an example where for four injections conducted under identical conditions, the fuel spray cone angle in the transient regime can differ by as much as 30% [31]. Modern breakup models allow simulation of the turbulent nature of the early spray buildup and subsequent quasi steady-state spray shape, and provide numerically calculated spray shapes in (very) good agreement with experiments [32][33].

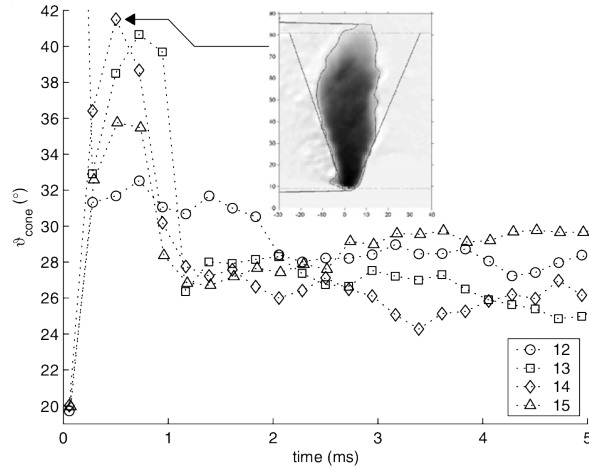


Figure 2.1.6: Example of the inconsistency of the early spray tip widening. Graph shows the determined fuel spray cone angle for four injections conducted under identical conditions. Note how in the first 0.8 ms of the injection the maximum fuel spray cone angle can attain any value between 31 and 42 degrees. Taken from [31].

2.1.3 Stable regime

Once the spray has attained a steady-state condition, the spray will resemble the schematic provided in Figure 2.1.3 for a high-temperature high speed direct injection (HSDI) engine. During the stable regime, most of the fuel is injected into the cylinder. Combustion quality and efficiency is for a major part dependant on the spray characteristics during the stable regime. In [8] the average spray behaviour during the transient SOI and the subsequent start of combustion have been described, ultimately leading to the quasi steady-state burning diesel plume, as depicted in Figure 2.1.3. Figure 2.1.3 however provides an artificially smoothed, idealized model of a combusting diesel spray, and combusting sprays measured in an experiment will show jagged edges due to local turbulence and injection to injection variations of the overall spray shapes. Contemporary investigations into the stable regime are conducted to understand interface properties and liquid–gas interactions, and on the details of spray formation and breakup.

A relative new field of research in the stable spray regime is the detailed study of the surface structure of the liquid core inside the atomized shell. This region is obscured for direct optical imaging by the dense atomized shell surrounding the core. The global structure and length of the liquid core has previously been studied with either direct-sampling methods (for example

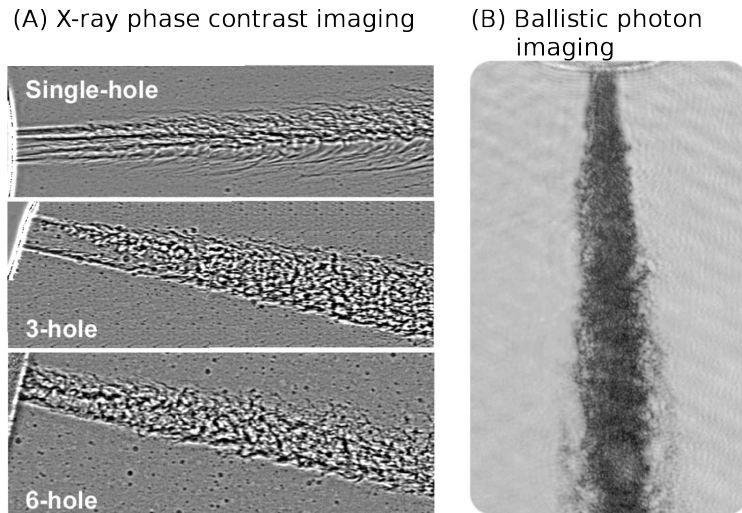


Figure 2.1.7: Measured liquid core present inside a stable diesel spray. The different images correspond to different imaging techniques and were taken from different articles. (A) X-RAY PCI image of the liquid core, showing the change in liquid core structure when changing the amount of orifices in the nozzle while maintaining same injection conditions [39]. Note the liquid itself is transparent to X-RAY radiation, allowing structures inside the liquid core to be resolved equally well as the surface breakup structures. (B) Ballistic photon image of a liquid core from a dodecane injection, recorded with an illumination window of only several picoseconds [41]. The surface of the core can be seen to have a complex breakup pattern.

wire probes [34]), or non-intrusively by using (most notably) mie-scattering of LASER light [35]. Contemporary high-power Light Emitting Diodes (LEDs) are capable of providing sufficient illuminating power to allow mie-scatter analysis of the liquid core as well [36]. Recent investigations apply X-RAY systems, utilizing either beam attenuation (absorption imaging, for example in [37]) to determine spray density, or phase alteration (X-RAY PCI, for example in [38][39]) to image detailed surface structures of the liquid core inside the atomized spray. Ballistic photon imaging [14] has been developed as a non X-RAY alternative technique using high-power lasers, to study surface structures of the liquid core. Measurements of the liquid core inside the evolving diesel spray provides additional information on the mechanism of atomization and breakup within the atomized cloud, and allows verification of existing models describing breakup. Figure 2.1.7 provides examples of the surface structure of the liquid core, measured with (A) X-RAY PCI, and (B) ballistic photon techniques. A more in-depth description of the techniques involved can be found in [40], which provides a review on imaging the liquid core inside atomizing sprays.

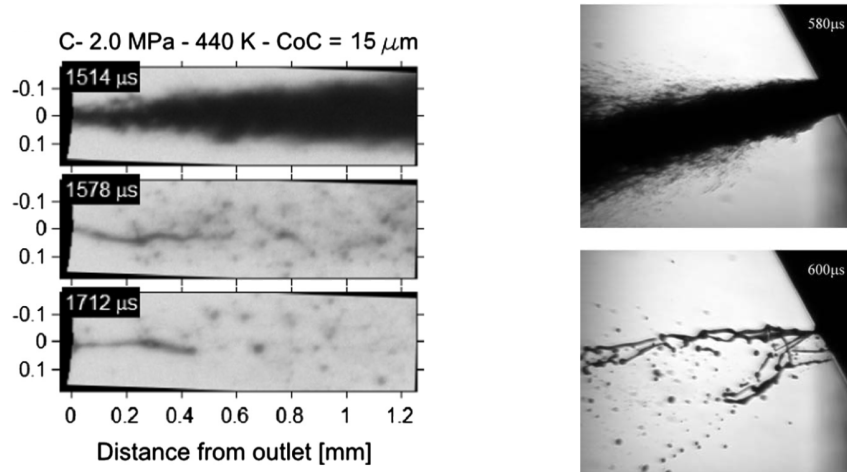


Figure 2.1.8: Expulsion of ligaments and droplets post-injection. Left image column taken from [43], injection pressure of 150 MPa into an ambient gas at 440 K pressurized to 2.0 MPa. Right image column taken from [15], injection pressure of 112 MPa into ambient atmospheric conditions. Note left image column was recorded from a mini-SAC nozzle, right image column was acquired from a VCO nozzle. The ligament expulsions are expected to be a universal characteristic of diesel injection systems, and not specific to any one nozzle configuration.

2.1.4 End of injection and post-injection

At the end of the stable regime, fuel injection is stopped by closing of the valve inside the nozzle. This termination of the fuel injection would ideally be discrete and abrupt, changing from a steady-state fuel injection during the stable regime to a completely ceased fuel flow, without the occurrence of any transient end of injection (EOI) effects. For real injection systems this termination of fuel flow is accompanied by a short transient period, leading to short-lived spray alterations. During, and directly following, termination of injection, a change in injection characteristics of the evolving diesel spray can be observed [42]. Most notably the expulsion of macroscopic ligaments and droplets after needle closure have been widely observed and recorded both for valve covered orifice (VCO) and SAC nozzles, see for example [15](VCO) and [43](SAC). Examples of the stable spray and the post-EOI expulsion of ligaments and droplets are provided in Figure 2.1.8. The images were recorded close to the nozzle providing only the liquid and atomized stages, leftmost images acquired from [43] and rightmost from [15].

In addition, stopping the fuel flow will alter the spray shape of the main injection, as there will be no further influx of fresh fuel to sustain the spray. The ending of the fuel flow can lead to recession of the liquid length [44],

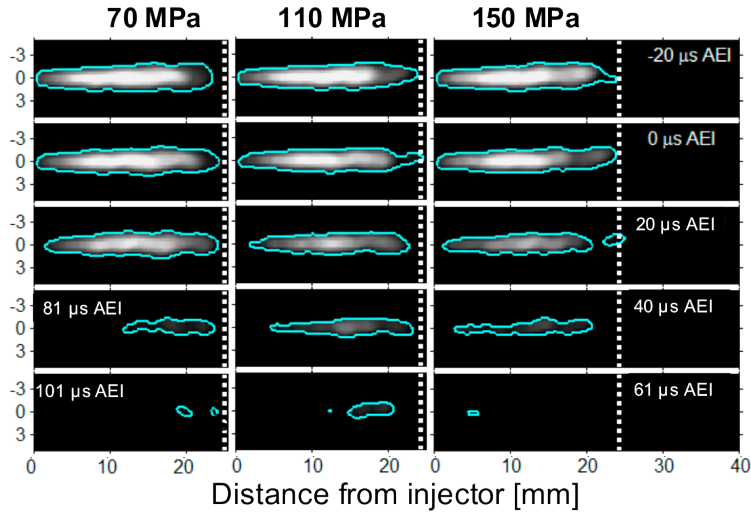


Figure 2.1.9: Recession of the liquid length in the atomized stage after the end of injection ($aEOI$) [44]. Except for injection pressure all parameters were maintained constant. Note how recession of the total liquid length for the lowest injection pressure requires more time than for the higher injection pressures (time indicated in bottom-left two images).

i.e. the total length of the liquid core inside the atomized spray will reduce when the injection stops. This is in itself not an unexpected feature of injection dynamics. When injection ceases the fuel flow is, after all, expected to stop while breakup and evaporation continues until all liquid fuel has evaporated. Imaging this process leads to furthering understanding of the EOI dynamics, as the observed reduction can be coupled to other observed changes in spray evolution and combustion. Figure 2.1.9 shows three time traces of the liquid length post-injection taken from [44], indicating injection pressure influences the liquid length recession, a higher injection pressure resulting in a more rapid decrease of the liquid length.

Similarly, terminating the fuel flow leads to a change in the flame lift-off length (FLOL) for combusting sprays, resulting in a flame front moving either towards or away from the nozzle once injection has ended. The dependence of the FLOL on the speed with which the needle closes has been studied in [45]. Slow EOI termination can lead to combustion recession, i.e. decrease of the FLOL [46]. A fast termination of the fuel flow can however lead to the FLOL increasing post-injection [45]. The graph presented in Figure 2.1.10 indicates the changes in the FLOL resulting from different ramp-down profiles controlling valve closing. Near-nozzle fuel–air mixing at EOI can lead to the formation of local pockets of lean mixtures, stagnated close to the nozzle, which remain present even after injection had ended completely [47].

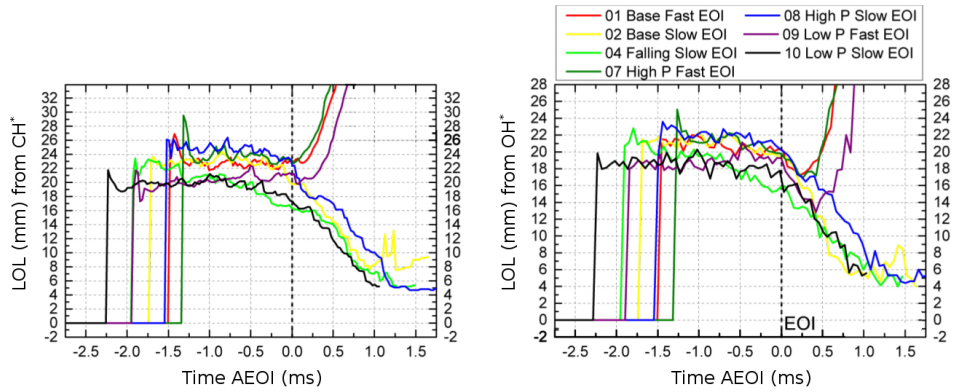


Figure 2.1.10: Dependence of flame lift-off length (FLOL) on mechanical EOI parameters. Graphs show FLOL determined through chemiluminescence of either CH^* or OH^* species, at indicated time after end of injection. It can be seen for rapid valve closing (*Fast EOI*) the FLOL increases $a\text{EOI}$ while for slow valve closing (*Slow EOI*) flame recession occurs. Graph acquired from [45], manipulated to show both graphs side-by-side. Cylinder conditions at start of injection were 860 K, 18.5% O_2 , ambient pressure of 11.3 MPa. Injection pressures varied for different combinations of *Fast EOI*–*Slow EOI*.

Once the needle has reached the closed position, fuel motion *inside* the nozzle continues for a short time. With the help of X-RAY PCI, gaseous bubbles have been observed to move inside the injector tip after needle closure, indicating liquid flow inside the nozzle post-injection [48]. The origins of the gas bubbles have not been researched extensively but are expected to be a combination of (vapour-filled) cavitation bubbles created inside the nozzle, and cylinder gas ingested into the nozzle. The latter type of bubbles are unwelcome in the nozzle holes, as hot combustion products in combination with (evaporating) fuel can lead to the formation of deposits inside the orifice. In [48] the authors observed such ingestion of cylinder gas into the nozzle at EOI, occurring simultaneously with the expulsion of ligaments. Figure 2.1.11 provides several images from [48] showing (left) a ‘raw’ recording of air bubbles trapped inside the nozzle, (middle) several algorithm-detected bubbles inside the nozzle at different ambient pressures, and (right) ligaments expelled after end of injection ($a\text{EOI}$) recorded in the same measurement series as the internal bubbles. Ligament and droplet images show a reduced contrast compared to Figure 2.1.8 due to the X-RAY PCI technique applied in [48].

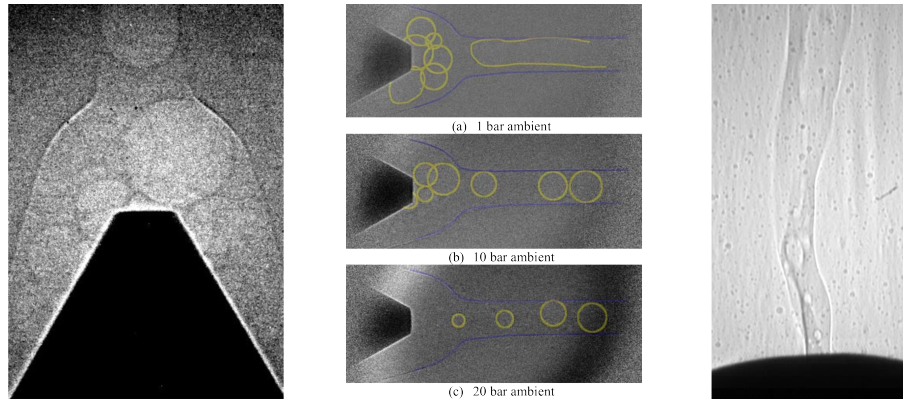


Figure 2.1.11: Gaseous bubbles present inside an injector nozzle after injection has ended, measured with X-RAY PCI. (left) Raw image showing the presence of several density gradients (bubbles) inside the nozzle, injection pressure of 150 MPa. (centre) Bubbles detected inside the nozzle post-injection for three different ambient pressures, injection pressure was maintained constant at 100 MPa. Images were recorded at least 1 ms $aEOI$ to ensure the bubbles were stationary. (right) Ligament ejection $aEOI$ observed to occur simultaneously with gas bubbles being ingested into the nozzle, for an ambient pressure of 0.1 MPa, 0.25 ms after the end of injection. All images taken from [48], left and right images have been rotated by 90° .

2.1.5 Combined characterization of fuel sprays

The steady state spray combustion cartoon provided in Figure 2.1.3 can now be expanded with the observations treated in Sections 2.1.1 to 2.1.4 to allow a qualitative description of the temporal evolution of a combustion spray.

As the needle inside the injector lifts at the beginning of injection, the inrush of fuel into the nozzle will expel any residual fuel and gas present in the tip from previous injection events. This will lead to a (tiny) mushroom cloud or atomized droplet spray entering the cylinder prior to the main injection. The subsequent start of the main injection shows transients associated with needle lift, as the spray builds up towards the spray shape in the stable regime. In the initial transient regime the spray length increases until the stable phase commences, at which time the spray will remain in a quasi steady-state until EOI . The fuel spray will show an irregular, widened spray tip, and often the first ignition occurs locally in this part of the injected spray. Total spray penetration and accompanying penetration rate (spray tip velocity) are commonly used to indicate the early evolution. Empirical relations for the spray tip penetration during the early injection regime are provided in Equation 2.5 and Equation 2.7. In the stable regime, a quasi steady-state spray with burning tip provides

a continuous combustion process in which the majority of all fuel is burnt. The stable regime does show jagged, turbulent edges around the combusting spray tip, but general spray characteristics remain fairly constant. Main spray characteristics are defined by:

- *Liquid length* - Total length of the core inside the atomized fuel spray that is in the liquid phase. Indicated by the maximum distance the liquid core reaches from the orifice.
- *Flame Lift-off Length (FLOL)* - Distance from the orifice to the nearest plane in which a flame is observed. The atomized spray close to the nozzle will not have evaporated and mixed sufficient to provide a combustible mixture. At fixed injection and ambient conditions, there ideally is a fixed distance downstream of the nozzle where entrainment and mixing has become sufficient to allow combustion.
- *Spray cone angle* - The apex angle of the cone formed by the atomized fuel spray, for combusting sprays reaching up to the FLOL. Evaporation and combustion downstream of the spray beyond the FLOL makes defining a spray cone angle impractical, and the fuel spray cone angle is mostly studied under non-evaporating conditions. The spray cone angle depends on injection conditions and nozzle geometry, and an empirical relation can be found in [1] to be

$$\theta = 2 \arctan \left(\frac{4\pi\sqrt{3}}{6A} \sqrt{\frac{\rho_a}{\rho_l}} \right) \quad (2.8)$$

where A is a constant dependant on nozzle geometry.

Although the outer layer of the spray is already atomized at the orifice exit, a jagged and turbulent liquid core is continuing breakup and atomization inside the atomized shell. At the end of injection, the termination of the fuel flow leads to a reduction of the liquid length while the remaining atomized droplets quickly evaporate. The rate at which the liquid length recedes is dependant on the injection pressure. A simultaneous change in FLOL is also observed, where depending on the speed at which the injection ends there can either be an increase (fast-closing), or a decrease (slow-closing) in the FLOL. Directly after these effects caused by cessation of the fuel flow, ligaments and droplets are expelled from the nozzle, while gaseous bubbles from the cylinder are ingested into the nozzle tip. The end of injection can lead to the formation of local

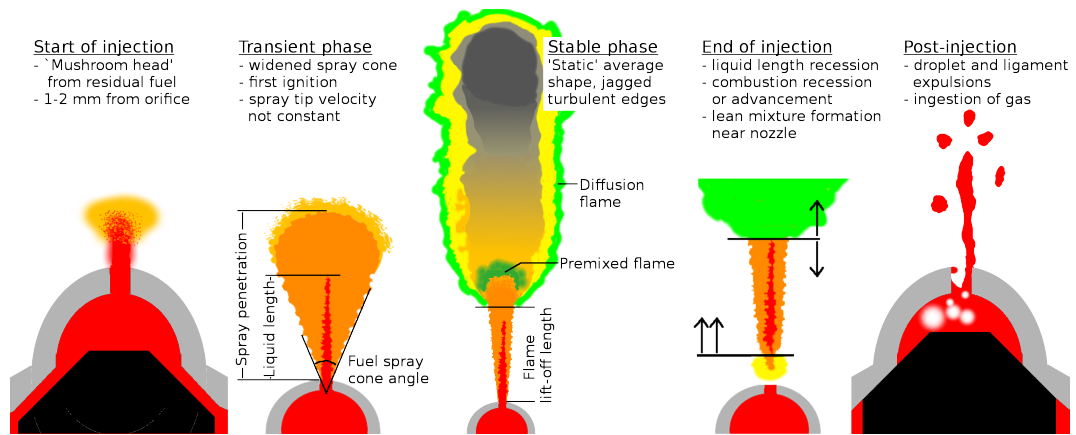


Figure 2.1.12: Qualitative description of the injection and combustion process, adding transient stages at SOI and EOI to the stable spray provided in Figure 2.1.3. An explanation of the depicted stages is provided in Section 2.1.5. Note the length scales are different for the five depicted spray stages.

fuel–air mixtures in close proximity of the nozzle tip. The complete injection process is qualitatively depicted in Figure 2.1.12.

2.2 Injector deposits

Injection sprays treated in the previous section have been optimized in combination with the cylinder geometry to provide the best possible combustion inside engines. This combustion is however not perfect, and the formation of small amounts of soot and unburned hydrocarbons (UBHC) will occur inside an engine cylinder. Carbonaceous deposits can form inside the cylinder, and these deposits *can* form at/in the injector, altering fuel flow and spray pattern. In addition, mechanical wear of injectors near the end of their life can also affect internal fuel flow. This is not new and both formation and removal of deposits at the tip of the nozzle have been investigated for decades [49][50][51]. Diesel engines have had this effect mitigated down to a minor issue by using robust fuel injection systems and addition of detergents to the diesel fuel, and under normal operating conditions nozzle coking and wear should not noticeably impact engine performance⁴. Application of HSDI engines in light-duty vehicles in combination with increasingly stringent emission regulations has led to the design of more complex, downscaled, high-pressure, and highly advanced injection systems since the turn of the century. This increase in the

⁴I.e. slight nozzle coking *will* occur, however diesel engines will not suffer a dramatic drop in performance as a result of these deposits within the injector lifetime.

complexity of the injection system has led to a reduced tolerance to deposits and increased sensitivity to fuel quality [52][53]. In addition, blending biodiesel (or bio-alcohols) with petrodiesel is considered a viable option for reducing net CO₂ -emission from diesel engines, creating a broad range of fuel compositions the fuel injection system is subjected to. The fuel quality of different biodiesels can vary widely as both fuel composition and the level of contaminants depend on the feedstock used for the production of biodiesel and the production methods. Using diesel-biodiesel blends of varying quality and possibly high levels of contaminants in contemporary, quality-sensitive, fuel injection systems can lead to unacceptable levels of deposit formation, degrading engine efficiency. A concise review on the different aspects of biodiesel production, engine emissions, and performance degradation can be found in [54], while [55] provides a review on six of the most commonly considered biofuel alternatives for diesel engines.

Early investigations into coking phenomena in common rail passenger cars identified metallic contaminants as one of the main constituents of the deposits [56]. Fuel additives, most notably acidic lubricants, were shown to dissolve small amounts of different metals into the fuel, and for fuels containing high levels of zinc, excessive deposit formation was observed. Detergents used in heavy-duty diesel engines had only little effect on reducing or preventing nozzle coking. Subsequent tests were performed to study the impact nozzle deposits have on torque loss and smoke emission, and how the use of detergents improved engine performance [57]. The impact of nozzle coking on future⁵ injectors would be severe, as up to 15% engine torque loss was measured for fouled experimental (EURO 5) injectors. Injector deposits and its adverse effect on engine performance is of concern for all diesel engine OEMs that are meeting EURO 6 emission regulations. Figure 2.2.1, taken from [58], provides an example of the torque loss over time for an engine running a zinc-doped fuel to accelerate deposit formation, for the indicated time. All injectors were clean at the start of these tests.

An extensive research, treated in [59], investigated the impact of contaminant concentration, nozzle tip temperature, and the presence of cavitation on

⁵The cited article is dated 2005, and ‘future injectors’ referred to injectors that were expected to be used in the near future, at high injection pressures and with small orifice diameters. The experimental injector treated in the article was an injector designed to meet ‘future’ EURO 5 standards.

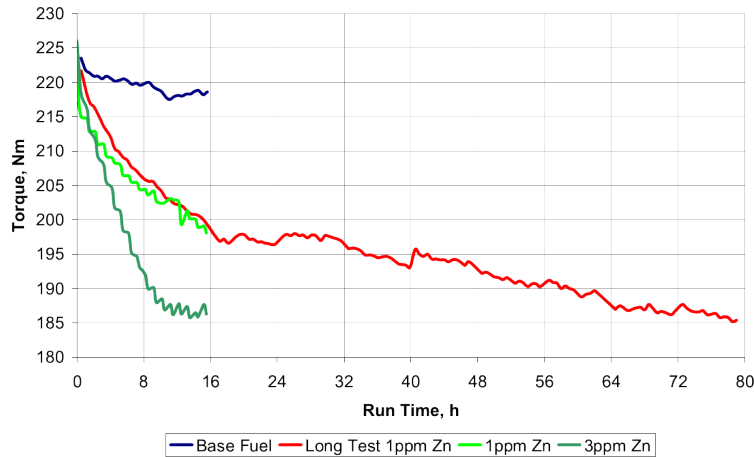


Figure 2.2.1: Impact of zinc concentration in the fuel on engine torque. Note the loss in combustion quality is the result of the formation of carbonaceous deposits and the zinc-doping was applied to accelerate the coking process. Taken from [58].

the formation of deposits in the nozzle. As a contaminant, zinc was once more applied to ensure rapid formation of deposits. The investigation indicated higher injector tip temperatures could lead to an increase in deposit formation, although the effect was less than the impact of zinc doping. In addition, the deposits formed inside the orifices were analysed to determine morphology and composition, and it was shown that the structure of deposits depended strongly on the accompanying formation rate. Figure 2.2.2 provides images from [59], indicating (left) power loss as a function of engine running time, and (right) Scanning Electron Microscopy (SEM) images of deposits near the orifice exit.

With the introduction of the CEC F-98-08 (DW-10) *Direct Injection, Common Rail Diesel Engine Nozzle Coking Test* in 2008, testing the effect of fuel quality on the formation of deposits has been standardized for common rail diesel engines. The test was primarily designed to determine the effect of fuel quality and detergents on preventing and/or eliminating deposits, but can be used as a standard protocol to study the formation of deposits. To produce deposits, and degrade combustion in a controllable way, the test indicates the use of zinc salt (zinc-neodecanoate) to create a 1 PPM zinc concentration in a high-quality fuel. The doped fuel can then be used as a reference low-quality fuel. Subsequent comparison of the DW-10 test protocol to a real-world engine [60] indicated the coking test protocol resulted in efficiency losses and injector deposits similar to those measured in real-world engines. Additional tests on the effect of biodiesel on deposit formation showed different batches

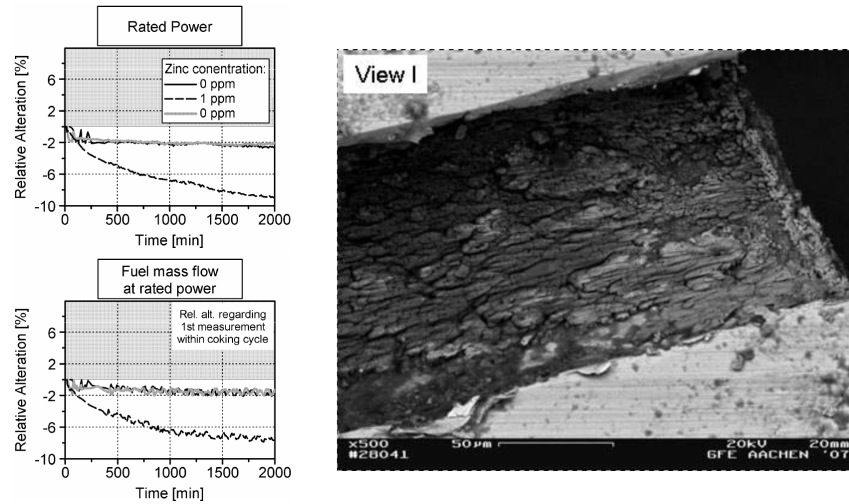


Figure 2.2.2: (left) Effects of deposits, induced by zinc-doping the fuel, on rated power and fuel injection rate. (right) SEM image of deposits present inside the nozzle close to the orifice exit, after a nozzle coking test. Both graphs and image taken from [59].

of the same biodiesel can have varying results on coking levels [60]. Application of biodiesels in the DW-10 test led to results ranging from no observable deposits to a severe deposit formation, worse than achieved by zinc doping a high-quality fuel. A recent review paper on the causes and effects of diesel injector/nozzle deposits, with several examples of biodiesel-induced coking, can be seen in [52]. Figure 2.2.3 indicates the power loss measured with the DW-10 test protocol for (left) three different batches of 10% biodiesel blends, and (right) for petrodiesel doped with zinc versus biodiesel. Without knowing the detailed composition of the biodiesel, it is impossible to determine *a priori* whether a given petrodiesel–biodiesel blend will produce injector deposits. A recent study on the impact of non-zinc metallic salts on nozzle coking, applying the same DW-10 protocol, is provided in [61].

In addition to deposits forming at the tip of the injector, the impact of internal injector deposits (IIDs) has also been investigated in recent years [62][63]. Internal deposits are however not formed as a by-product of combustion, as the injector internals are never exposed to high temperatures or reactive conditions as present at the tip of the injector. Here, fuel chemistry is responsible for the formation of soft soap layers or hard polymeric deposits inside the fuel injection equipment. While zinc appears to play a negligible role in the internal deposit formation, sodium salts play a dominant role. Reactions of sodium salts with corrosion inhibitors, and a reduced oxidation stability of the fuel, appeared to be the major causes for internal deposit formation [64]. Another investigation

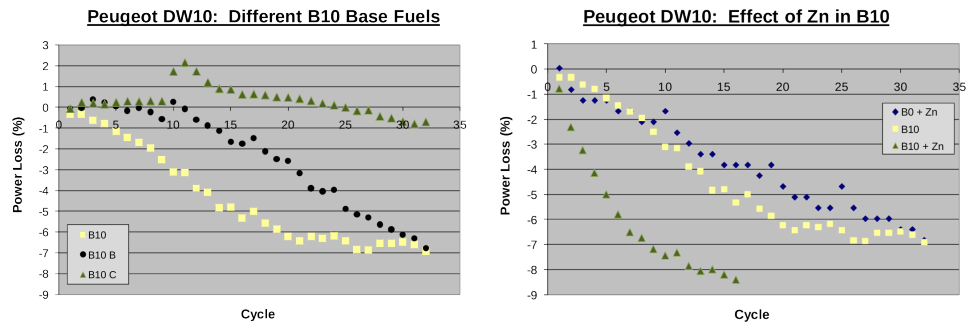


Figure 2.2.3: (left) DW-10 nozzle coking test applied to three different commercially available 10% biodiesel–diesel blends. (right) Same test, comparing a zinc-doped mineral diesel to the bottom B10 blend from the left graph, and to the same B10 blend with additional zinc doping. Both graphs taken from [60].



Figure 2.2.4: Example of an injector needle covered by IIDs. Left image provides a needle free of deposits, right image shows a same type needle removed from an injector after the injector failed proper operation. Both images taken from [66].

[65] indicated sodium in combination with pure petrodiesel led to no noticeable IID formation, however a blend containing 10% high-quality biodiesel did lead to the formation of IIDs. In addition it was found that combustion enhancers can lead to an increased IID growth rate when thermal decomposition of these enhancers occurs inside the injector. Copper contamination in combination with high-sulphur fuels can also lead to internal deposits [65]. An example of an injector needle covered in IIDs is shown in Figure 2.2.4 [66], analysis of these deposits revealed that they contain high levels of both sodium and calcium. Some fuel additives designed to reduce deposit formation can accidentally enhance the formation of IIDs when the fuel contains fatty acids [67].

The presence and formation of deposits is a well-documented process in diesel engines and, as treated above, some metallic salts can accelerate the deposit formation inside the injector, nozzle, orifices, and at the injector tip. In general, deposits will form by the very nature of the combustion cycle. The formation of deposits from high-quality, high-purity fuels is however negligible over the lifetime of the injector. Low quality fuels, or fuels which enhance

contaminant uptake due to fuel chemistry, show an increased rate of deposit formation and may lead to combustion degradation well before the injector has reached its EOL. To prevent issues with existing engines, biodiesels from different feedstock and different production methods can be tested with the DW-10 cycle, to determine susceptibility to deposit formation [68][69].

2.3 Spray degradation from fouled injectors

Nearly all the research work treated in Section 2.2 measured power loss or increased fuel consumption, and was related to the amount and type of deposits. The impact of the presence of these deposits on the spray evolution as treated in Section 2.1, is however researched only recently. Initial investigations on the impact of nozzle coking on spray evolution for modern direct injection (DI) diesel systems were conducted as early as 1992 [70]. This investigation revealed that sprays were not noticeably altered, although the engine and injection system used were not representative for contemporary common rail HSDI passenger car engines. A later investigation in 1997 on the effect of nozzle coking on spray structure for two-stage injectors [71] did reveal minor alterations of the spray pattern, and a reduced early penetration rate was observed. The authors of the latter paper [71] indicated that several observations were not well understood and would require further research. Surprisingly, the optical investigation of sprays from fouled injectors received negligible attention after publication of the 1997 paper. Investigations continued, as described in the previous two sections, on the understanding of the spray structure and evolution from new or research-grade nozzles, the effect deposits and nozzle coking have on engine performance, and the formation of deposits resulting from the use of biodiesels.

In 2012, at the start of this research, the lack of investigations into (possible) spray shape deformations from fouled nozzles was considered by us⁶ to be an interesting research opportunity to further knowledge in the field of diesel sprays and combustion from real-world engines. In addition to the research started in 2012 at the Brunel University London, a few other groups started

⁶Finding a suitable and promising research subject at the start of my Ph.D. research was not done by me alone. The decision on the research question to investigate has been agreed upon in collaboration with the supervisor and the industrial sponsor. Claiming *I* considered this a promising research subject would be inappropriate.

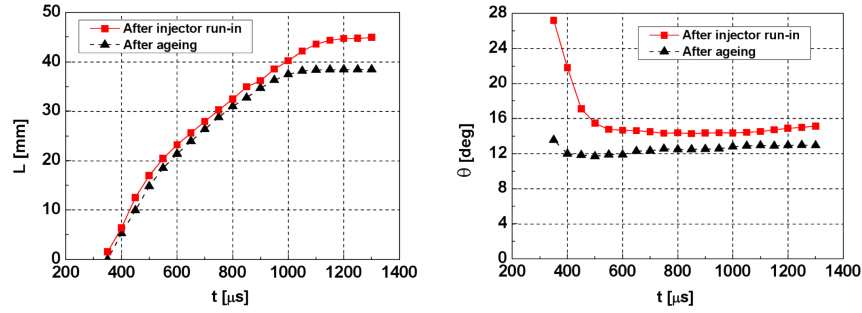


Figure 2.3.1: Reduction in (left) spray penetration and (right) spray cone angle caused by deposits on/in the injector nozzle. Red *after injector run-in* trend lines correspond to spray behaviour of a clean injector. Black *after ageing* trend lines indicate the characteristics from the fouled injector. Both graphs taken from [72].

looking at spray shape alterations from deposit rich injectors.

A broad investigation in 2012 [72] studied deposits both optically and chemically, and investigated the effect of deposits on spray shape evolution and engine performance. Based on the results, the authors concluded nozzle coking led to a significant reduction in both fuel spray cone angle and penetration length. These two effect were expected to lead to a reduction in fuel–air mixing, thus degrading combustion quality. Figure 2.3.1 provides two graphs from [72], indicating the reduction in spray cone angle and penetration resulting from nozzle coking.

Another optical investigation into the effect nozzle coking has on the fuel spray evolution was conducted in [73](2013) and [74](2014), both investigations conducted on the same test engine. In agreement to [72], a reduced spray penetration was observed for the fouled injector. The fuel spray cone angle measured in [74] however showed an increase for the majority of the measurements on the fouled injector. Analysis of the combustion characteristics indicated that fouled injectors produced on average higher soot concentrations, higher NO_x emissions, and more particulate matter (PM) in the exhaust. The increase in NO_x formation was attributed to local ‘hot-spots’ observed during combustion when using the fouled nozzle. Figure 2.3.2 provides the NO_x and PM exhaust measurements from [74].

The few investigations highlighted here provide an indication of the effect deposits have on the fuel spray evolution. A more detailed investigation of the impact of nozzle deposits on the spray shape evolution throughout the whole life cycle of the injector has however not been conducted to-date. The research presented in this thesis aims at filling this void by investigating, time resolved,

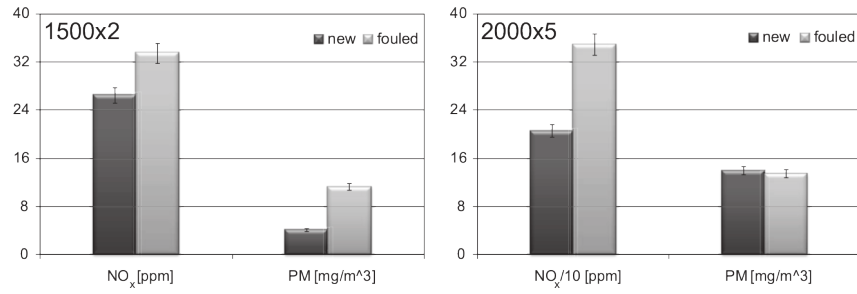


Figure 2.3.2: Comparison of engine emission of NO_x and PM for a new and a fouled injector at different operating conditions. 1500×2 indicates results measured at 1500 rpm engine speed, 2 bar brake mean effective pressure (BMEP). Similarly 2000×5 indicates tests at 5 bar BMEP and an engine speed of 2000 rpm. Graphs taken from [74].

the fuel spray evolution from injectors at different stages in their life. Although the injectors used in the present investigation showed clear signs of deposits both at the tip of the nozzle and inside the orifices, the deposit rich injectors are referred to as *used injectors*. The used injectors investigated in the present research were not purposefully fouled in a test bench by adding metallic salts, but were acquired from light-duty vehicles in the UK commuter car parc. It is expected that all observations were primarily caused by the presence of deposits. For the highest-mileage injectors researched in this investigation, it can however not be excluded that some mechanical wear might have influenced the results.

Chapter 3

Characterising sprays by injecting high pressure diesel into water

An initial investigation on the spray shape evolution from used, end of life (EOL) injectors was conducted in a high density liquid backpressure medium. By application of a liquid backpressure medium, experiments at atmospheric conditions were possible, greatly reducing complexity and safety issues of the experimental set-up. Although a liquid backpressure medium is not a realistic combustion-capable and reactive medium, it is suitable for a more fundamental, comparative study of spray shapes. By comparing in a systematic, reproducible way tens to hundreds of fuel injection events, any differences in the behaviour of used versus new injectors could be determined, at the very least qualitatively. Injection into a liquid backpressure medium allowed determining *if* there was a structural difference in spray behaviour between fuel sprays from a new or an EOL injector. Apart from the ease with which a liquid backpressure set-up could be built from readily available materials, this method proved very successful as an initial study on spray evolution alterations from different injectors. In addition to the use of a liquid backpressure environment, the experimental set-up was used as a testing facility for controllers, LED light sources and other hardware, making it an ‘initial experimental set-up’ in the broadest possible sense.

This chapter provides the reader with an alternative approach to recording and analysing fuel sprays under conditions not directly suitable for combustion research. The approach treated here was found to be very useful for a com-

parative study on spray shapes and their evolution. The minimal amount of required resources and the ease of use of the set-up presented here might prove valuable to researchers and groups who would benefit from a quick, qualitative, injection rig for testing purposes. It should be stretched the set-up is not intended as an alternative for, but as an addition to, pressurized chambers or optical accessible engines in fuel spray research.

As a result of the broad testing, recording and analyses done on the imaged fuel sprays, sufficient data (and understanding) was generated to allow publication of part of the results. The results presented in Sections 3.3.2 and 3.3.3 have been treated in [75] and additional measurement results on Rape-seed Methyl Ester (RME), not treated in this thesis, have been presented at FISITA 2014 [76].

3.1 Experimental set-up

The experimental set-up applied in this part of the research contained several alternatives to commonly used methods of recording fuel sprays. The initial set-up was built to test whether *any* difference in fuel spray evolution from a used injector with respect to a new injector could be recorded, and the practical minimum demands on the set-up were that it should:

- allow time-resolved optical recording of an evolving fuel spray,
- allow easy replacement of the fuel injector,
- provide good reproducibility,
- not require significant safety measures or expensive equipment.

By considering injection into a liquid backpressure medium the second point, the third point, and part of the fourth point, were immediately satisfied. A container filled with a liquid medium does not require air-tight constructions, high pressure systems, or any accompanying safety measures. A liquid-filled tank would not require a closed system, provided the injector was sufficiently immersed in the liquid to prevent the fuel spray from breaking through the surface upon injection. The liquid has a fixed density at atmospheric conditions, and pressure and temperature dependence of the density is low, resulting in highly reproducible ambient conditions. To satisfy the first point, a high

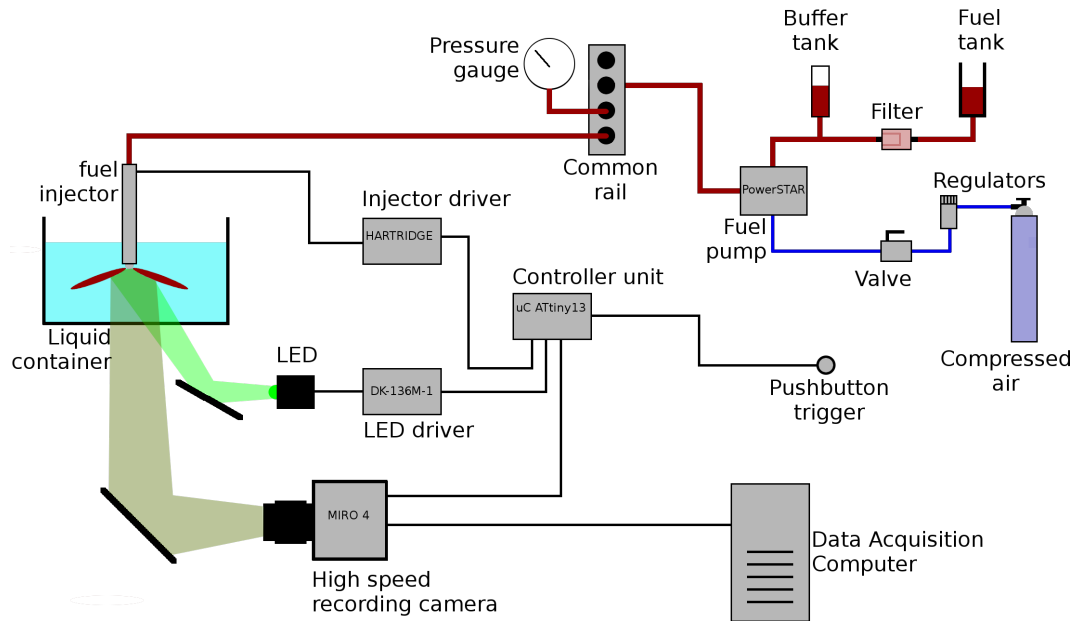


Figure 3.1.1: Schematic of the experimental set-up used in the initial investigation, where injections were conducted in a high density ambient environment.

speed camera suitable for recording the spray evolution during injection was borrowed from the EPSRC¹.

In order to record an injection event at high frame rates, additional illumination of the fuel spray was required. The fuel spray was illuminated in a front-lit configuration, as the injectors under consideration were multi-orifice injectors, making back-illumination (shadowgraphy) impractical. An additional advantage of a front-lit configuration is that the alignment of optics is less critical compared to, for example, Schlieren imaging. Taking the last point in the above list into consideration, the use of LASERS was ruled out as a light source in this part of the research. Based on the successful application of LED light sources in other researches reported in literature, a high power PhlatLight CBT-120 LED was chosen as an illumination source, inspired by the application of this specific LED in [77]. For the high pressure fuel delivery to the injector, a passenger car common rail pressurized by an air-driven pump was utilized. A schematic overview of the set-up used in this investigation is provided in Figure 3.1.1, the corresponding equipment is listed in Table 3.1. A detailed description of the main apparatuses is provided in the following sections.

¹The Engineering Instrumentation Pool of the EPSRC provided high-end (expensive) cameras, laser systems, light sources, microscopes, and what-not on a free loan basis to affiliated organizations and universities. The loan pool facility has however been discontinued in 2015.

Material	Brand, type number
Fuel filter	FFR-G12P In line Filter (20 μm)
Fuel pump	PowerSTAR 4 P4333EVN
Common rail	4-injector passenger car CR, maximum rail pressure 150 MPa
CR pressure gauge	Hi-Pro 104482, 0–250 MPa
Injectors	Several types, 5- and 6-hole light duty injectors, new and EOL
Injector driver	Hartridge
Injection chamber	Plexiglass water tank, 50 l
Backpressure medium	Clear tap water, ambient air at 18 $^{\circ}\text{C}$
Camera system	Phantom MIRO 4, monochrome camera
- Lens	Nikon Zoom 24–85 mm f2.8
Illumination source	Phlatlight CBT-120-G, green high power LED
- Central wavelength	521 nm
- FWHM	40 nm
- Driver board	Luminus Devices, DK-136M-1
Pulse/delay generator	In-house built timing and control unit
- Micro-controller	ATMEL ATtiny13-20PU (9.6 MHz)

Table 3.1: Details of materials used in the experimental set-up for the liquid backpressure investigation.

3.1.1 Fuel pump and common rail

The fuel assembly consisted of a pneumatically driven fuel pump, working at a pressure ratio of 1:333, powered by compressed air at a maximum pressure of 0.6 MPa. The pressurized fuel, filtered through an in-line fuel filter upstream of the fuel pump, was collected in a common rail. The pressure of the common rail was determined by use of an analogue pressure gauge, connected directly to the common rail. Pressure was set and maintained at 40, 60 or 80 MPa by varying the input/drive pressure. A short (roughly 45 cm) fuel line connected the common rail to the injector. Commercially available mineral diesel (EN590 compliant) was used as fuel.

3.1.2 Injector driver and injectors

Six different types of EOL injectors, showing the clear presence of external deposits, were acquired for this initial investigation. For comparison purposes, a new injector was acquired for one type of the used injectors, and a full comparison of spray shape evolution conducted on this one type of injector

is treated in Section 3.3. For the remaining five deposit rich injectors, an unused counterpart was not acquired and analysis was limited to recording the occurrence of transients only. All injectors were common rail multi-orifice injectors, having 5 or 6 orifices, depending on the injector type.

A Hartridge injector driver, specifically designed for use in research environments, was used to control injections. By use of an external TTL-compatible triggering port, the injector driver was triggered time-synchronized with the camera and illumination source. The injection duration was varied from 300 μ s to 3 ms in order to determine optimal injection and recording conditions. For the optimal recording conditions the injector driver was set to produce injections lasting approximately 0.6 ms.

3.1.3 High speed camera

Injections were recorded using a monochrome VISION RESEARCH Phantom MIRO4 camera, borrowed from the EPSRC Engineering and Instrumentation Pool. The MIRO4 is a hand-held high speed camera, recording at frame rates and resolutions ranging from 800 \times 600 pixels at 1265 fps to 32 \times 16 pixels at 111 100 fps. For testing purposes several combinations of frame rates and resolutions were used, and after analysis of the initial results, the majority of the recordings were done at a resolution of 128 \times 128 pixels and a frame rate of 24 390 fps. Shutter times were varied in combination with pulsed illuminating of the evolving fuel sprays, and this led to the selection of two optimal shutter times of 2 μ s and 39 μ s, depending on the pulse mode of the light source.

3.1.4 High power LED

The evolving fuel spray was illuminated by a high power LED in a front-lit configuration. The LED provided green light at 521 nm with a FWHM of 40 nm and was designed for operation at a maximum current up to 36 A, for a duty cycle below 50%. The LED was driven by a DK-136M-1 LED driver board, and accepted external control of pulse width through TTL-input. Several combinations of pulse widths and LED currents were tested in this research, and the pulse modes applied in the major part of these experiments were fixed at two optimal recording modes. *Mode 1* corresponded to a pulse driven mode with 4.5 μ s pulses at a repetition rate of 24.39 kHz, for a total of 35 pulses while the camera shutter speed was set at 39 μ s. *Mode 2* provided a single pulse of

1.5 ms in combination with a camera shutter time of 2 μ s, essentially resulting in a temporal continuous wave (CW) illumination mode for the duration of the injection.

To minimise set-up complexity, illumination with the use of a LED was preferred over LASER illumination. A possible drawback of using a LED could be a lack of optical power to allow clear imaging of the fast evolving fuel spray. Available articles on research involving high-power LED sources [77][78] show contemporary LEDs allow high-current pulsed operation and should be capable of producing pulses suitable for spray imaging. Moreover, LEDs do not emit coherent and monochromatic light, while they do have a fairly small bandwidth. The use of LEDs instead of LASERS prevents the occurrence of speckle patterns, which might give artefacts in images due to the coherence of LASER light. The occurrence of speckle patterns could be reduced by using a diffuser in combination with a LASER, however this would only lead to a further increase in the complexity of the system.

The added advantage of using LEDs instead of LASERS stretches to the physical experimental set-up as well. LEDs require less safety measures and no interlock, LASER safety courses, or controlled zone is required due to the relative low power and incoherence of the light. The physical size of a typical high power LED with accompanying cooling and power supply, in this research less than three litres, allows easy incorporation in an experimental set-up. The use of an arc light as an (incoherent) alternative to a LASER has been considered but deemed less favourable than the use of a LED for two reasons. In the experiment conducted, the small spectral bandwidth of the LED was preferred to the broadband emission of an arc light preventing chromatic aberrations. Additionally, a high powered LED can be pulse driven at a high repetition rate and short illumination time, while an arc lamp generally provides flashes of the order of milliseconds at a low repetition rate, potentially increasing motion blur when recording high velocity transients.

3.1.5 Control and timing

For the synchronization of the injector driver, camera, and LED, a controller unit was developed and built in-house. At the heart of the controller resided an ATMEL ATtiny13 microcontroller, programmed to produce several parallel TTL output signals, with the appropriate delays and repetitions required for the experiment. The main reason for using a bare microcontroller, opposed to an

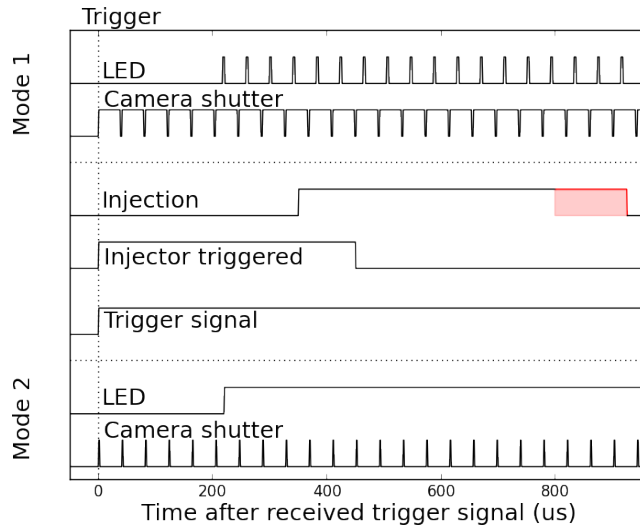


Figure 3.1.2: Graphical representation of the pulse/trigger timing. In order to record both the dark and the illuminated backgrounds, the control unit has been set to trigger the LED delayed w.r.t. the triggering of the camera. Injection of fuel is retarded w.r.t. the triggering of the injector driver. The red region at the end of the *injection* graph shows the overshoot in measured injection duration with respect to the programmed injection duration.

off-the-shelf delay generator, was the possibility of the controller to allow the output of highly asymmetric signals and pulse trains with varying pulse widths and inter-pulse times coming from the same output channels². Although the ATtiny13 microcontroller is a low-end general purpose controller, the investigation treated here did not require synchronization to a higher precision than $1\ \mu\text{s}$, which lies well within the capabilities of the ATtiny13.

After the initial testing to find optimal combinations of injector times, illumination modes and camera settings, the microcontroller was programmed to operate in two modes, designated *mode 1* and *mode 2*, already shortly described in Section 3.1.4. Figure 3.1.2 provides a graphical representation of the timing and synchronization of the camera, LED and injector for the two different modes. In this figure *Trigger signal* represents input to the controller (the closing of a switch), the *Injector triggered* represents the output of the controller to the injector driver. The actual fuel injection (*Injection*) is both delayed and elongated with respect to the programmed injection pulse. This

²For example, during the initial tests the microcontroller was programmed to output on one port a signal consisting of two subsequent pulses spaced $500\ \mu\text{s}$ apart with the second pulse having a fourfold increased pulse width. This two-pulse combination was repeated nine times with $70\ \text{ms}$ delay between every set of pulses. Programming such an asymmetric pulse train into a microcontroller is not more complex than programming a single, symmetric, output signal.

Parameter	Parameter range initially tested	Applied settings for final measurements
Injection pressure	40, 60, 80 MPa	60 MPa
- Duration	0.3 ms to 3.0 ms	0.6 ms
Backpressure density	1.2 kg m ⁻³ (air), 10 ³ kg m ⁻³ (water)	predominantly water
Recording conditions	800x600 @ 1265 fps to 32x16 @ 96 kfps	128x128 @ 24 390 fps
<i>Mode 1</i> shutter time	1/frame rate	39 μ s
- Illumination	3 μ s to 15 μ s	4.5 μ s
- Pulses	30 to 60	35
<i>Mode 2</i> shutter time	1 μ s to 10 μ s	2 μ s
- Illumination	CW, 1.5 ms	CW, 1.5 ms
- Pulses	1	1

Table 3.2: Experimental parameters varied in the initial investigation.

delay is the result of a combination of an electronic delay inside the injector driver ($\sim 20 \mu$ s), and mechanics inside the injector ($\sim 350 \mu$ s). The injection delay was deliberately not compensated for by piloting the injector trigger with respect to the start of recording, although the LED was delayed with respect to the start of recording. Recording of both the non-illuminated and illuminated injector nozzle prior to the start of injection provided dark and light background images, which were required for image analysis. The LED signals represent the pulses sent to the LED driver board by the controller and the *Camera shutter* signal represents the shutter-open time of the camera. The camera was triggered by a continuous high signal from the controller, and the block/spike graphs depicted as *Camera shutter* provides the shutter behaviour, controlled by the camera software.

3.1.6 Initial measurement parameters

In the initial phase of the investigation parameters were varied over a wide range in order to determine optimal recording conditions. After determination of the optimal conditions, several hundred recordings were conducted. An overview of the investigated parametric space is provided in Table 3.2, showing both the initially tested and ultimately applied settings.

3.2 Measurement results

3.2.1 Spray anomalies

Measurement data consisted of monochrome images of fuel injection events, showing the evolution of the fuel spray when injecting into either a liquid backpressure environment or into air at atmospheric conditions. A set of images of different injection events are shown in Figure 3.2.1, accompanied by an elaborate explanation of visible details and image quality. Based on comparable qualitative determinations of image properties, the parameters provided in the second column of Table 3.2 were optimized, resulting in the parameters listed in the third column. These settings have subsequently been used in the measurements treated in the following section.

When recording the fuel spray development from different injectors under identical conditions, direct comparison of the acquired spray images is possible. Such a comparison of injections from a new and used injector demonstrated the occurrence of anomalous transients when using an EOL injector. Figure 3.2.2 provides image sets of injections from different used injectors along with one set of images recorded from the new injector. All injectors were fitted with a six-orifice nozzle, except for the injector on the second row, which had five holes. The new injector (bottom row) provided a symmetric and highly reproducible spray shape. The EOL injectors all produced similar radial expanding transients and it was decided to continue the research with the one injector for which a new counterpart was available³.

³It was considered excessive to acquire a new injector for every used injector and to do all subsequent experiments for all available injectors.

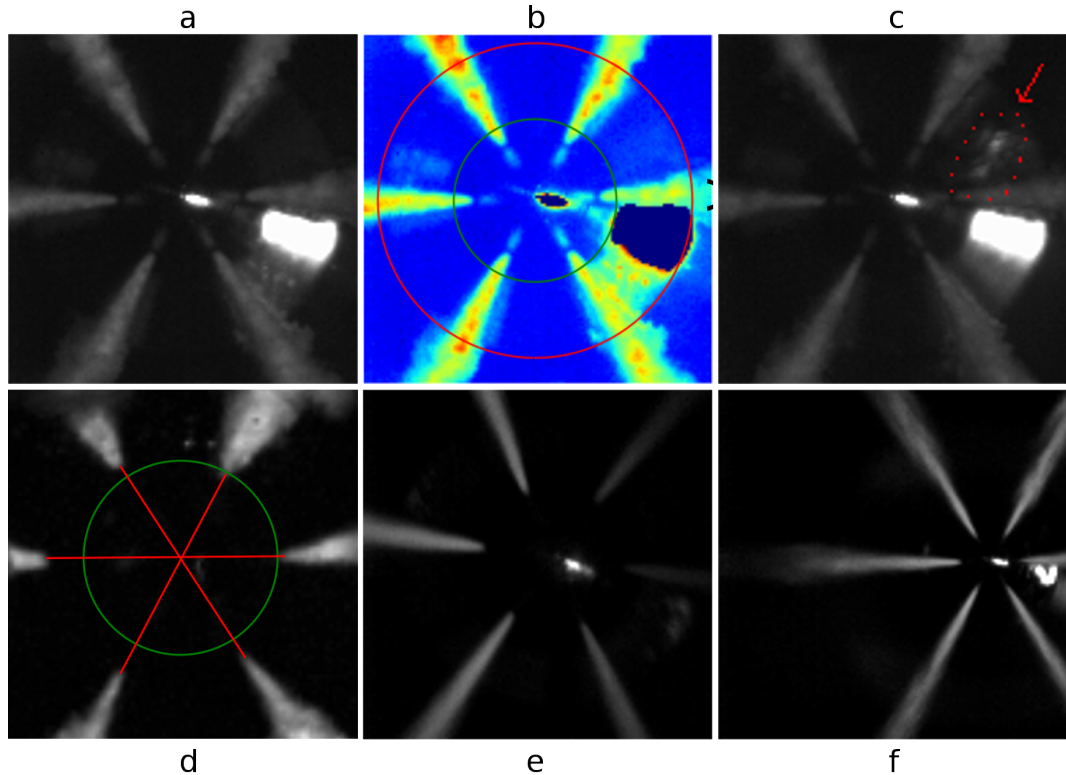


Figure 3.2.1: Examples of typical recordings. (a) Typical injection of diesel into water, unaltered image. The bright, saturated part is the result of specular reflections off the tip of the nozzle. (b) Same image as (a), false coloured for clarity. Saturated part has been masked out, and two circles have been added to indicate the injector tip. The red circle shows the outer diameter of the injector nozzle. The hemisphere at the injector tip, containing the six orifices, is indicated by the green circle. (c) An injection event in water, where the red arrow and dotted area indicate the presence of an air bubble at the tip. Recordings showing air bubbles at the tip were rejected for analysis as it is unclear what the effect of these air bubbles could be on spray evolution. The air bubbles were not stationary during injection, and they followed the flow field of the surrounding water. (d) Misalignment of the injector with the focal plane, the nozzle of the injector appears warped. The red lines connect opposing orifices of the injector and should form a symmetric hexagon if the orifices all lie in the horizontal (focal) plane. As a guide to the eye, the green circle is placed with the origin centred at the intersection of the three lines, the radius equal to the shortest distance to the nearest orifice. (e) Injection into air at atmospheric pressure. The lower background density of air leads to a higher initial fuel spray velocity. This in turn reduced quality of the spray edge by motion blur, creating (falsely) a perfect straight spray edge. (f) Injection into air at atmospheric pressure with the injector placed off-centre and the magnification reduced compared to the image in (e). The fuel spray from the left orifice was visible over a longer distance, but illumination was no longer uniform.

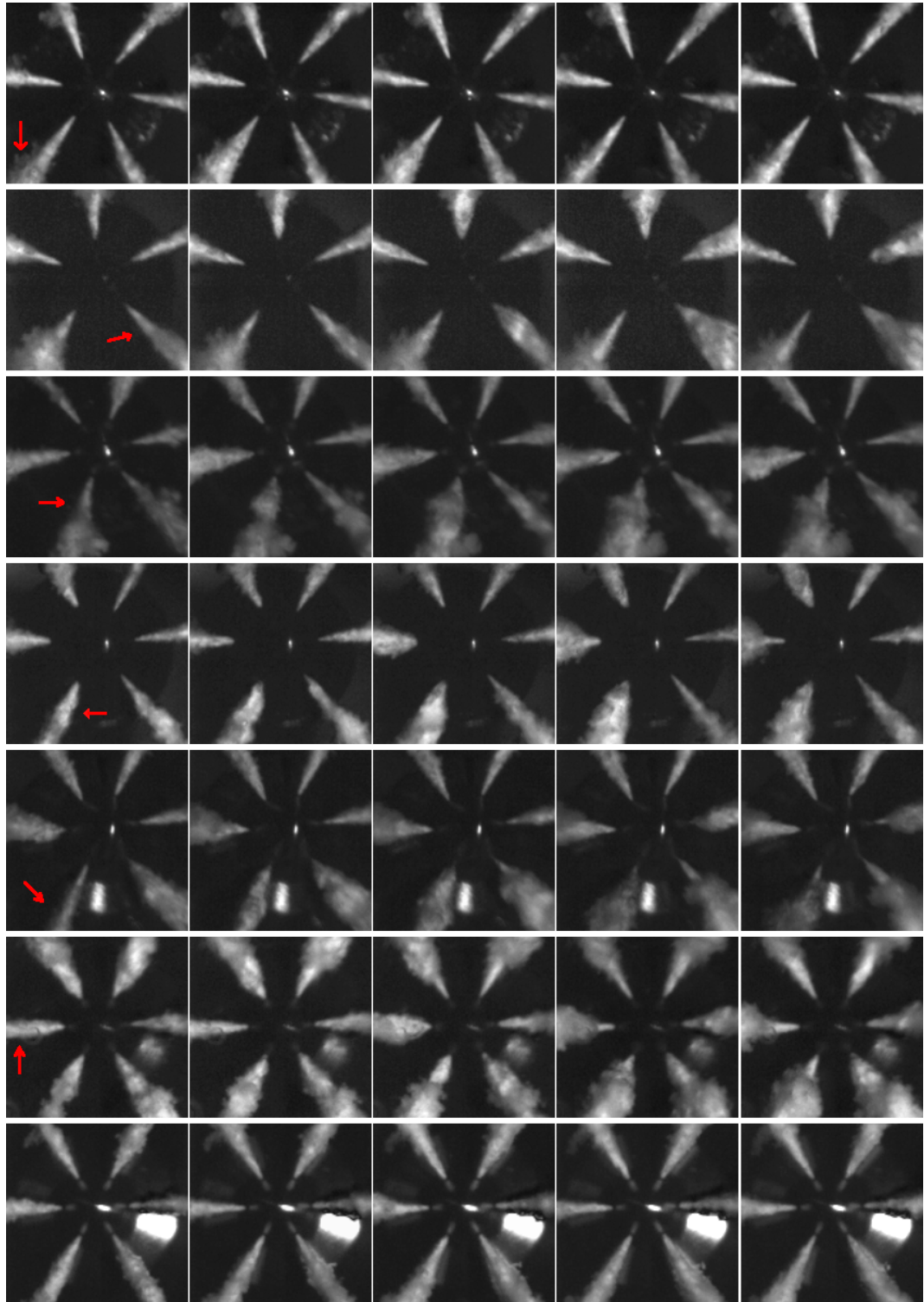


Figure 3.2.2: Image streaks of injections from different end of life (EOL) injectors and a new injector, injecting into a liquid backpressure medium, injection pressure 60.0 MPa. Every row corresponds to a single injection from one injector, first six rows for EOL injectors, bottom row for a new injector. Red arrows in the first frame have been added to indicate where a radial bulge is/will be occurring in subsequent frames. Time between subsequent frames was 40 μ s, recorded at a frame rate of 25 000 fps.

3.2.2 Comparison of a new and end of life injector

Figure 3.2.2 shows the new injector produced a stable fuel spray shape during injection, as would be expected. EOL injectors produced transient anomalies, recognizable as off-axis bulges indicating a change in fuel momentum from a primarily axial to an increased radial component. This aspect was further studied by recording several hundred injections from both the new injector and a same-type EOL injector. During this investigation, experimental parameters were varied over a narrower field than in the previous section, the recording conditions are listed in the third column of Table 3.2. The injectors were both of same type and the recording conditions were kept constant in between measurement series to allow direct comparison of recorded images. Transient anomalous ‘bulging’ of the spray was observed in nearly every recording for the used injector, although shape, evolution velocity, moment of occurrence, and participating orifices varied from injection to injection. To illustrate the inconsistency of the spray evolution from the EOL injector, Figures 3.2.3 (shape) and 3.2.4 (time of occurrence) provide image sets of the used injector, showing the mentioned transient aspects.

To ascertain the observed anomalies are not induced by the liquid back-pressure environment, additional measurements in free air (0.1 MPa, 18 °C) were conducted. The high velocity of the injected fuel in combination with the relatively low recording speed of 24 390 fps resulted in images of insufficient quality to allow analysis. It was however possible to show the used injector produced comparable anomalies under atmospheric conditions. The anomalies could be seen in one to two frames of every recording, making analysis of the evolution of the bulges impossible, but the *presence* of the bulges was successfully established. Several measurements conducted into atmospheric air are provided in Figure 3.2.5, alongside the evolution of a fuel injection from a new injector for comparison.

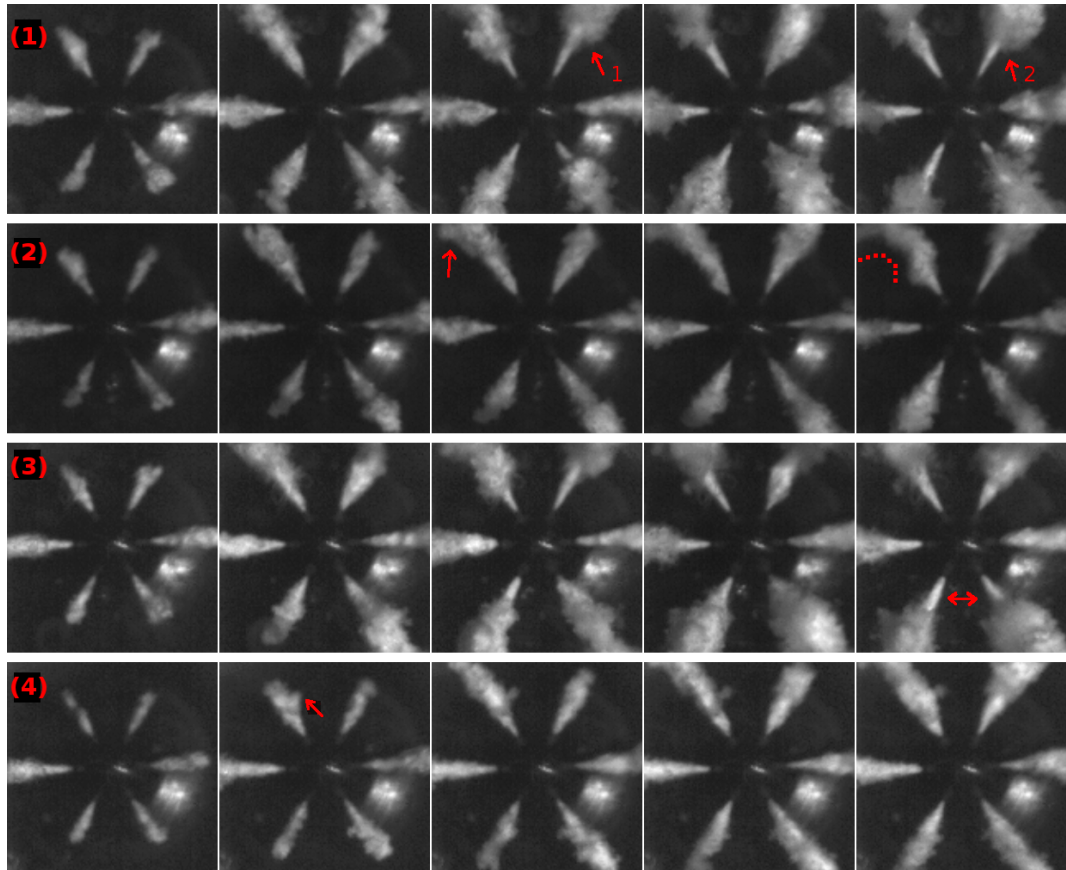


Figure 3.2.3: The shape and size of transient bulges vary for different injections when injection conditions are maintained constant. The only common trait appears to be the increased radial momentum, although the magnitude of the effect does not appear to be constant. Every row provides one injection and different anomalous behaviours have been emphasized with the help of small red arrows. (1) A double-bulge occurring from the same (top-right) orifice. (2) Top-left orifice produces a strongly skewed spray. (3) The two sprays from the two bottom orifices produce two comparably large anomalies. (4) A small atomized cloud is separated from the main spray and remains stationary during the remainder of the injection.

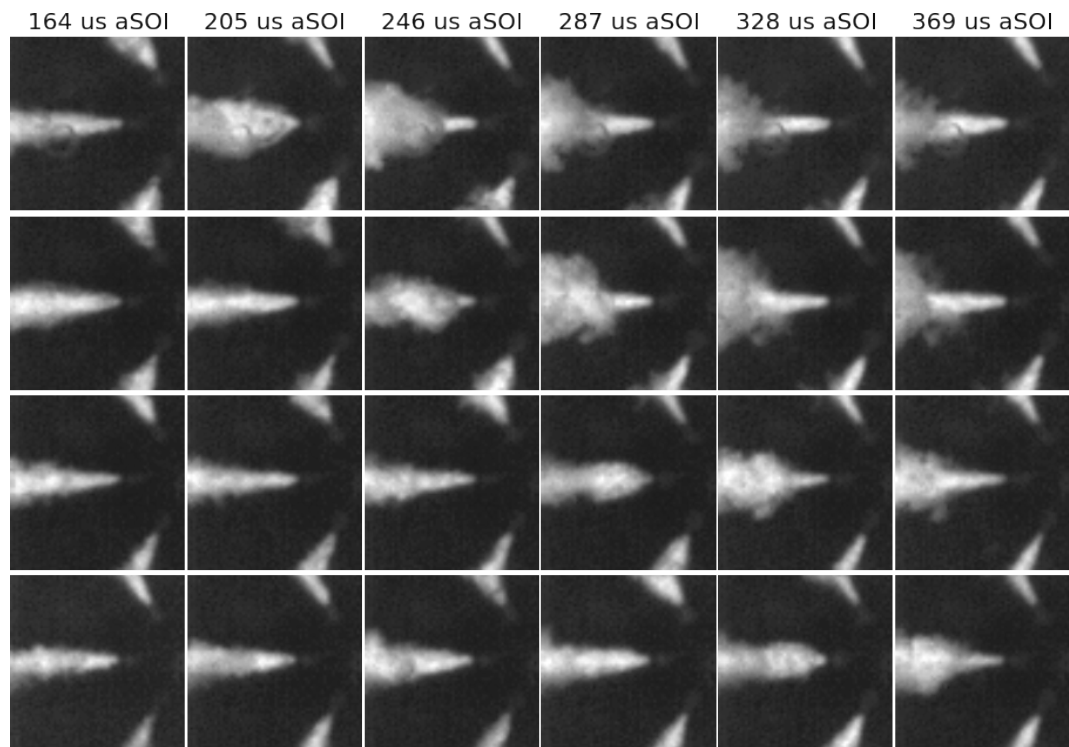


Figure 3.2.4: The moment of occurrence of transient anomalies is not constant from injection to injection. The earliest anomalies can be observed 205 μs after the start of injection, and in some cases anomalies will start occurring only 328 μs after the start of injection. Other orifices might produce bulges even more advanced or retarded compared to the numbers given here. Injection and recording conditions were identical for all injections.

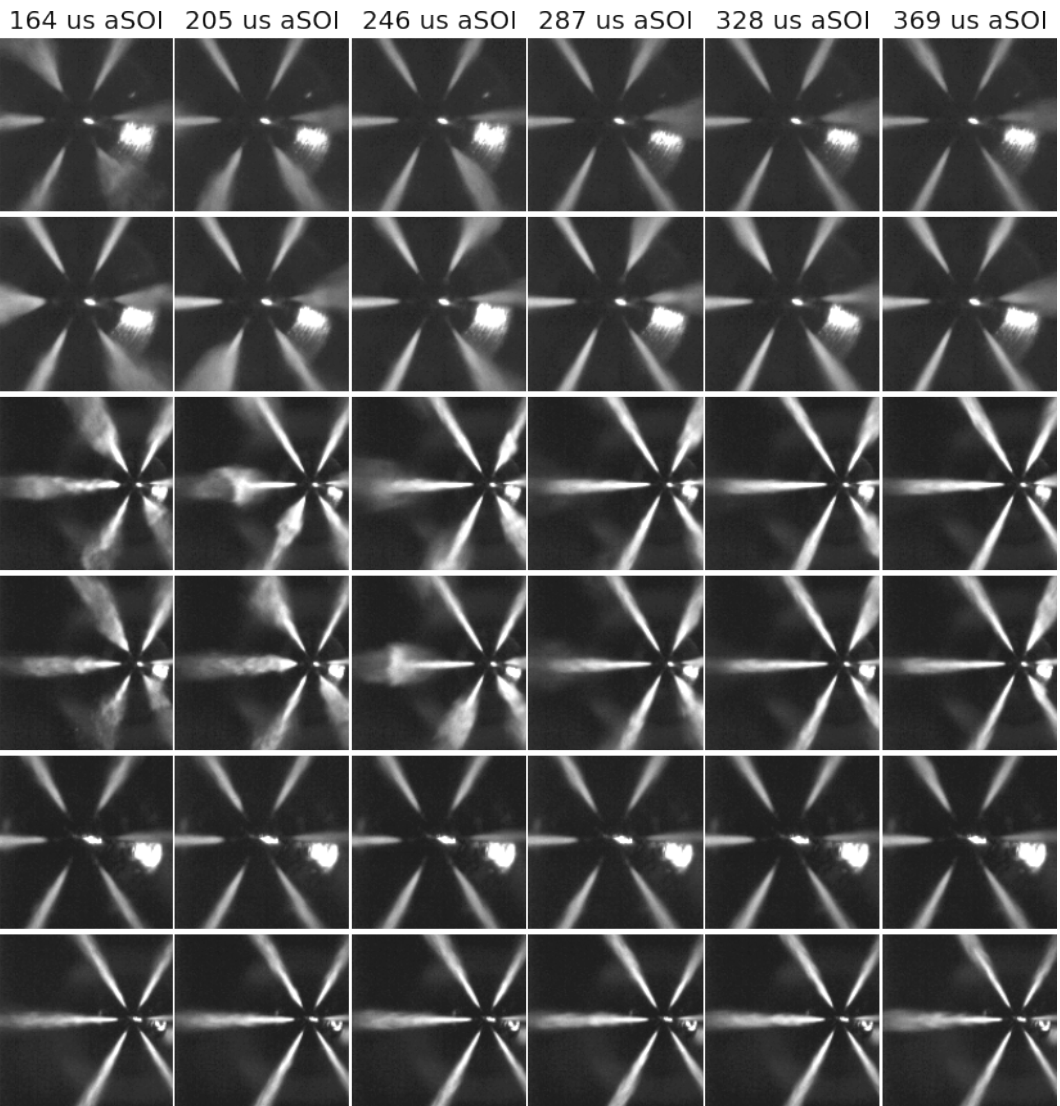


Figure 3.2.5: Bulging anomalies can be observed when injecting fuel into free air, affirming the transients are caused by the EOL injector, and are not induced by the use of a liquid backpressure medium. The camera can record the presence of bulges, but is too slow to record their evolution. First two image rows show two injections from the EOL injector at a magnification of $62\ \mu\text{m}$ per pixel, Third and fourth row show injections from the same injector at a magnification of $125\ \mu\text{m}$ per pixel, with the injector placed off-centre. Fifth and sixth row show injections into free air from a new injector, at $62\ \mu\text{m}$ and $125\ \mu\text{m}$ per pixel respectively.

3.3 Analysis of recorded sprays and anomalies

Identification of transients observed in the previous section was done by direct comparison of images of injections from the new and the deposit rich injector. A quantitative analysis of the observed effects requires image analysis to determine typical fuel spray characteristics, for example spray cone angle and penetration. This section treats the analysis of the observed spray anomalies, recorded both in free air and in a liquid backpressure medium. Injection in either a liquid backpressure medium or into free air are uncommon conditions for diesel spray investigation, and therefore the analysis does not provide results that can be compared to literature. Nonetheless the observed *trends* in some of the results proved illuminating for understanding the effects of injector age on sprays. The analysis done in this section only applies to the new and EOL injector treated in Section 3.2.2.

3.3.1 Pre-analysis manipulations

Before analysis of the images to determine spray characteristics, several basic image manipulations were applied in this investigation, and are treated in this section. Although there are numerous ready-to-use image manipulation packages available, the image quality of the recorded data was relatively low and applying standard image filtering packages sometimes led to erroneous results. To prevent eccentric results, part of the analysis was done with the help of purpose-written filters, generally incorporating existing manipulation software libraries in a post-processed stadium for further analysis. In order to ensure the results were cross-comparable, all recordings were analysed with the same filters and libraries. As a result, some cumbersome preprocessing steps have been applied to ensure sanity of the results. These manual preprocessing steps are treated in the subsequent paragraphs, and if applicable a short discussion and comparison to existing manipulation techniques is offered.

3.3.1.1 Pulsed versus continuous light source operation

Two different illumination/exposure combinations were used in this investigation, as listed in Table 3.2. The two modes led to a total exposure of the camera CMOS of either $4.5\ \mu\text{s}$ (*mode 1*) or $2\ \mu\text{s}$ (*mode 2*) for every image. Main reason

for application of two different modes was to determine optimal conditions for future investigations, by studying the trade-off between high illuminating power (longest exposure time) versus reduction of motion blur (shortest exposure time). After studying several recordings, it was found the increased exposure did not lead to either an increased motion blur or to an enhanced image brightness for the water-injected experiments. Irrespective of the exposure time motion blur was not observed when injecting into a liquid environment, and motion blur when injecting in air was clearly present, but not significantly different for the two exposures. Image brightness seemed slightly better for the longer exposure when looking at features in the central core of the injected spray, however these features were not studied as a full 3D-reconstruction of the spray was not possible. For edge detection and threshold determination, the added brightness did not significantly increase image quality. There was therefore effectively no difference between *mode 1* and *mode 2* data sets when injecting into a liquid backpressure environment. The investigation of the two different pulse modes did not allow determination which setting would be better suited for future experiments⁴. An advantage of this conclusion was, that both pulse modes provided data of indistinguishable quality and both data sets could be combined together into one set.

3.3.1.2 Intensity corrections and specular reflections

When illuminating in a front lit configuration, specular reflections off flat metallic surfaces can lead to saturation of the camera CMOS. The first preprocessing step was to correct for these specular reflections. Timing and recording were configured to ensure illumination of the injector before the start of injection, and pre-injection recorded images allowed correcting for specular reflections. Based on the illuminated background recordings, sprays that evolved through saturated areas could be (partially) reconstructed, but spray shadows coinciding with saturated parts could lead to additional reconstruction of ghost sprays, as will be shown below. It was therefore decided to use a simple masking scheme to eliminate saturated parts altogether, and accept the loss of spray parts as a result of the masking operation. The amount of specular reflections depended on the state the injector was in, a used injector producing far less

⁴Based on ease-of-use the *mode 2* ‘local CW’ mode was easier to apply, however the LED die temperature limit sets an upper limit on the total illumination time of roughly 3 ms, when the LED is operated at the maximum current of 36 A.

reflections due to the deposits at the tip. It was not feasible to apply one mask to all recordings, and an individual mask was determined and applied for each recording. To compensate for intensity fluctuations resulting from different illumination and shutter times, a single threshold was applied to determine whether reflected light in any area of an image was intense enough to require masking. Certain areas of the recorded images would never show specular reflections, and by determining the maximum image intensity in these regions for a fully developed fuel spray, an upper limit for the spray intensity could be determined. To clarify this masking and correction, Figure 3.3.1 provides a step-by-step analysis, including an initial attempt at spray reconstruction leading to ghost sprays. After masking all images from any recording, the image intensity was rescaled to the maximum intensity still present in the image. This was to ensure one threshold could be applied to all recordings, irrespective of their initial recorded intensities. The binarized images in Figure 3.3.1 were acquired by using an OTSU threshold, and have been inserted for illustrative purposes only. Section 3.3.1.3 treats a more rigorous threshold determination.

3.3.1.3 Threshold determination for binarization

Masking of all saturated parts and subsequent intensity rescaling allowed binarization of the spray by application of a single fixed threshold⁵. Numerous standard libraries are available which provide more flexible threshold determination methods (OTSU- or adaptive thresholds, for example), but these threshold methods rely on intensity histograms of the individual images. Here, depending on the spray shape (bulging or not-bulging) the histogram could change dramatically over the complete set of images from a single injection recording. Application of a flexible threshold algorithm, redetermining the optimal threshold for every individual image, might lead to artificial spray expansions or contractions as a result of changing thresholds from one image to the next. It would be possible to use, for example, an OTSU threshold to determine an averaged threshold based on several images, subsequently applying the determined threshold to all images within a single recording. This would have resulted in the application of one fixed threshold to all images, which is operationally identical to what was done here, except the single threshold in

⁵As 2D images were recorded, intensity variations inside the sprays did not provide any information on the spray evolution; a 3D reconstruction is not possible from these images. Only the spray circumference provides ‘real data’, justifying binarization.

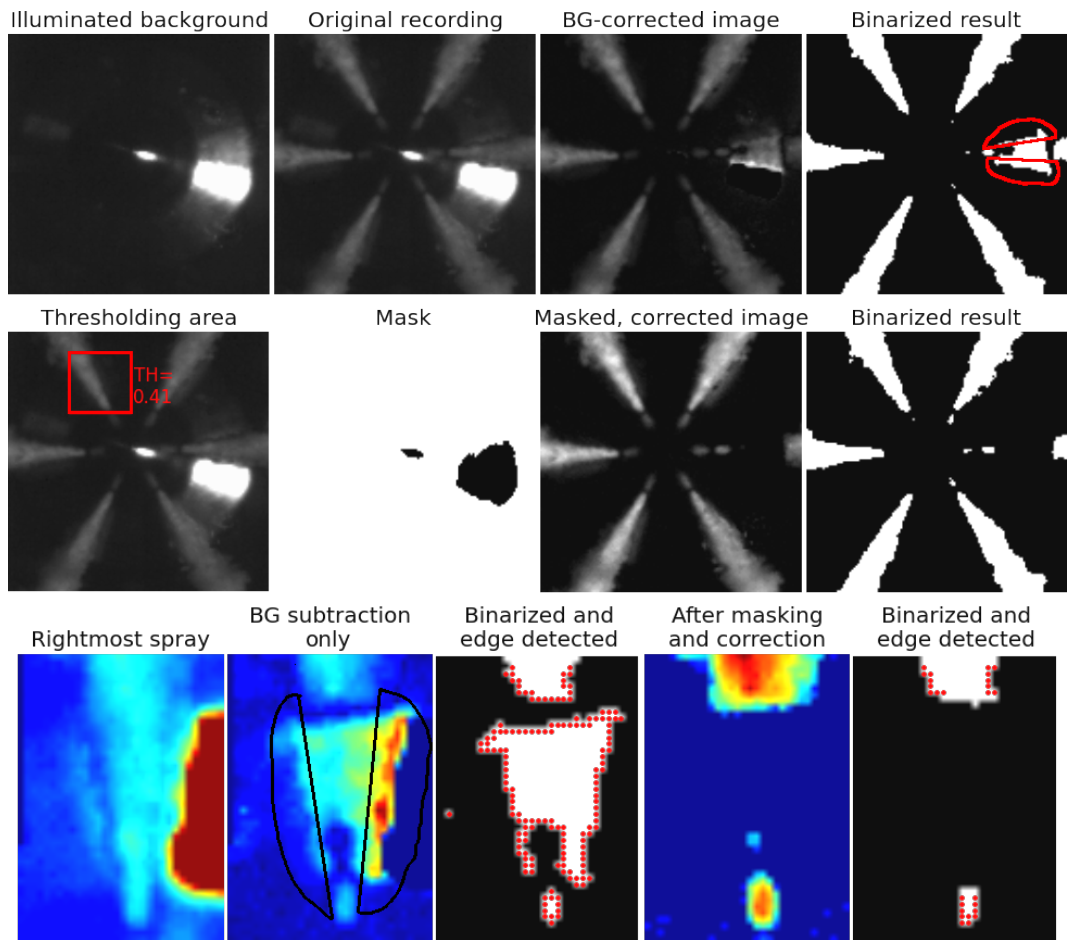


Figure 3.3.1: Correction for specular reflections of the recorded images. First image row shows a spray reconstruction which was rejected as the rightmost spray had an artificial ‘ghost spray’ interpreted by the algorithm (indicated in red). The second image row shows the determination of the mask that would be applied to all images to correct for specular reflections. The third row shows the effect of the resulting correction for the rightmost spray, including the interpreted spray edges, where black half-ellipses in the second image indicate ‘ghost sprays’. Red dots correspond to the determined spray edge.

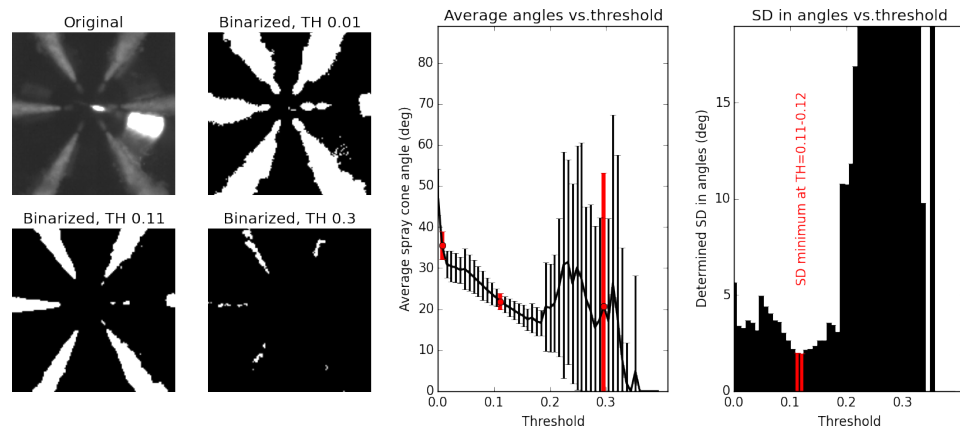


Figure 3.3.2: Determination of the binarization threshold. Left images show the impact different thresholds have on binarization results of the images. Middle graph provides the spray cone angles with accompanying error margins (vertical) versus the applied binarization threshold (horizontal). Red data points correspond to the thresholds applied in the leftmost images. Right graph provides the standard deviations in the spray cone angles, plotted versus the binarization threshold. Red bars in the right graph show the optimum threshold for spray cone angle determination.

this instance was determined by error analysis.

The threshold applied for binarization was calculated by optimizing an analysis algorithm that determined the fuel spray cone angle. By varying the threshold and calculating the resulting fuel spray cone angle with accompanying error margin for a large subset of images, it was possible to determine the threshold that provided optimal binarized images for subsequent analysis. Care was taken the angle determination algorithm was not applied to images containing transient anomalies, as these spray cone angles would have been error-rich due to bulges in the spray, distorting the quality of the angle determination routine. Figure 3.3.2 provides a graphical clarification of the method used to determine the optimal threshold for binarization. All recordings were done under identical conditions and by considering data from the new injector only. For identical injection and recording conditions the spray cone angles should therefore be the same, which is required to allow minimizing of the standard deviation.

3.3.1.4 Further manipulations

After application of the binarization filter using the threshold as determined above, standard libraries for further analyses were applied, in some cases augmented by additional purpose-written filters. Most filters and regression algo-

rithms were imported from the SciPy *Scientific Tools for Python* library[79], most notably the `scipy.odr`[80] procedure for variable fitting of data, and the `scipy.ndimage.filters.sobel`[81] filter for edge detection in processed images.

3.3.2 Variations in the start of injection

The start of injection (SOI) was sometimes retarded by one, sometimes two, frames w.r.t. what was expected based on injector mechanics⁶. The microcontroller triggered camera, LED, and injector synchronized within $0.5\ \mu\text{s}$, and an injection delay of more than one frame should not occur. Based on the detailed settings and generated delays in the controller, the actual injection was expected to start $20\ \mu\text{s}$ before illumination of the sixth frame in any recording. This provided five illuminated pre-injection images suitable for light-background subtraction and specular correction, see also Section 3.3.1.2. The sixth frame *should* provide an image where a spray had been evolving for $22\ \mu\text{s}$ to $24.5\ \mu\text{s}$, depending on whether the recording was a *mode 1* (24.5) or a *mode 2* (22) recording. For the new injector the SOI indeed proved highly reproducible, as can be seen in Figure 3.3.3, left three columns. The six recordings of the new injector show an almost identical penetration in the sixth frame. It can additionally be seen in the rightmost three columns of Figure 3.3.3, identical settings and conditions for the EOL injector did not result in a reproducible SOI. Injections starting in the expected, sixth, frame provided different spray penetrations, indicating not all injections started exactly at 22 or $24.5\ \mu\text{s}$ before the start of the sixth frame. The change in the exact time at which injections started was however below the temporal resolution of the camera. The bottom two SOI image sets of the EOL injector showed two extreme cases where injections started as late as in the seventh frame, corresponding to a minimum *additional* injection delay of $24.5\ \mu\text{s}$.

⁶The mechanics/inertia of the valves and needle lead to a delay between the start of the inrush current, the start of the needle lift, and the start of the fuel injection. This delay is highly reproducible, and was typically $350\ \mu\text{s} \pm 5\ \mu\text{s}$ for a new injector. At a frame rate of $24.4\ \text{kfps}$, a delay of 2 frames constitutes an additional delay of $46\ \mu\text{s}$ to $82\ \mu\text{s}$.

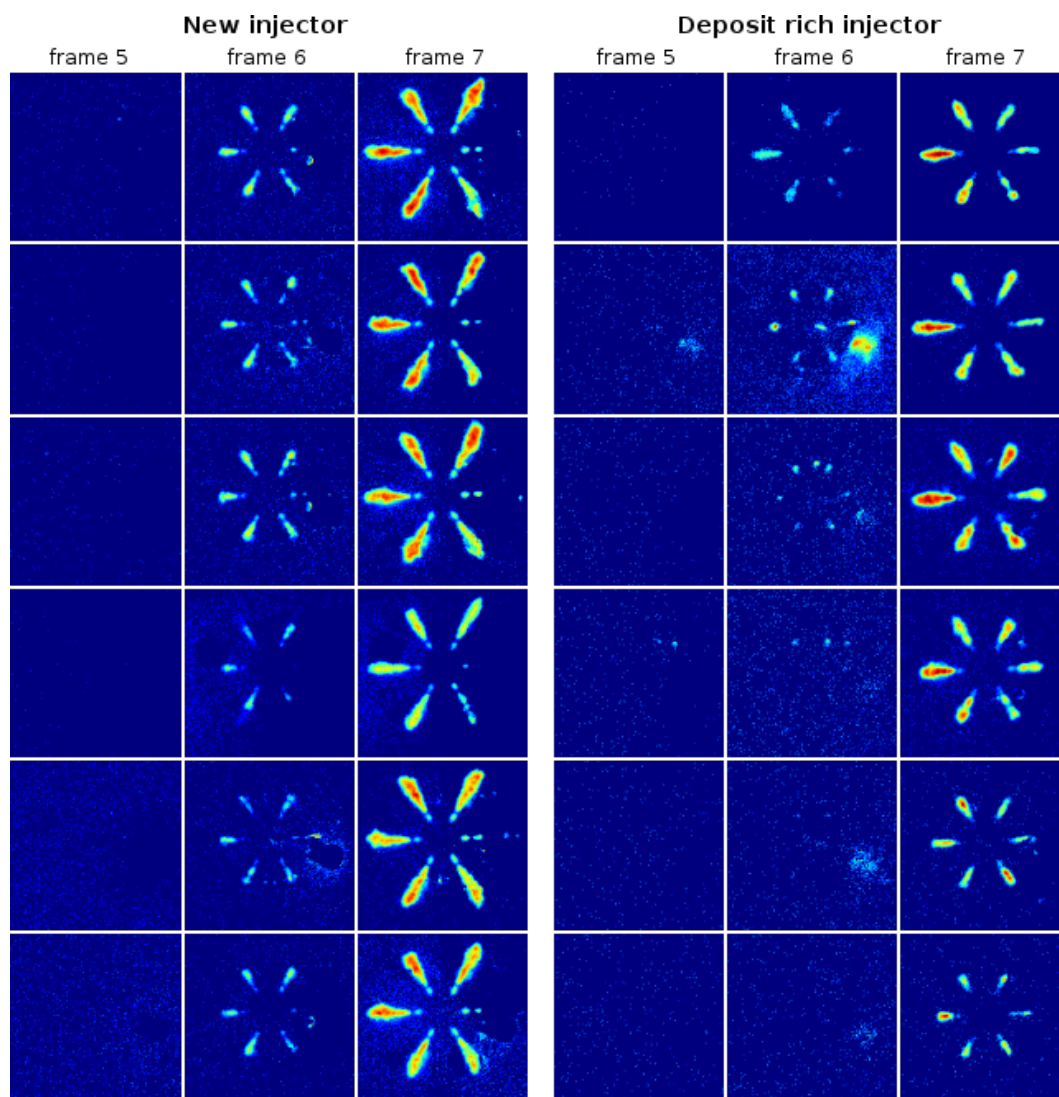


Figure 3.3.3: SOI repeatability for the new and EOL injector, injecting in water at a rail pressure of 60 MPa. Images have been partially background corrected and false-coloured for clarity, but have not been binarized. Apparent loss of the rightmost (and sometimes lower-right) spray from the new injector is the result of background corrections.

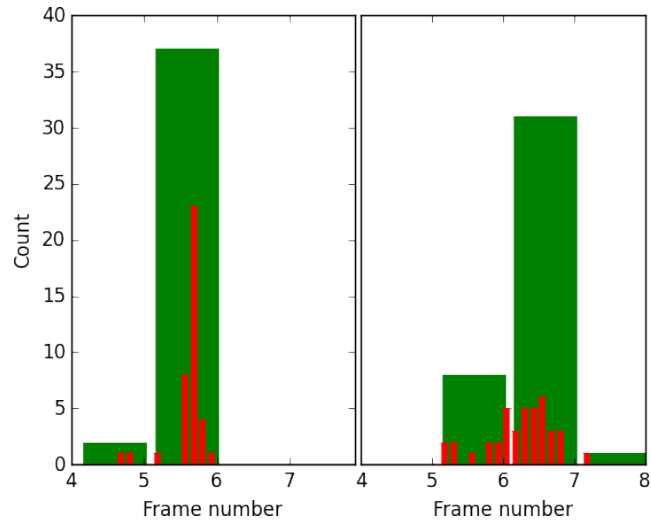


Figure 3.3.4: Determination of the frame number in which injection started, and extrapolated sub-frame time SOI. The green bars show in which frame the first occurrence of an evolving spray became apparent, where the right side of the bar has been aligned with the frame number, i.e. the tall green bar in the left figure shows that for 37 injections the spray was first visible in frame number 6. Red bars show the SOI histogram extrapolated under the assumptions as mentioned in the text, and binned into eight bins of approximately $5 \mu\text{s}$ per frame.

To quantify the observed delay in the SOI, analysis of the first occurrence of a fuel spray from all recordings was conducted. An estimate at sub-frame rate resolution of the SOI-delay was determined by considering the length of evolved sprays, assuming the early spray penetrated at a constant velocity for a given injection pressure. This assumption is strictly speaking incorrect, however for a first-order estimate it would suffice. The EOL injector showed large injection to injection fluctuations with regard to early spray evolution, and a more rigorous treatment of this data would only lead to complex calculations resulting in the same qualitative conclusion. In order to reduce calculation time and complexity only the evolution of the leftmost spray for every injection was considered, as hole to hole fluctuations for different injections from the EOL injector would not allow cross comparison of different orifices. The histogram in Figure 3.3.4 shows the results of these analyses. For the new injector nearly all (except two) injections were first visible in the sixth frame. Detailed comparison of the recorded penetrations at the beginning of the injection showed there was a slight jitter in the start of the actual fuel injection of up to $10 \mu\text{s}$, where it should be reiterated this jitter has been determined under the assumptions that the early spray penetration velocity is both constant and identical for all injections. For the EOL injector the start of injection could

occur in either frames six, seven, or (in one case) eight, and back-calculating the moment at which the injection started provided a wide range of possible SOI-times as can be seen in the right histogram in Figure 3.3.4. It should be understood that, as these determined starts of injections for the EOL injector are based on the leftmost orifice only, the actual start of *any* spray from *any* orifice will significantly impact the right histogram in Figure 3.3.4. The observed spread is expected to be reduced, and shifted towards the lower frame numbers, as including more data can shift the observed SOI only to earlier times.

3.3.3 Fuel spray cone angle determination

The fuel spray cone angle was determined for injections both in air at atmospheric conditions and in water. These two extreme backpressure densities made comparison of determined spray cone angles to existing literature impractical, however from the point of view of *analysis*, and especially error analysis, resulting spray cone angles and their evolution over time proved a useful method for identifying anomalous spray behaviour. After initial basic image clean-up (see Section 3.3.1) an edge detection algorithm provided the evolution of the spray cone edges. Assuming the spray cone edge should ideally be a straight line, the determined edges can be fitted using an orthogonal regression algorithm [80]. Subsequent fuel spray cone angle determination, including proper error propagation, will result in a list of fuel spray cone angles for all sprays from all orifices in all recordings. The ‘proper error propagation’ is an essential part of the analysis. Fuel sprays from EOL injectors produced radially expanding anomalies, which led to a departure of the assumed straight spray cone edge. Subsequent application of a linear fitting routine led to an increased error margin, and by inverting the argument it was possible to determine the occurrence and presence of off-axis anomalies by monitoring sudden increases in the standard deviations (SDs) of determined spray cone angles. An increase in the overall spray cone angle could be indicative for the occurrence of an anomaly, but an increase in the SD additionally indicated the spray edge was no longer straight, and proved a better indicator for the onset of anomalies. To clarify the procedure and analysis, Figure 3.3.5 provides a step-by-step determination of the fuel spray cone angle from a new injector. Figure 3.3.6 shows the effect of applying a linear algorithm to determine the fuel spray cone angle when a radial anomaly occurs.

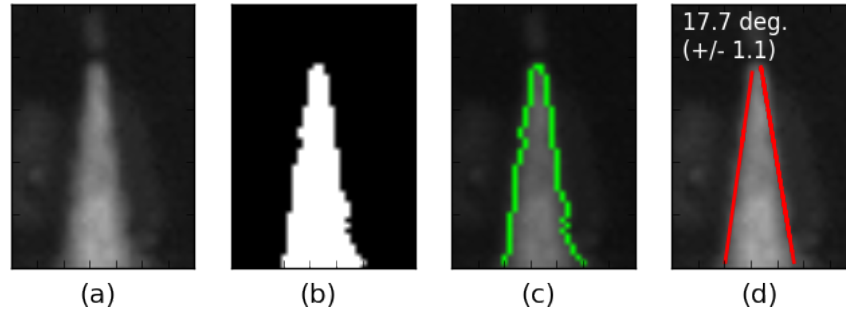


Figure 3.3.5: Spray cone angle determination for a single spray. (a) Original recording of the fuel spray injection. (b) Binarized version of the recording. (c) Spray edge determination (green), edges were detected using the `sobel` filter from SciPy. (d) The determined spray cone angle was 17.7° with a standard deviation of 1.1° . Linear fitting to the data was done with the SciPy `odr` package.

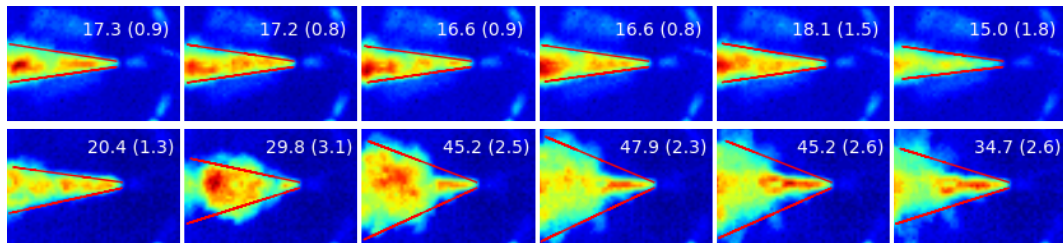


Figure 3.3.6: Application of the same algorithm as applied in Figure 3.3.5 to a spray suffering a radial expanding anomaly. Top row: Injection from the new injector with the determined spray cone angle and SD. Bottom row: Injection from the EOL injector.

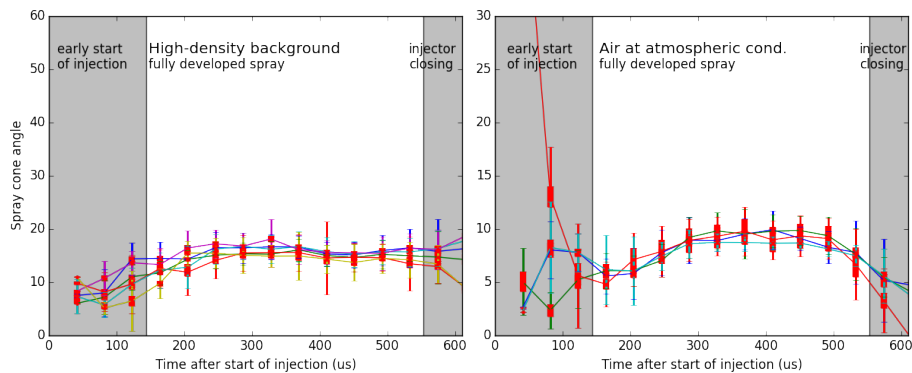


Figure 3.3.7: Determined average fuel spray cone angles for a new injector, injecting into (left) a liquid backpressure medium, or (right) free air at atmospheric conditions. Red solid error bars provide the error margins of the determined averages, thin coloured error bars show the variation in measured spray cone angles. At the start of injection, up to $150 \mu\text{s}$, the spray has not yet evolved beyond the view screen, leading to incorrect angle determinations. The rightmost graph provides the spray cone angles from four out of six orifices. The fuel sprays originating from the remaining two orifices were unsuitable for analysis.

After determination of all fuel spray cone angles from all orifices in all recordings, spray reproducibility was determined by considering the variation in spray cone angle from injection to injection. By averaging all determined fuel spray cone angles from the new injector, it became clear the new injector provided a highly stable and reproducible spray, Figure 3.3.7. All determined spray cone angles were contained within the angle interval of 13.5° to 19° , with an average angle of $15.2^\circ \pm 1.1^\circ$ when injecting into a liquid backpressure environment. The fuel spray cone angle remains highly reproducible when analysing injections into free air at atmospheric pressure, which confirms the low fuel spray cone angle fluctuations are not caused by the liquid backpressure medium. For the injections conducted into free air the determined angles for two out of six orifices have not been plotted. Due to specular reflections a significant amount of the spray had been masked out, and the remaining spray was too short to properly apply the analysis algorithm.

Comparable analysis of the data acquired from the used injector provided a less uniform spray cone angle. Anomalous bulges occurring when using the EOL injector did not always occur at the same time $aSOI$ (see Figure 3.2.4). The presence of a bulge has a severe impact on the determined spray cone angle, see Figure 3.3.6, and the onset of bulges will lead to an increase in the average spray cone angles determined from used injectors. This effect will become more severe at later times $aSOI$, as more bulges will have started evolving. Additionally, orifice to orifice fluctuations led to a less uniform spray cone angle during the early start of injection, before the first anomalies occurred. The determined fuel spray cone angle evolution from an EOL injector is provided in Figure 3.3.8, for injections both into a liquid backpressure medium and into free air.

3.3.4 First occurrence of radial expanding anomalies

The first appearances of anomalies from the individual orifices were determined for all recordings of the EOL injector. Figure 3.3.9 provides a histogram of the determined starts of radial expanding anomalies, indicating anomalies started occurring between $280 \mu s$ and $550 \mu s$ after the start of injection. Different orifices show clearly distinct histograms, indicating the occurrences of anomalies are not purely stochastic. There appears to be both a preference for bulges to start occurring at specific orifices, and a tendency for the spread in the time of occurrences to be dependant on the orifice under consideration. For example,

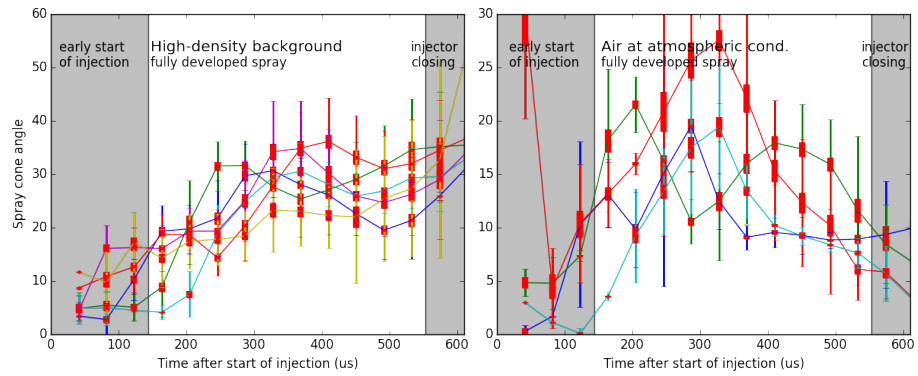


Figure 3.3.8: Determined average fuel spray cone angles for the used injector, injections into liquid (left) and 0.1 MPa air (right) backpressure media. The determined spray cone angles differ for different orifices even prior to the onset of radial bulges from $\sim 300 \mu\text{s}$ onwards. The onset of radial bulges is recognizable as a sudden increase in the variance of the determined averages in the left graph. Red solid error bars provide the standard deviations of the determined average angles, while the thin, coloured, error bars provide the accompanying variance.

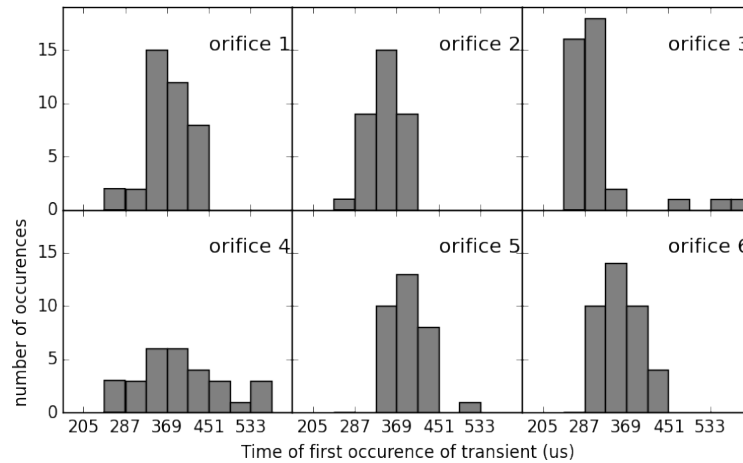


Figure 3.3.9: Determination of the start of occurrence of radial expanding anomalies for every individual orifice. Horizontal axis provides the time after the start of injection, binned in $41 \mu\text{s}$ bins equalling the recording inter-frame time. Vertical axis provides absolute occurrence counts for the determined start-of-anomaly time. Not every orifice would suffer a radial expanding anomaly for every injection, and total recorded amount of anomalies can differ from orifice to orifice. The earliest anomalies occur $240 \mu\text{s}$ *aSOI* (orifices 2, 3 and 4), while the most retarded anomalies appear $575 \mu\text{s}$ *aSOI* (orifice 3).

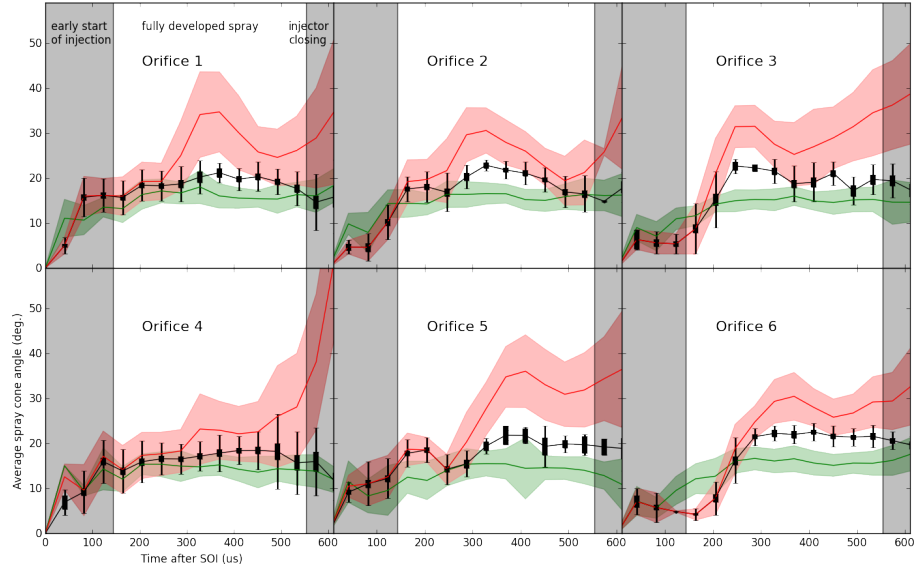


Figure 3.3.10: Determined average spray cone angles from individual orifices of a used injector, after rejection of all data in which anomalous radial expansions occurred. The light green band provides the average spray cone angles (with spread) determined for a new injector, the light red band shows the enveloped average angles determined from the EOL injector if transient anomalies are not filtered out.

most bulges occurred at *orifice 3* before $320\ \mu\text{s}$ *aSOI*, whilst for *orifice 5* all anomalies occurred $320\ \mu\text{s}$ or more *aSOI*. *Orifice 3* in Figure 3.3.9 provides a slim histogram, indicating good reproducibility of the time *aSOI* at which bulges occur, whilst *orifice 4* produced a nearly flat histogram, showing no preference regarding the onset of bulges.

Having determined the onset of bulges for every individual recorded injection and orifice, Figure 3.3.8 can be corrected by truncating data whenever an anomaly has occurred. Re-determination of the spray cone angle evolution from the EOL injector then provides trends suitable for comparison to the spray cone angle evolution from the new injector. Figure 3.3.10 provides the spray cone angle evolution from the used injector, calculated in a similar fashion as for Figures 3.3.7 and 3.3.8, using datasets that have been truncated when radial anomalies started occurring. For clarity the data for every individual orifice has been plotted in a separate graph, and the average spray cone angles determined from a new injector were added for comparison. As can be seen in Figure 3.3.10 orifice to orifice variations in the spray cone angles remain present, and the evolution differs from the angles determined from a new injector. The variance in the determined spray cone angle for a used injector, after rejecting anomalies, is comparable to that of the new injector which indi-

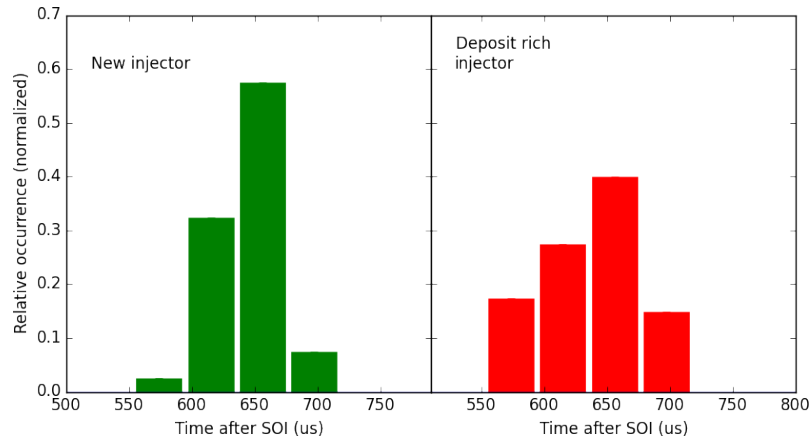


Figure 3.3.11: Histogram of the time of EOI, providing a measure of EOI-reproducibility. The histograms show the relative occurrences of the observed end of injection time with respect to the time after the programmed start of injection, binned in 41 μs intervals.

cates injection to injection reproducibility has become of the same order. The average spray cone angle from a used injector tends to be slightly higher than from a new injector after correcting for the anomalies, the graphs remain on the upper side (or above) the green band in Figure 3.3.10.

3.3.5 Variations in the end of injection

The end of injection was studied to determine if there was jitter present upon termination of the injection, comparable to the spread in the start of injection treated in Section 3.3.2. By defining an injection as ended when the spray was no longer connected to the injecting orifice, the time at which a fuel injection ceased was determined for both new and used injector. The EOI depends solely on the termination of the solenoid current and subsequent internal mechanical actions, and correction for the jitter in the start of injection was not required. The controller unit terminated the driver current at a fixed time ($\pm 0.5 \mu\text{s}$) with respect to the triggering of both LED and camera, irrespective of any earlier transients. Any inconsistencies in the time of EOI were therefore the result of internal injector dynamics. Figure 3.3.11 provides a histogram of the determined EOIs, providing horizontally the time with respect to the *programmed* start of injection (*pSOI*), related to the triggering of the injector driver unit. The left histogram shows injections from the new injector predominantly (>90%) ended at 600 μs to 680 μs after SOI, with a slight overshoot on either side of the main two peaks. The right histogram in Figure 3.3.11 indicates EOI of the EOL injector was less reproducible, providing a flattened

distribution where in the same time interval of 600 μs to 680 μs *aSOI* slightly less than 70% of the injections ended. The spread in the EOI was for both injectors contained within four frames, corresponding to a maximum time interval of 164 μs . The most notable difference between the results for the two injectors in Figure 3.3.11, was the relative flatness of the right histogram. This flatness indicated the used injector *on average* suffered more jitter at EOI than the new injector, whereas the more Gaussian shape of the histogram for the new injector indicated the new injector provided a higher reproducibility of the time at which the injection ended.

3.4 Discussion of the results

The investigation showed several interesting phenomena, however there were some drawbacks of the method applied and injectors used in this initial investigation. Resolving several of the shortcomings of the research presented so far was the starting point for the research as treated in the next chapter. The main discussion points regarding the relevance of the observed effects are treated in this section, divided into several subsections.

3.4.1 Injectors

The injectors used in this investigation were all EOL injectors acquired from a servicing station. Although mechanically and electrically the injectors were still in working condition, it is not known if internal wear and deposits were indeed the main cause of the observed anomalies. All injectors clearly showed the presence of carbonaceous deposits, but none of the injectors was dismantled in order to thoroughly check the internals. This point has been addressed by conducting further research on injectors which were acquired from passenger cars at mileage intervals well within the expected life time of the injectors. In the subsequent chapter the injectors investigated were all still in working conditions, and were acquired from cars that had driven approximately 30.000, 60.000 and 90.000 miles. The new batch of used injectors showed comparable behaviour as treated in this chapter, and as these injectors (especially the 30k-miles ones) are expected to be relatively free of wear, it was concluded the observed anomalies were the result of the presence of deposits in/on the injectors. Other injector issues degrading spray quality can however not be excluded in this spray investigation under extreme backpressure conditions.

3.4.2 Liquid backpressure medium

The majority of the experimental data was acquired by recording the fuel spray evolution when injecting into a liquid backpressure medium. Needless to say, this is not a realistic condition for a combusting diesel spray and comparison of any observations to sprays as measured inside an optically accessible engine are at least complicated by the choice of this backpressure environment. Injection into a high temperature, high pressure gaseous medium would represent a realistic injection condition, but then some of the observations done in this chapter are expected to disappear. For example, the radial expanding anomalies consist of very small amounts of fuel in an atomized state, and these bulges are expected to quickly evaporate under engine-like conditions. Measurement of the fuel spray evolution in a more realistic environment was considered essential for verification of the significance of the observed effects as reported here. To this end subsequent tests were done inside a CVC and injections were conducted into a pressurized gaseous background, with the temperature kept sufficiently low to prevent rapid evaporation of the atomized droplets. These measurements are treated in the next chapter.

3.4.3 Numerical data

This chapter provided primarily a qualitative treatment of the impact of injector age on fuel spray evolution. Although some numerical data was provided regarding spray cone angles measured from the new injector when applied in different backpressures, no comparable figures were presented regarding the EOL injector. (nearly) All comparisons were done by comparing different graphs or histograms, where often the direction of the trend line and the relative size of the variance was used to motivate conclusions, avoiding numerical conclusions where possible. The numerical determinations were deliberately omitted for several reasons, of which the most important considerations were:

- The orifice to orifice variations of the fuel spray evolution for the used injector was large. Calculations and averaging would have resulted in numerical results for the spray cone angle, start of injection time, and end of injection time for a used injector that *could* be numerically compared to a new injector. When taking the individual orifices and the corresponding spread in the averaged numbers into consideration, this

would result in the conclusion the comparison should be considered for its qualitative nature only, defying the point of determining numerical values.

- Radially expanding transients provided a static or slow-evolving distortion of the spray cone shape, and the resulting fuel spray could no longer be treated as a classical, straight-edged, and rapid evolving injection. The notion of ‘fuel spray cone angle’ loses part of its significance under these conditions, and the main reason for determining the fuel spray cone angle was to analyse the accompanying error margins in the spray cone angles, *precisely because* the determination of an angle will generate erroneous results for transient-rich sprays. The accompanying error margin was a significant bit of information and was required, together with the spray cone angle, to determine if a deviation from a straight-edged fuel spray cone did occur.
- In the subsequent chapter, results from an investigation under more realistic backpressure conditions are treated. An extensive determination and comparison of data acquired in this chapter seemed disproportionate, considering the end result would most likely be suitable only for qualitative comparisons.

For the purpose of comparison *within the data generated in this investigation*, numerical results are provided in Table 3.3 to allow qualitative comparison of the behaviour of the new and the EOL injector in high density environments. This data is, for the reasons stated above, deliberately not included elsewhere in this chapter.

The standard deviations (SDs) reported in Table 3.3 reflect a combined effect of different uncertainties. Uncertainties in determined spray cone angles can arise from several causes, and upon calculation of overall error margins, the combined effect of all errors should be accounted for. In the present investigation the limiting camera resolution and slight mismatches in the focal and injection planes, see Figure 3.2.1 (d) for an extreme example, were the main contributors to uncertainties in individually determined spray cone angles. The limited camera resolution was responsible for a typical error of 1.1° , the plane mismatch would lead to an additional error of at most 0.13° . Upon averaging *all* spray cone angle data, the combined contribution of these two uncertainties will be approximately 0.22° . The measured SD for the new injector is 1.1° ,

Parameter	New injector	EOL injector
Occurrence of SOI		
- Frame number	5 or 6	6 to 8
- Sub-frame extrapolation	351 μs ($\pm 9 \mu\text{s}$)	376 μs ($\pm 19 \mu\text{s}$)
Occurrence of EOI after SOI		
- Frame number	14 to 17	14 to 17
- Time estimate	644 μs ($\pm 26 \mu\text{s}$)	637 μs ($\pm 39 \mu\text{s}$)
Average fuel spray cone angle		
- Complete injection	15.2° ($\pm 1.1^\circ$)	26° ($\pm 6^\circ$)
- Before onset of transients	-	21° ($\pm 6^\circ$)
- Complete injection, truncated data	-	19.2° ($\pm 2.9^\circ$)
Average fuel spray cone angle for injection in air	7.5° ($\pm 1.1^\circ$)	16.3° ($\pm 4.9^\circ$)

Table 3.3: Numerical results acquired from the investigation as presented in this chapter. Data refers to injections into a liquid backpressure medium, except for the last row where the average spray cone angle is provided for injections into atmospheric air.

indicating a 1.0° uncertainty will be the result of injection to injection variations. For the end of life injector, the camera resolution and plane mismatches led to the same error contributions, indicating the reported SDs of 6° and 2.9° were primarily caused, $>5.9^\circ$ and $>2.8^\circ$ respectively, by injection to injection variations.

3.5 Conclusion

Without analysis of spray characteristics of the used injector inside a real, firing, diesel engine it is not possible to determine the effect deposits and wear have on combustion. Considering the clearly observed anomalous behaviour of used injectors it is reasonable to state some preliminary conclusions based on the observations as noted in this chapter. It was shown in Figure 3.2.2 *all* EOL injectors suffered anomalous spray evolutions after the start of injection. By recording the spray evolution when injecting into a liquid backpressure environment, the formation of transient anomalies, recognizable as off-axis bulging, became apparent. If these radial expanding anomalies persist when injecting into a compressed gaseous background, comparable to conditions inside an engine, it is expected combustion is at least qualitatively influenced by alteration of the air entrainment. For one specific injector an analysis of the observed effects has been provided, and subsequently compared to the observed spray pattern from a new, same type, injector. The main conclusions related to fuel

spray evolution, based on the observations discussed in this chapter, consist of:

- Different orifices of an EOL injector produce different early spray shapes, and the observed differences can be consistent over several injections. This can be seen in Figure 3.3.8, by looking at the leftmost data points in the graph. Different orifices provide very different early spray cone angles, but the variance in the measure data indicates a high reproducibility of the individual early spray cone angles.
- Used injectors produce radially expanding anomalies during the early stage of fuel injection. Participating orifices, time of occurrence, and total width of these anomalies are not constant from injection to injection. Figure 3.2.2 provides a selection of recordings of radial anomalies, measured from different EOL injectors. The effect these anomalies have on the evolution of the fuel spray cone angle is provided in Figure 3.3.8.
- Observed transients are not caused by the application of a liquid backpressure medium, as none of the observed effects remained present when a new injector was used in a liquid backpressure medium.
- *In general* the EOL injector provided a fuel spray that deviated both in shape and evolution from the fuel spray recorded from a new injector.

It is not possible to draw firm conclusions on the effects these transients have on combustion quality, but several reasonable predictions can be made based on the observed effects. It is *expected*⁷ these anomalies can lead to the following unwelcome fuel spray alterations inside a firing engine, affecting combustion quality:

- *Suboptimal fuel-air mixing* - Although an altered fuel spray does not necessarily lead to a reduced air entrainment in itself, modern cylinder-injector combinations are co-designed based on the assumption the injected spray resembles a straight, uninterrupted fuel spray cone with a fixed spray width and penetration. Any occurrence of radial anomalies will temporarily alter the air entrainment process, and a change in fuel-air mixing can occur. Considering the level of sophistication involved

⁷This can not be stressed enough. I *definitely did not* observe any of the stated expectations, but I consider these expectations to be quite reasonable, based on the observations done up to this point. But they remain '*guesstimates*'.

in the design of injector and cylinder, it is assumed any alteration in fuel–air mixing is deemed to lead to a reduced combustion quality.

- *Temporally reduced spray penetration* - When a radially expanding transient occurs, momentum conservation dictates the axial momentum must be temporarily reduced to redirect kinetic energy to allow the radial expansion to occur in the first place. This is not a permanent condition, and the initial spray penetration is expected to fluctuate as a result of these anomalies.
- *Local rich mixture/combustion* - Any radial, off-axis, fuel mass flow redirects the corresponding atomized (and evaporating) fuel droplets out of the main fuel injection path. Further air entrainment and mixing is not augmented by back-impingement from the continued fuel injection, and lack of mixing can locally lead to relative rich fuel–air mixtures. This effect is not expected to be of major importance at low backpressures, as injection into air at 0.1 MPa (Figure 3.2.5) shows the forward velocity of radial anomalies is still significant. At higher backpressures the axial momentum *might* become too low during radial expansion to allow sufficient air entrainment. In the extreme case of injection into a liquid backpressure medium radial anomalies remain stationary at close proximity to the nozzle, an example of which can be seen in the fourth row in Figure 3.2.3 where the small (red arrow indicated) sideways expansion of the atomized fuel cloud remains stationary.

Chapter 4

Characterising sprays from used injectors in a high-pressure constant volume chamber

In the wake of the observed anomalies and transients reported in Chapter 3, a new experimental set-up was designed and commissioned to determine the prevalence of these observations when measuring in an engine-like environment. This required a heated and pressurized gaseous backpressure medium, and the liquid container was replaced with a constant volume chamber (CVC) that would allow ambient pressures up to 8.0 MPa for continuous operation, and peak pressures up to 12.0 MPa for short-lasting, pulsed operation. In addition thirteen more injectors were acquired, all with identical nozzles. The newly acquired injectors were provided by servicing stations, and were removed from passenger cars during routine maintenance. These injectors offered the unique possibility of studying the effect on fuel spray evolution of ‘naturally grown’ deposits and wear from normal on-road use of production injectors.

Apart from these two major modifications, a new injection chamber and thirteen same injectors, the rationale of this additional study was the same as for the high ambient density investigation treated in the previous chapter. The spray shape evolution of fuel injections were studied, a comparison of new versus used injectors was done and the appearance of transient anomalies was studied. The new measurements were done under more realistic conditions and the application of new camera systems allowed for an increased temporal and spatial resolution. The results provided new insights in the effects prolonged on-road usage of injectors has on the evolution of fuel sprays.

The present chapter first treats the improved experimental set-up, followed by a treatment of the two main measurement series, in turn followed by analysis of the observed differences in fuel spray evolutions between new and used injectors. The resulting conclusions and observations are treated in the final two sections of this chapter. Chapter 5 will compare the observations done in this investigation to literature, incorporating part of the results attained in Chapter 3.

Part of the observations and analysis treated in this chapter proved suitable for publication, and additional results have been published in a conference proceeding. To prevent numerous self-referencing in this chapter, the articles are referenced to at this point and will not be referred to further in the text. Part of the results as presented in Sections 4.3.1 and 4.3.2 have been published in [82]. Observations presented in Section 4.3.5 have been presented at the IMECHE ICE2015 Conference [83], extended results have been published in [84].

4.1 Experimental set-up

The main changes of the set-up w.r.t. the set-up described in Section 3.1 consisted of the application of a CVC and the replacement of the high speed camera by better cameras. Based on the new requirements for the experimental conditions some of the existing apparatuses were tuned or modified to allow more control over the experimental parameters. Although the new operating conditions provided very different results, the basic working of the set-up remained unaltered. Diesel fuel, fed from a common rail to an injector, is injected into a high density ambient environment. By synchronizing illumination and the start of recording with the moment of injection, time resolved recordings were acquired of fuel injection events, and the spray evolution was studied close to the nozzle.

Two main measurement series were conducted in the CVC. Most measurements (*series 2*, based on chronology) were continued along the same line as in the liquid backpressure investigation, illuminating with a green high powered LED in a front lit configuration, and using the same ATtiny-based controller for synchronizing purposes. Prior to this measurement series, the very early spray evolution was studied with the help of a highly specialized SIM16 imaging system (measurement *series 1*). For this system, capable of recording up

to 200 million frames per second, timing and recording conditions proved too challenging for the basic controller and LED. An additional light source was incorporated and part of the control tree was covered by the camera hardware.

Table 4.1 provides a list of all applied materials for both measurement series and Figure 4.1.1 provides a schematic of the experimental set-up. A detailed description of the main apparatuses used in this research is provided in the following sections, descriptions of systems already treated in the previous chapter have been reduced.

4.1.1 Fuel pump and common rail

Apart from replacing the fuel filter every few months, no alteration had been applied to the fuel rig itself, see Section 3.1.1 for further details on the fuel system. The fuel used in this investigation was an EN590-compliant diesel fuel, specifications are provided in Table 4.1. The injection pressures applied in the experiments in this chapter were varied over a broader range, varying from 60.0 MPa to 150.0 MPa. An overview of the applied injection pressures for both measurement series will be provided in Section 4.1.3, Table 4.3.

4.1.2 Injector driver and injectors

For control of the injectors studied in this investigation the same injector driver was used as in the previous chapter, see Section 3.1.2. The injection durations were varied more throughout this part of the investigation. There was no additional alteration of the driver required, as any change in injection duration or repetition was achieved by changing the TTL control signal.

The injectors studied in this investigation were acquired from a servicing company that additionally provided the mileage and maintenance history of the used, deposit rich injectors. Injectors were taken from passenger cars and were assumed to have been used for all kinds of normal daily driving (i.e. commuting, shopping, etc.). All the injectors clearly showed deposits at the nozzle tip. These injectors were *not* EOL injectors, and the injectors showed no signs of excessive wear, were not removed for a lack of drive-ability of the vehicles, and were not in any other way faulty. It was therefore expected the used injectors would not produce as clearly distinct sprays as observed in the initial project. These injectors were real-world injectors at different mileages and different levels of spray degradation was expected for different

Material	Brand, type number
Fuel filter	FFR-G12P In line Filter (20 μm)
Fuel pump	PowerSTAR 4 P4333EVN
Fuel	EN590 compliant
- Density	830 kg m^{-3}
- Cetane number	52
- Viscosity	3.4 $\text{mm}^2 \text{s}^{-1}$
Common rail	4-injector light duty CR, maximum rail pressure 150 MPa
CR pressure gauge	Hi-Pro 104482, 0-250 MPa
Injectors	13 pcs. see Table 4.2
Injector driver	Hartridge
Pressure chamber	In-house designed CVC
- Volume	1.8 dm^3
- Working pressure	8.0 MPa cont, 12.0 MPa peak, pulsed
- Ambient gases	Any mix of C_2H_2 , H_2 , air, oxygen-free N_2
- Working temperature	Up to 145 $^\circ\text{C}$ electrically heated, up to 1550 K by pre-combustion
- Pressure sensor	Kistler 4005B
Pulse/delay generator	In-house built timing and control units
- Micro-controller	ATMEL ATtiny13-20PU (9.6 MHz), ATtiny26-16PU (1-10 MHz)
<i>Measurement series 1</i>	
Camera system	SIM16 Specialised Imaging
- Sensor	16 individual ICCD's, $1280 \times 960 \text{ px}^2$
- Lens	Nikon 24–85 mm, augmented by additional $f=300 \text{ mm}$, $d=101.6 \text{ mm}$ lens
Illumination source	$2 \times 500 \text{ J}$ discharge lamp
- Wavelength	Full-spectral, IR to (soft)UV
- Control	Through camera system
<i>Measurement series 2</i>	
Camera system	Photron SA-X2 colour camera
- Sensor	CMOS, $1024 \times 1024 \text{ px}^2$
- Lens	Tokina $f=100 \text{ mm}$
Illumination source	Phlatlight CBT-120-G, green high power LED
- Central wavelength	521 nm
- FWHM	40 nm
- Driver board	Luminus Devices, DK-136M-1

Table 4.1: Details of materials used in the experimental set-up for measurements in the CVC.

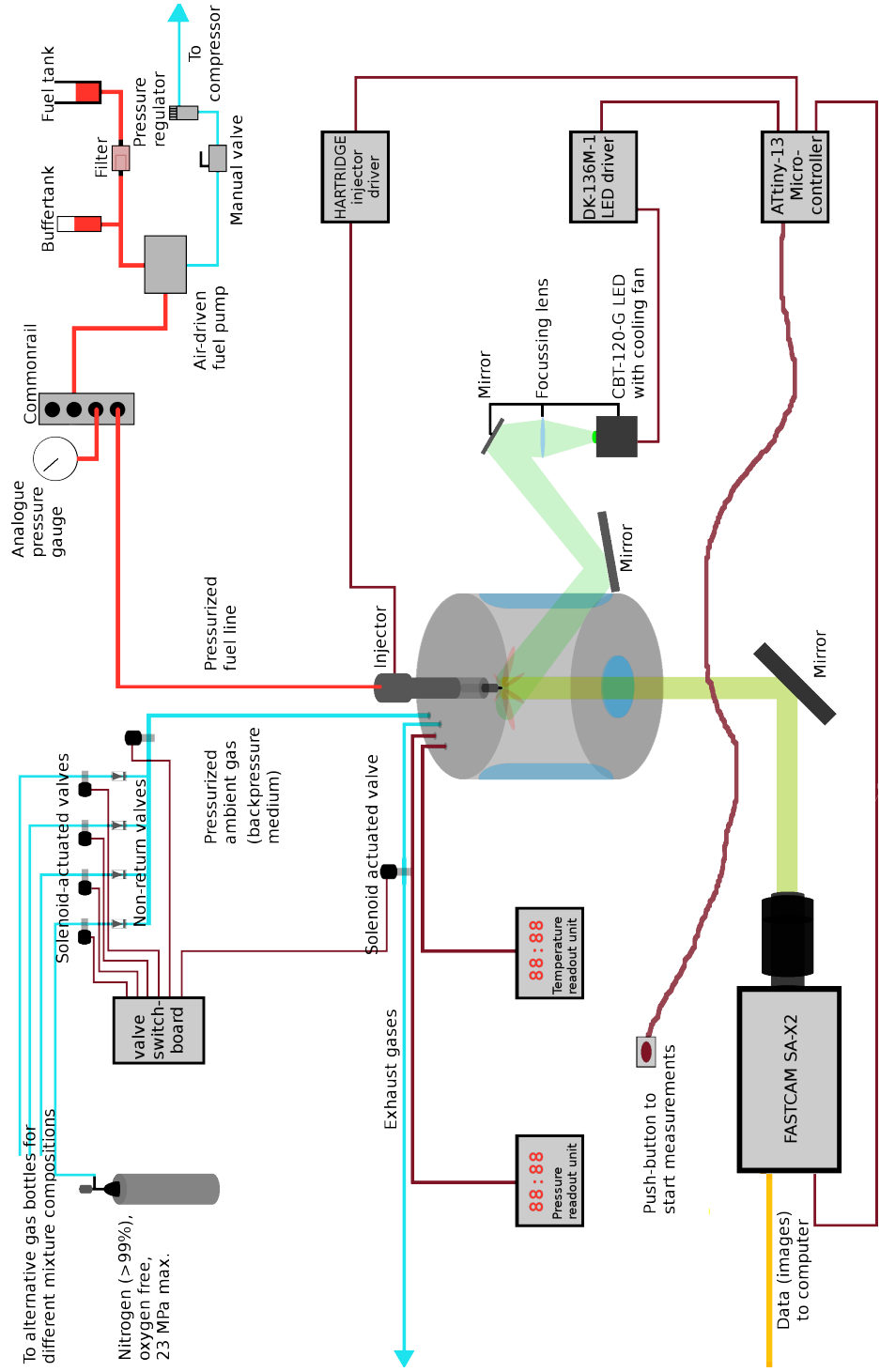


Figure 4.1.1: Schematic of the modified experimental set-up, as used for measurement *series 2*. For the *series 1* measurements, the camera was replaced with the SIM16 camera, the LED was replaced by two flash heads, and the single focussing lens for the LED was removed. A schematic of the relevant alterations of the set-up applied for *series 1* is provided in Figure 4.1.3.

Nozzle characteristics	
Investigated nozzles	13 pcs. total, all identical nozzle numbers
- New	(<i>New</i>) 2 pcs. brand new, unused
- 30k	(<i>Set 1</i>) 4 pcs. removed at 30021 miles
- 60k	(<i>Set 2</i>) 4 pcs. removed at 62856 miles, received after market cleaning agent at 30000 miles.
- 90k	(<i>Set 3</i>) 3 pcs. removed at 92316 miles,
Nozzle type	6-orifice SAC nozzles
Orifice	Rounded orifice inlet
- length	0.98 ± 0.05 mm
- inlet diameter	178 ± 4 μ m
- middle diameter	155 ± 5 μ m
- outlet diameter	142 ± 2 μ m

Table 4.2: Technical specifications of the injector nozzles investigated in this work.

aged injectors. Apart from three sets of used injectors, two new injectors were acquired for comparison.

The used injectors all came from the same car/engine type, were all common rail, six-orifice injectors, and were divided into four batches based on mileage. The injectors were all fully interchangeable but two different type numbers occurred in the injector batches. Three injector batches ended with a recent type number and one batch ended with an older designator. The old-type injectors had been superseded by the newer type as of 2008, and engines serviced after 2008 would have the injectors replaced by the newer type if the injectors needed replacement. This was in line with the observation that the highest mileage injector batch came from a pre-2008 vehicle, which never had the injectors removed or replaced. The nozzle type numbers were identical for all injectors, i.e. both old and recent injector types incorporated nozzles with identical SAC configurations. The internal geometry of the nozzles from the two different injector type numbers was confirmed to be identical by making silicone moulds of several nozzles, and comparing the internal nozzle geometries, determined by SEM. The injector needles and solenoid valve systems were also closely studied, and no differences were found between the two different injector type numbers. It was therefore assumed the different type numbers were introduced for administrative purposes and do not reflect a change in the workings of the injectors. Details on the orifice geometries of the nozzles used in this research are provided in Table 4.2.

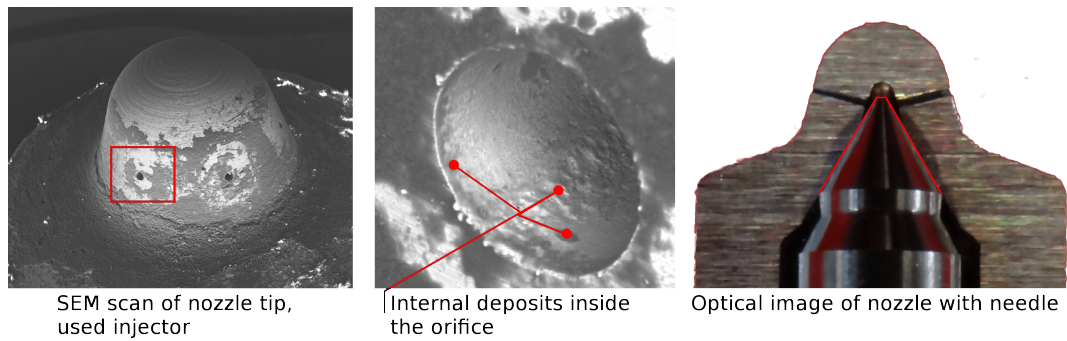


Figure 4.1.2: SEM and optical images of a used injector. Red square in the first image indicates the orifice of which a magnified view is provided in the second image. The magnified view in the middle image clearly shows the presence of deposits inside the injector orifice. The axial structure (middle red dot) has been confirmed to be a carbonaceous deposit. Third image provides an optical image of a cut injector nozzle, with the needle reinserted. Red lines in last image have been added to indicate the edge of the needle.

Figure 4.1.2 shows a SEM image of the tip of one of the *Set 1* nozzles studied in this work, alongside an optical image of a cut injector nozzle with needle. The SEM image clearly shows the presence of deposits both at the tip of the injector and inside the orifice. Analysis of the composition of the deposits showed the deposits consisted primarily of carbon.

As can be seen in Table 4.2, the *Set 2* injectors had received an after-market cleaning agent at approximately 30,000 miles. The impact of this cleaning agent on injector behaviour was *a priori* unknown, however two extreme cases can readily be imagined. If the cleaning agent was *perfect*, the injection characteristics of the *Set 2* injectors should be the same as those from the *Set 1* injectors, assuming the 60,000 mile injectors had been cleaned to an as-good-as-new state and subsequently been used for 32,000 miles. The other extreme case is the situation in which the cleaning agent had *no effect* on deposits present at the nozzle tip. In the latter case, the *Set 2* injectors should produce sprays and anomalies that would resemble something in between the behaviours of the *Set 1* and *Set 3* injector groups. It was expected the actual behaviour of the injectors would be in between those two extreme cases. Without extensive knowledge on the detailed working of the cleaning agent it is however not possible to estimate the effect of the cleaning agent on the deposits that were present at 30,000 miles.

4.1.3 High speed cameras

Two different high speed recording systems were utilized for the two different measurement sets recorded in this stage of the research. In the first stage, *series 1*, the very early start of the fuel spray was investigated and the recordings were done with a highly specialised SIM16 recording system. In the second stage, *series 2*, the complete fuel spray evolution was recorded at a reduced frame rate and magnification with a FASTCAM SA-X2 camera system.

4.1.3.1 Specialised Imaging System, SIM16

For the recording of the near-nozzle initial spray evolution (*series 1*) an ultra high frame rate Specialized Imaging System SIM16 was borrowed from the EPSRC Engineering and Instrumentation Pool. The SIM16 system consisted of sixteen individual ICCD sensors aligned along the same optical axis, allowing the user to take sixteen images of the same object, with a highly flexible programmable time delay. With a minimal time resolution of 5 ns, a theoretical frame rate of 200 million frames per second is possible, but at a maximum of sixteen frames only. The ICCD sensors were individual sensor arrays and the system recorded at the full¹ CCD resolution of $1280 \times 960 \text{ px}^2$ irrespective of the frame rate. The initial spray evolution was recorded at a much lower frame rate than the maximum of 200 million fps. The main reason for application of such a high end system was the capability of maintaining full resolution irrespective of frame rate. Sprays evolved from six orifices simultaneously and moved in different directions. Recording all sprays to a sufficient resolution required a CCD with a high total pixel count to provide sufficient spatial resolution at every orifice to determine changes in the evolving fuel sprays.

The level of control the SIM16 system provided regarding timing, delay, and external triggering on a nanosecond time-scale made it appropriate to use the SIM16 as the primary controller, driving the ATtiny control unit as a secondary controller. Figure 4.1.3 depicts the changes in the experimental set-up with respect to the camera, controller, and illumination source used.

¹The physical CCD size was $1360 \times 1024 \text{ px}^2$. The outer border of the CCD's was used for alignment corrections, reducing the effective image size to $1280 \times 960 \text{ px}^2$. This was a fixed setting and could not be altered.

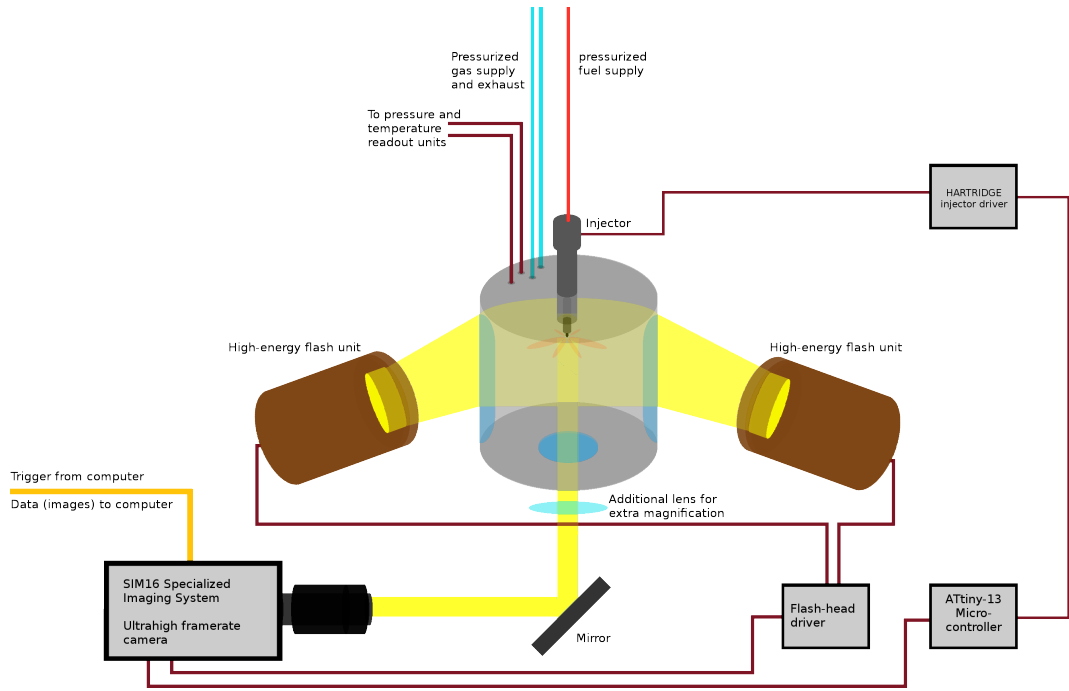


Figure 4.1.3: Changes in the experimental set-up with respect to the set-up treated in Section 4.1, Figure 4.1.1. Note the ATtiny controller now only drives the injector driver, based on input triggers from the SIM16 system.

Settings	<i>Series 1</i>	<i>Series 2</i>
Camera	SIM16	FASTCAM SA-X2
- Frame rate	200, $66\frac{2}{3}$, $33\frac{1}{3}$ kfps	45 kfps
- Sensor area	1280×960 px ²	512×512 px ²
- Imaged area	21×16 , 44×33 mm ²	30×30 , 39×39 mm ²
- Image scale	16.6, 34.7 μ m/px	59, 77 μ m/px
- Shutter time	0.1 μ s	5.0, 2.5, 1.25 μ s
Injection pressure	60.0 MPa	60.0 MPa to 150.0 MPa
- Duration	770 μ s	1.3, 1.5 ms
Ambient pressure	3.0 MPa to 3.1 MPa	3.2 MPa to 3.4 MPa
- Temperature	104 $^{\circ}$ C to 112 $^{\circ}$ C	114 $^{\circ}$ C to 119 $^{\circ}$ C
Investigated injectors	<i>New, Set 1, Set 2</i>	<i>New, Set 1, Set 2, Set 3</i>

Table 4.3: Applied recording and injection conditions.

A Nikon 24–85 mm f=2.8 zoom lens was fitted to the camera and an additional large 101.6 mm diameter lens could be fitted between camera and CVC for enhanced magnifications. Frame rates varied depending on the aspects studied, see Table 4.3, from 200 000 fps to 33 333 fps with the exposure held constant at 0.1 μ s for every recording. At this short exposure, the LED light source provided insufficient illumination power without driving the LED beyond its (factory-default) safe operation current regime. The LED would allow

pulsed operation at much higher current densities with a purpose-built power supply [77], possibly providing sufficient illumination power in the present experiments. The SIM16 camera system was however provided with an additional set of high power flash heads designed for use in combination with the SIM16. Designing and building a purpose-built driver unit for the LED was therefore deemed disproportionate.

4.1.3.2 Photron Fastcam SA-X2

Recording the full spray evolution (*series 2*), requiring more than 16 consecutive frames, was done with a Photron FASTCAM SA-X2 camera. The FASTCAM SA-X2 camera incorporated a colour CMOS chip that allowed recording at $1024 \times 1024 \text{ px}^2$ up to 12 500 fps and higher frame rates were possible at a reduced resolution, up to a maximum frame rate of 480 000 fps at $128 \times 48 \text{ px}^2$. Initial tests with frame rates and resolutions indicated the optimal setting for most experiments would be a recording frame rate of 45 000 fps at a resolution of $512 \times 512 \text{ px}^2$. The shutter time was varied from $1.25 \mu\text{s}$ to $5.0 \mu\text{s}$, depending on magnification. The camera was fitted with a Tokina 100.0 mm lens. Details on the camera settings and applied injection pressures are provided in Table 4.3.

4.1.4 Illumination source

Apart from the flash heads mentioned in 4.1.3.1 when recording with the SIM16 system, illumination was provided by the same LED and driver boards as discussed in Section 3.1.4. For all measurements, the LED was operated in a ‘locally CW’ mode, switched on prior to the start of an injection and maintained on for a total duration of 2.6 ms, lasting up to 1 ms after the end of fuel injection to capture all relevant aspects of the fuel spray evolution. The higher sensitivity of the FASTCAM camera with respect to the MIRO4 camera used in the pilot research made a pulse driven high-current operation mode unnecessary.

4.1.5 Control and Timing

For measurement *series 2*, recorded with the FASTCAM camera, timing and control was provided by the ATtiny13-based controller unit discussed in Section 3.1.5. The controller was programmed to generate output trigger signals

corresponding to the *mode 2* operation depicted in Figure 3.1.2, as pulsed operation of the LED was no longer required. The duration of the injection was varied depending on the aspect studied, and injection durations are listed in Table 4.3. For the reduced injection duration of 1.3 ms the illumination time was deliberately kept unchanged at 2.6 ms to allow studying post-injection expulsions of ligaments and droplets.

4.1.6 The constant volume chamber

The main difference between the set-up used for measuring injections into a liquid backpressure environment, and the set-up used for the study in this chapter, was the incorporation of a constant volume chamber (CVC) that allowed the use of a compressed and heated gaseous environment. The CVC was designed by a group of Master students at the *Brunel School of Engineering and Design*, a detailed description is provided in [85] as *Design 5*. The CVC is treated here to a sufficient degree to understand the possibilities and limitations of the system, and the peripherals required to operate the CVC will be discussed.

The CVC consisted of a stainless steel cylinder with four view ports along the cylinder wall and one view port in the bottom of the cylinder. One of the four ports was fitted with a steel flange and was used for gas inlet and outlet. The top face of the cylinder contained a water cooled injector seating. The injector seated in the CVC at the top face incorporated a multi-orifice nozzle, and the sprays were ejected radially outward from the centre of the top flange. Imaging was done from the bottom window, illumination from the windows along the side of the cylindrical body of the CVC. The total inner volume of the CVC was approximately 1.8 l, cylindrically shaped with a diameter of 130 mm and height of 135 mm. Due to the finite sizes of the windows, the available visible and illuminable volume for experiments was a cylinder of roughly 70 mm diameter and total height of 110 mm. A photograph showing the inlet manifold, injector seat, and one view port is provided alongside an isometric rendered view of the CVC in Figure 4.1.4.

Windows applied in the CVC were made from UV-grade fused silica, allowing future use of UV LASERS or LEDs for fluorescence imaging. To prevent condensation of diesel vapour on the windows during operation, the body and windows of the CVC were maintained at a minimum temperature of 110 °C by the application of eight cartridge heaters in the CVC body. For four of

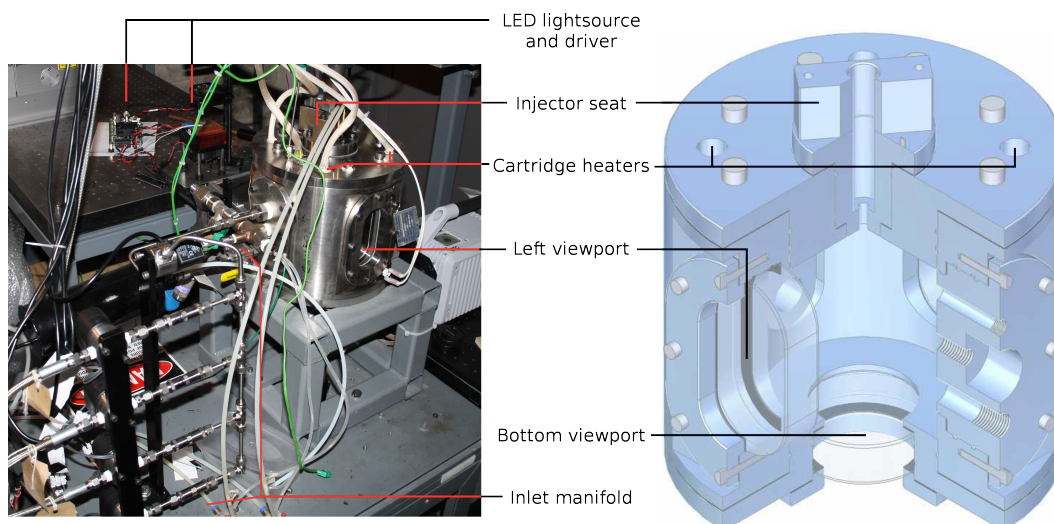


Figure 4.1.4: (left) Photo of the CVC February 2015, showing the inlet manifold (left side), the injector seat (top) and one view port. (right) Isomeric rendered view of the design of the CVC showing one side window and the bottom window, along with the inlet flange on the left/behind side of the view. Right schematic taken from [85].

the eight cartridge heaters the power leads can be seen in Figure 4.1.4, exiting at the top of the chamber as four shielded white cables. Four additional heaters were placed in a similar fashion in the bottom of the CVC. Fused silica has a low tolerance to thermal stress, therefore the CVC was heated with a maximum temperature increase of $0.5\text{ }^{\circ}\text{C min}^{-1}$, requiring a minimum of four hours to attain the required temperature and allow thermal stabilization of the steel body. All temperature measurements were done using K-type thermocouples allowing simultaneous measurements of CVC surface temperature, body temperature, and temperature of the gas inside the chamber.

The CVC was pressurized with oxygen free nitrogen (>99.9% purity) from a compressed gas cylinder. Due to pressurization the gas heated to a temperature of roughly $135\text{ }^{\circ}\text{C}$ to $150\text{ }^{\circ}\text{C}$ inside the CVC during filling. The additional thermal energy was allowed to dissipate into the cylinder walls to ensure a constant gas temperature during measurements. Thermal (re)stabilization of the in-chamber gas required roughly 15-20 minutes². A Kistler 4005B pressure sensor with amplifier type 4618A0 was connected to the CVC through a 5 cm tube to measure the pressure inside the CVC. The pressure sensor provided a

²Allowing the chamber and compressed gas to stabilize for twenty minutes resulted in a fairly stable end temperature. Variations in exact fill pressures, slight leakage after injector replacement, and fluctuating environmental temperatures resulted in the gas temperature varying by a few degrees from injection to injection.

measuring range from 0.1 MPa to 25.0 MPa with an uncertainty of 0.025 MPa. The sensor was mounted in a cooling jacket type 7525A, to ensure sensor temperature would remain below the safe operation temperature of 125 °C.

4.1.6.1 Safety measures of the CVC

To satisfy health and safety requirements the CVC and accompanying peripherals were fitted with several safety features, ensuring at least two safety features for every determined risk factor.

To prevent overheating, especially during the four-hour ramp-up of the CVC heating systems, the controller unit was configured to switch off in the case of power fluctuations, and the controller was powered by an independent mains socket from the rest of the set-up. The CVC was fitted with a thermal fail-safe switch cutting all power to the heaters if the surface temperature reached 150 °C. All materials in proximity of the CVC were non-flammable, except for the diesel fuel. The fuel supply for the injector had a maximum storage capacity of 125 ml and was located roughly 1 m from the CVC.

All electrical circuitry was fitted with a fuse, earthed, and power to all units was supplied through a leak current detector tested for correct operation at the start of every measurement day.

The CVC was tested and certified by ISI INDUSTRIAL SAFETY INSPECTIONS LTD. for safe operation at continuous pressures up to 8.0 MPa and peak pressures up to 12.0 MPa. A Pressure Relieve Valve was incorporated in the inlet manifold, fixed at an operating pressure of 6.3 MPa as intended operation pressure would not exceed 6.0 MPa in the initial investigations. An additional rupture disk served as a redundant overpressure safety measure, certified to burst at a chamber pressure of 9.0 MPa at 500 °C. 12.0 MPa rupture disks were available for future research.

Inlet and exhaust gas supply lines were suitable for operating pressures of at least 40.0 MPa, valves were operated remotely allowing (de)pressurization without the need to be physically near the CVC during pressurization or evacuation. A manual valve was incorporated in the exhaust line to allow throttling of exhaust gas flow.

4.2 Measurements

Measurements in the CVC were split into two series, *series 1* recorded with the SIM16 ultra-high speed camera system, and *series 2* recorded with a FASTCAM high speed camera, both of which have been treated in Section 4.1.3. Main reasons for the division into two series was the chronology, *series 1* recordings pre-dated the *series 2* by nearly a year, and the different recording conditions (see Table 4.3) motivated by the different capabilities of both camera systems. Although the sprays evolved in a similar fashion and showed the same basic characteristics, the different levels of visible detail allowed studying different aspects within each group of recordings. The division into two groups based on camera system was maintained for treatment in this chapter. Measurements conducted with the SIM16 system do not include *Set 3* injector results, as the *Set 3* injectors were acquired after the *series 1* measurements.

4.2.1 SIM16 measurements (series 1)

The SIM16 system was designed for recording a limited number of frames at extreme high frame rates, and the first measurement series was aimed at recording the start of injection with a high temporal resolution. Under varying conditions (see Table 4.3) sixteen subsequent images were recorded, providing the evolution of the fuel spray at a high recording frame rate. Figure 4.2.1 provides a complete recording of the start of an injection. Due to high noise levels caused by the integrated intensifiers, recordings were not as sharp as expected based on the high pixel resolution. Figure 4.2.2 provides a magnified view of a single spray showing high noise levels.

Direct comparison of the imaged start of injections from new and used injectors immediately led to two observations. First, several of the used injectors showed an asymmetric spray evolution, some orifices providing a retarded SOI and/or reduced penetration compared to other orifices during the same injection. Second, the very early spray evolutions of all injectors, *including* the injectors that showed large hole to hole variations, proved highly reproducible³. Although an altered spray evolution for the used injectors was

³In the analysis section it will be shown that for some injectors this statement is not completely accurate. By side-by-side comparison of the images without thorough analysis the changing spray shape is however not visible.

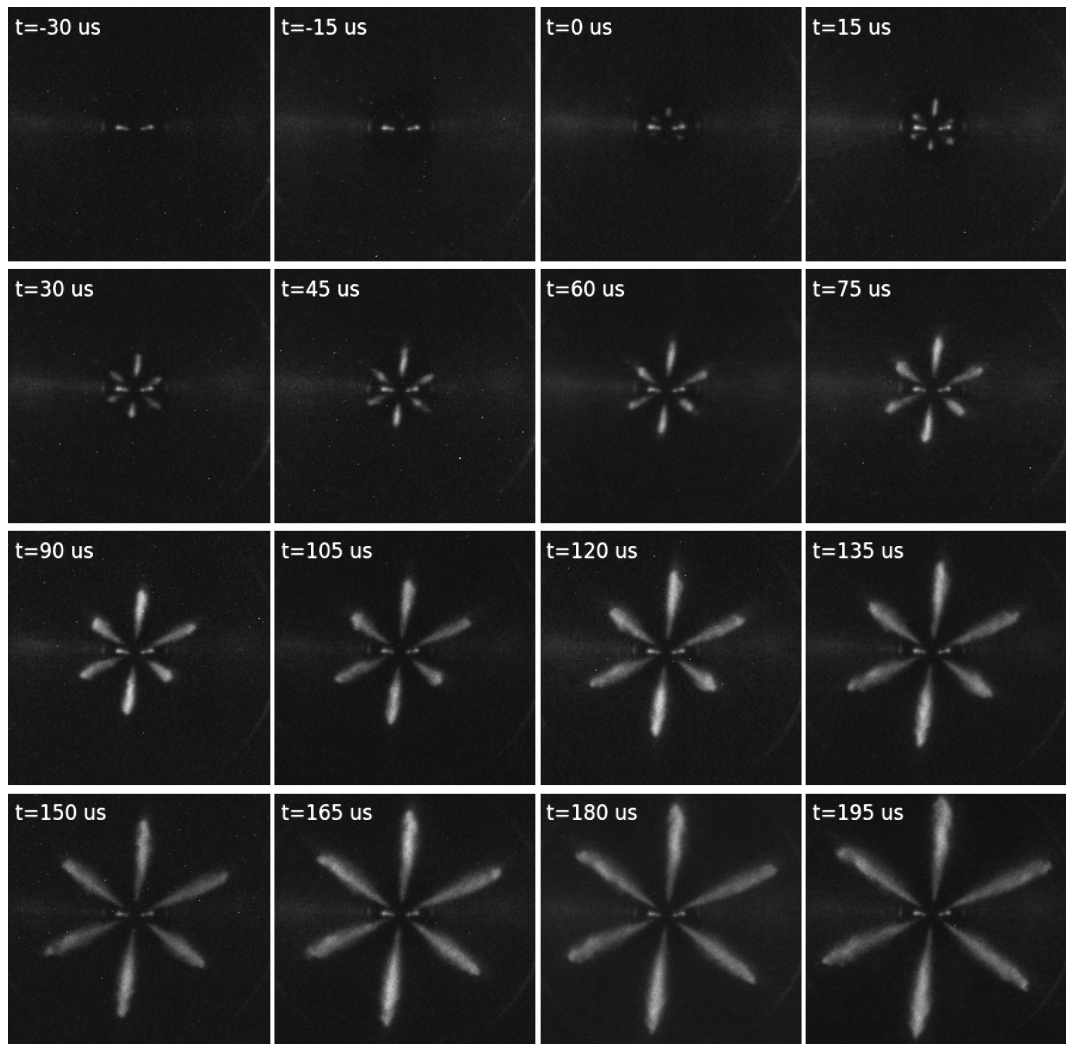


Figure 4.2.1: Image sequence recorded with the SIM16 system. Recordings show the evolution of the fuel spray at the start of injection from a new injector. Recorded frame rate was 66.7 kfps, injecting mineral diesel into a compressed N_2 environment at 3.1 MPa, 105.3 °C. The injection started in the third frame. The two horizontal bright areas, clearly visible in the first two frames, are specular reflections off the tip of the injector nozzle.

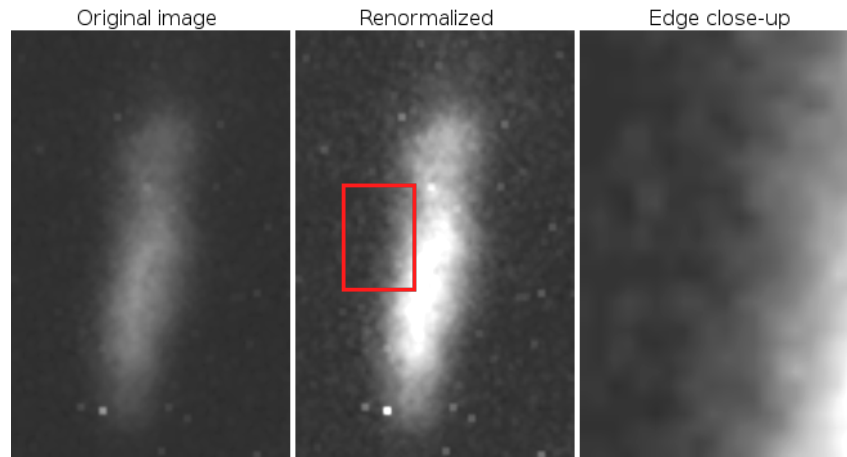


Figure 4.2.2: High noise levels from the intensifiers degraded image quality. Image shown provides an enlarged version of the upper evolving spray, sixth frame of Figure 4.2.1. First image provides the raw recorded spray, second image has been histogram-renormalized to enhance intensity, third image shows a zoomed-in part of the left spray edge. The third image clearly shows the high noise level of the ICCD smeared out the spray edge.

expected based on the investigation in the previous chapter, the high repeatability of the reduced penetration and delayed start was not expected. Not all used injectors suffered from a retarded or asymmetric early evolution of the fuel spray. Some injectors provided spray patterns which were indistinguishable from those emerging from a new injector. The investigated used injectors were still in working conditions and there were no known issues with these injectors, therefore severe spray degradation was not expected. Figure 4.2.3 provides examples of the high repeatability of the spray shape at the start of injection for both new and used injectors.

The reduced penetration from part of the orifices at start of injection, observed from several used injectors, led to an asymmetric early spray evolution lasting nearly the full recording time of sixteen frames. Figure 4.2.4 shows the evolution of spray penetration for one injection from several injectors. Used injectors have been qualified as being ‘good’ or ‘bad’ by purely considering orifice to orifice spray penetration variations. In Figure 4.2.4 it can be seen spray penetrations from several orifices of a used injector tend to be reduced compared to the penetration from a new injector, indicating the net fuel flow could be less at the early start of injection for a used injector. The ‘good’ used injectors produced nearly symmetrical spray evolutions, although the total penetrations seem slightly reduced compared to new injectors. For clarity red circles have been added to Figure 4.2.4 to indicate penetration from a

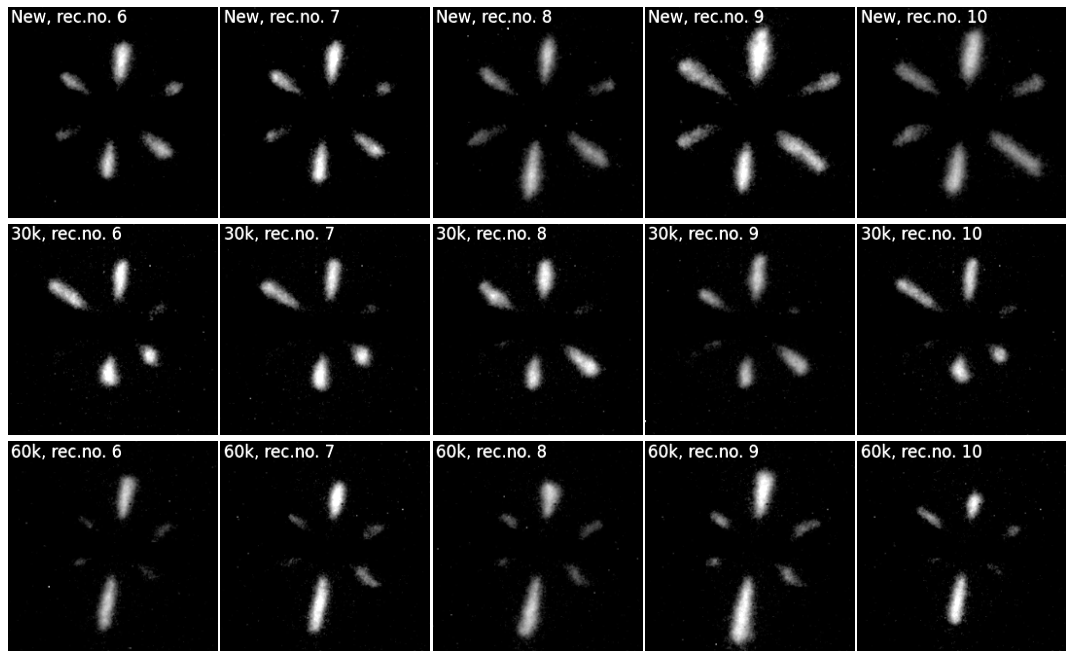


Figure 4.2.3: High repeatability of the early evolution of fuel sprays. All images were recorded $30\ \mu\text{s}$ after the start of injection, for five subsequent injections (columns). First row: new injector. Second row: *Set 1* injector showing an asymmetric early spray evolution. Large orifice to orifice variations in spray penetration are visible at the start of every injection. Third row: *Set 2* injector showing an asymmetric spray evolution. Note the injection to injection constancy of observed hole to hole variations. All recordings were done under identical conditions. Rail pressure of 60.0 MPa, N_2 ambient medium at 3.1 MPa, $114\ ^\circ\text{C}$, recorded at 66.7 kfps. Images correspond to an area of $9.7\times 9.7\ \text{mm}^2$, specular background reflections have been removed and the image intensities rescaled to enhance visibility.

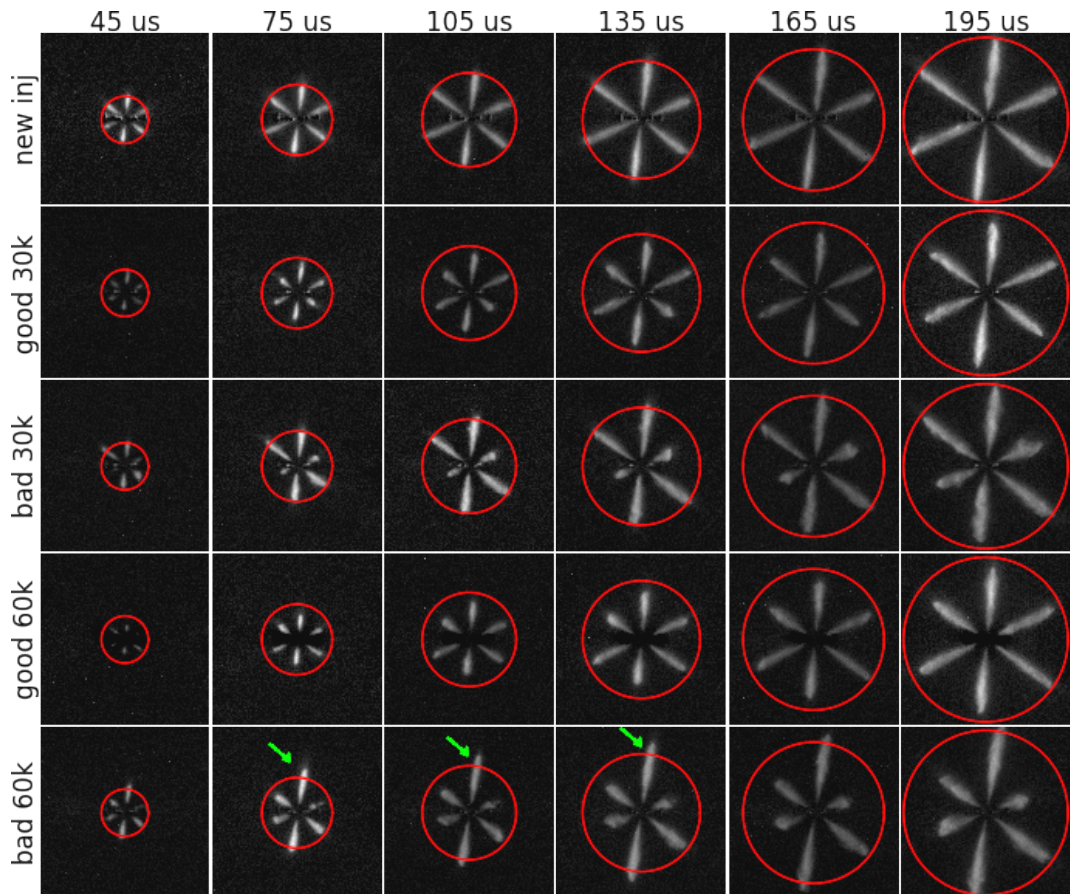


Figure 4.2.4: Comparison of spray penetration from a new injector to four used injectors (one injector on every image row), which have been deemed ‘good’ or ‘bad’ based on observed orifice to orifice penetration consistency only. For the worst performing injector from the *Set 2* injector group, the strongly reduced penetration from several orifices apparently led to an increased spray velocity for the remaining two orifices (green arrow). Red circles have been added to show penetration of the new injector. Times reported above the first image row indicate time after SOI.

new injector at the given time after the start of injection. Orifice to orifice variations in early spray evolutions could incidentally lead to an *increased* injection velocity from non-retarded orifices with respect to a new injector, as indicated by the green arrow in the bottom image row in Figure 4.2.4.

The occurrence of radial anomalies observed in the previous chapter (see for example Figure 3.2.2) were not clearly visible when recording the early start of injection. Closer investigation shows spray anomalies *do* occur, however due to the lower ambient pressure the radial expanding transients evolve while maintaining a significant forward momentum. The widening of the spray therefore appears to be less pronounced. The last image in the third row (*bad 30k*) of Figure 4.2.4 shows a radial expansion starting from the top-right spray.

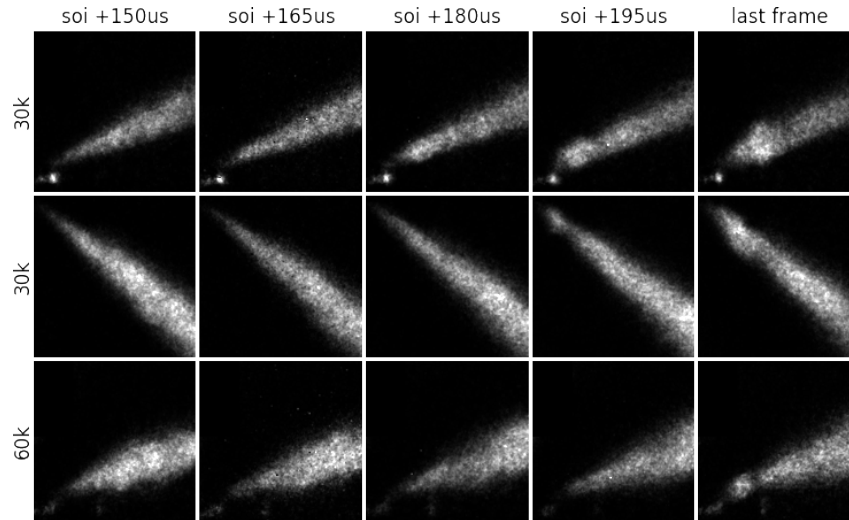


Figure 4.2.5: Start of a radial expanding spray anomaly, recorded near the end of the recording time frame. Earliest visible radial transients occur 195 μs after the start of injection. The anomalies result in a minor increase in width of the unperturbed fuel spray. Images have been corrected for specular reflections, contrast was artificially increased, and only the relevant sprays are shown.

In several recordings, one example is provided in Figure 4.2.5, the onset of additional transients were observed which started at the end of the recording time frame. Significant radial expansions were not observed, probably due to the limited time window recorded with the SIM16 system.

4.2.2 Fastcam SA-X2 measurements (series 2)

The FASTCAM SA-X2 camera allowed recording the full fuel spray evolution at a reduced frame rate, instead of a maximum of sixteen frames at a higher frame rate as was possible with the SIM16 system. A full injection recorded with the FASTCAM camera is provided in Figure 4.2.6, showing every 5th frame of one recording. Although CMOS pixel count was roughly one-fifth of the available resolution of the SIM16 system, the CMOS-sensor's higher sensitivity allowed imaging the fuel spray without intensifiers, greatly improving signal to noise ratio. For the early start of a fuel injection, comparable observations as noted in the previous section were made. The new injectors provided same spray penetrations from all orifices, and several (explicitly not all) used injectors showed hole to hole variations in the early spray evolution, the higher mileage injectors tended to provide higher hole to hole variations than the lower mileage ones. Similar transients as depicted in Figure 4.2.5 were observed when recording with the FASTCAM camera, and the longer recording time allowed prolonged

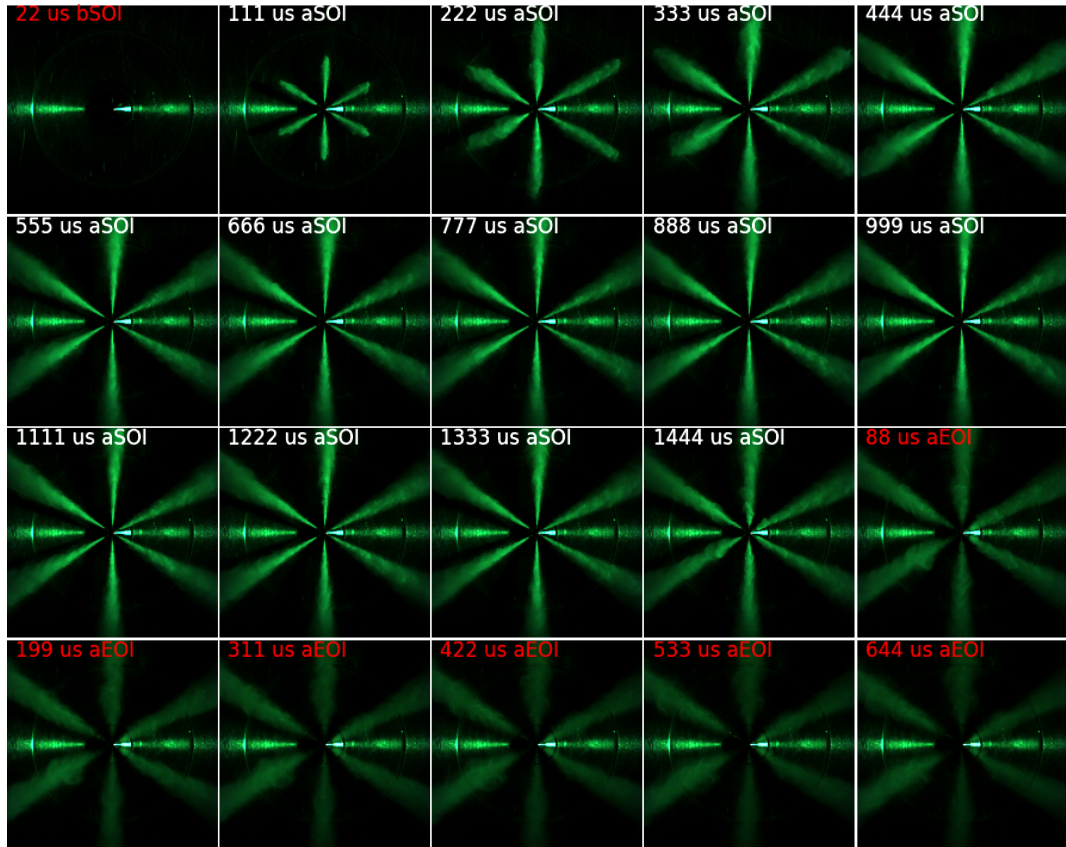


Figure 4.2.6: Example recording from the FASTCAM camera, showing 20 frames from a single injection event, covering the full injection. Every 5th frame of the original recording is provided unaltered. First (top-left) image is recorded just before the start of injection, providing a ‘light background’ reference image. The last six images were recorded after the injection ended and show the persistence of the atomized cloud in the ambient environment, which was maintained at a sufficiently low temperature to minimize evaporation. The horizontal bright band already visible in the first frame corresponds to specular reflections off the top of the CVC.

study of the evolution. Figure 4.2.7 provides (top two rows) a side by side comparison of the early start of injection for both camera systems from a new injector, (middle two rows) a starting radial expanding anomaly (white arrow) recorded from a used injector, and (bottom row) a side by side close-up of a single spray to show the difference in image quality between the FASTCAM and SIM16 system. In addition to the onset of a possible radial bulge as was observed with the SIM16 system, the improved sensitivity allowed recording of an early spray widening for sprays that suffered a reduced initial penetration.

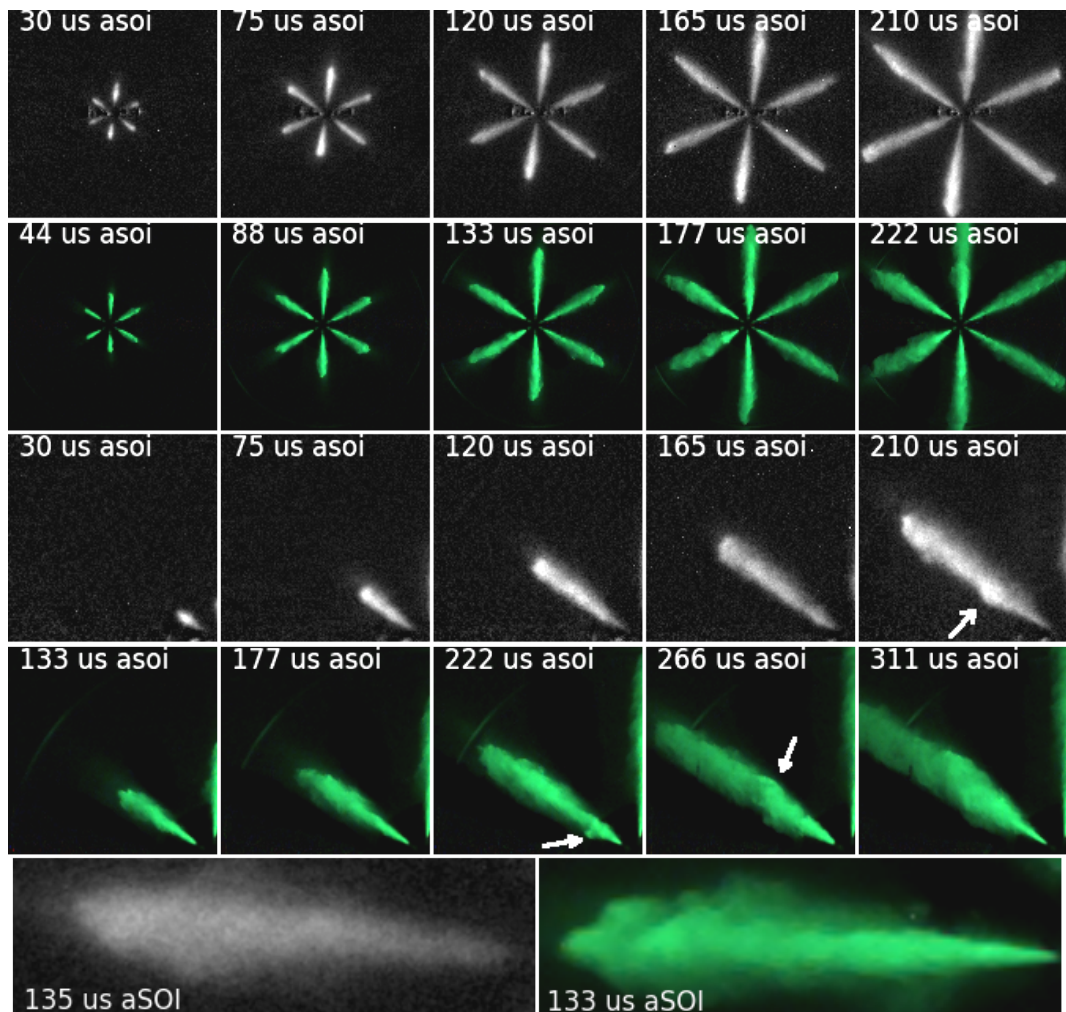


Figure 4.2.7: Typical image galleries of FASTCAM SA-X2 recordings (green), with comparable frames recorded with the SIM16 system (b/w) for comparison, cropped to provide roughly the same area. Top two rows provide the start of injection from a new injector. Frames have been selected to correspond as closely as possible to similar times $aSOI$ as both cameras recorded at different frame rates. Third and fourth row show the continuation of a radial expanding anomaly (white arrow), where the FASTCAM is capable of recording the evolution beyond the sixteen frames available with the SIM16 system. The anomaly is visible 311 μs $aSOI$, the width marginally larger than the width of the unperturbed spray. Bottom row provides a magnified image of a single spray, showing the reduced noise level of the FASTCAM compared to the SIM16. The lower resolution of the FASTCAM leads to slight pixellating in the bottom right image.

After the initial transient phase at the start of injection, all new and used injectors produced similar quasi steady-state spray shapes in the stable regime, with no clearly visible differences from injector to injector. Any reduced initial penetration was resolved by subsequently injected fuel, leading to a similar spray shape for all orifices in the stable regime. This stabilization was often accompanied by self-impingement transients, visible as small, radially expanding anomalies. Figure 4.2.8 shows two image galleries where the transient initial regime, the subsequent stable regime, and the transient end of injection period are provided for a new injector and a used injector from the *Set 3* pool. The new injector suffered from both SOI transients associated with needle lift and EOI transients associated with needle drop, but for a used injector the magnitude of the SOI transients appeared more severe. A quantitative analysis of the difference in the early spray transients is treated in more detail in the analysis section.

The onset and evolution of additional transients were closely studied in the CVC. These additional anomalies differ from the anomalies shown in Figure 4.2.8 by occurring after the initial transients at SOI associated with needle lift, but before the spray had stabilized to the quasi steady-state spray shape. Figure 4.2.9 provides image sets of several radial expanding bulges after the initial transient regime has passed, recorded from one injector from every *Set 1–3* batch. The anomalies show a reduced radial expanding component when compared to recordings in the previous chapter, Figure 3.2.2. This is expected to be the result of a reduced ambient density, as radial expansions observed in Chapter 3 for injections into free air also showed a reduction in radial size, see Figure 3.2.5. The anomalies often remained within the outline of the initial transient spray shape at the start of injection, but by overlaying a spray shape from the stable regime, it can be seen the additional anomalies are wider than the quasi steady-state spray, see Figure 4.2.10.

Continued recording after the injection had visibly ended allowed the recording of fuel expulsions after needle closure, comparable to the expulsions treated in Section 2.1.4. These expulsions of ligaments and droplets were observed for every injection, and from every injector. From an observational point of view, the post-injection expulsions may prove interesting in comparing new and used injectors, to determine if there is a relation between droplet expulsion, injector condition, and early spray characteristics. Typical post-injection expulsions from a new and a used injector are provided in Figure 4.2.11.

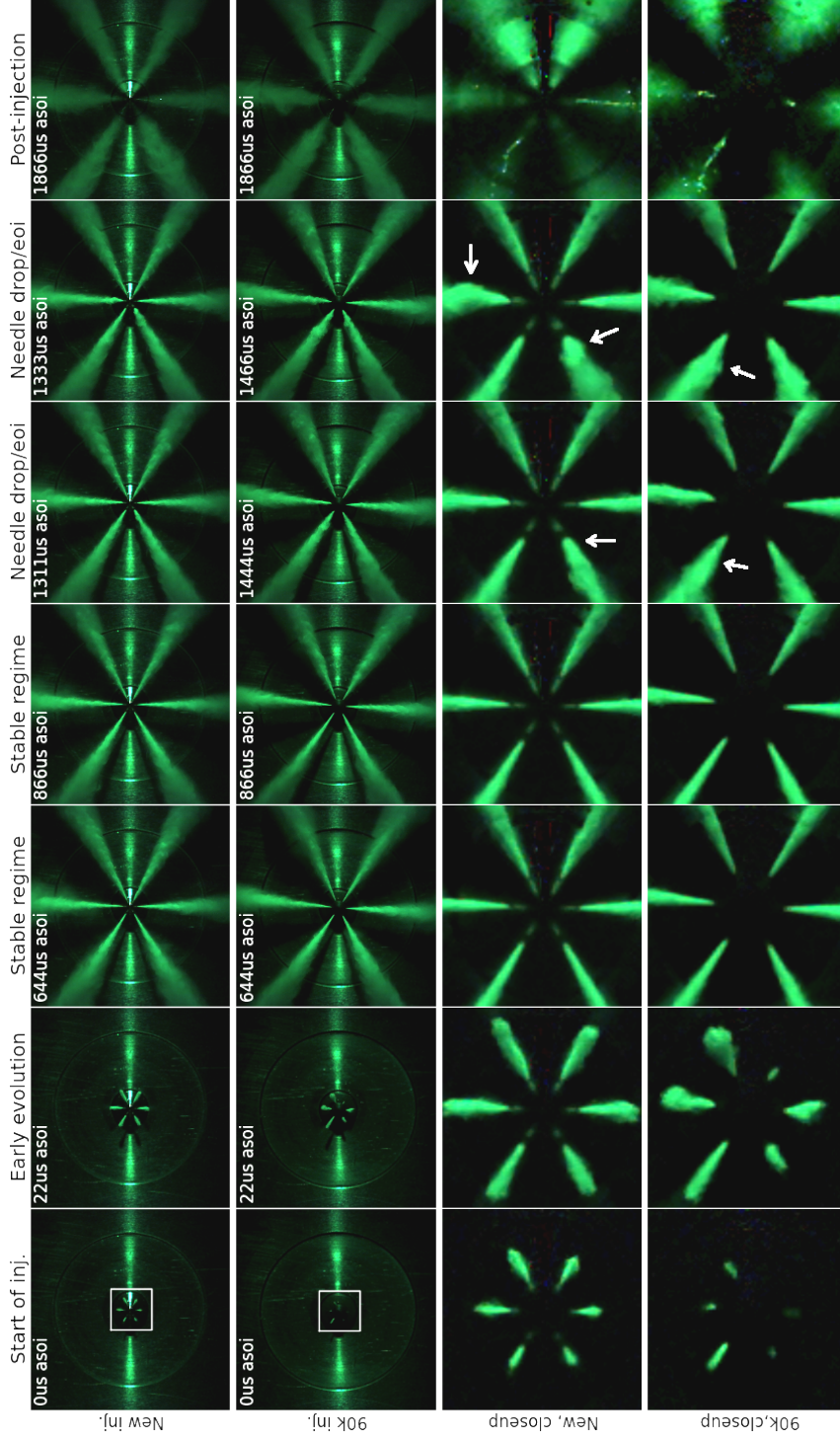


Figure 4.2.8: Selected time windows of a spray evolution from a new and a used injector. Both injectors have a stable regime in which spray shape differences are minimal. The new injector produces anomalies during the start of injection, the magnitude of the effect much less than for a used injector. First and third row show seven images taken at stated times *asoi* from a new injector, where the third row provides a zoomed in view of the white square depicted in the top-left image in the first row. Second and fourth row provide similar images recorded from a *Set 3* injector. First two images in both magnified sets show the new injector produces a symmetric hole to hole penetration in contrast with the used injector. Fifth and sixth frames were recorded during needle drop at the end of injection, the magnified images in the bottom rows show the spray width increases slightly (indicated by white arrows) with respect to the spray width in the stable regime. Last image column shows the shape of the residual fuel cloud after injection has ended, and the magnified views clearly show the expulsion of liquid ligaments and droplets post-injection.

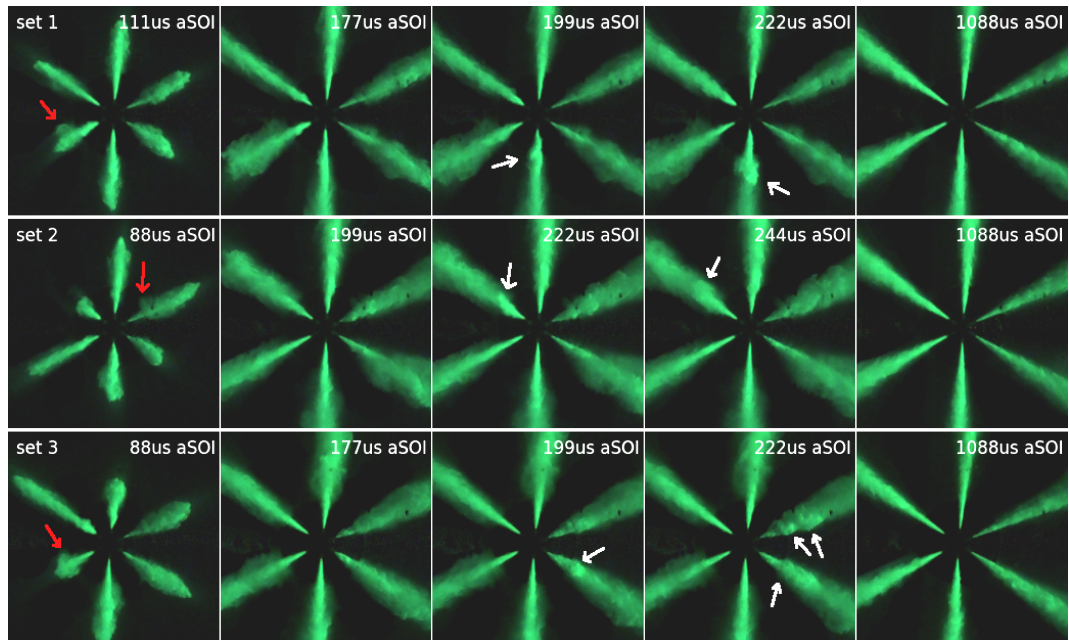


Figure 4.2.9: Radial expanding anomalies, occurring after the initial SOI transients have passed for three different used injectors, one from each set. Leftmost images (red arrows) show the initial transient widening of the sprays associated with needle lift dynamics. Three central frames in each row show the evolution of the spray after the initial transients have passed, before the stable regime. Radial expanding ‘bulges’ are visible as sudden intensity increases *within* the atomized envelope resulting from initial SOI transients (white arrows). Images in the last column provide the spray shape in the stable regime. Recording times provided in the top-right of every frame are not equal for all recordings.

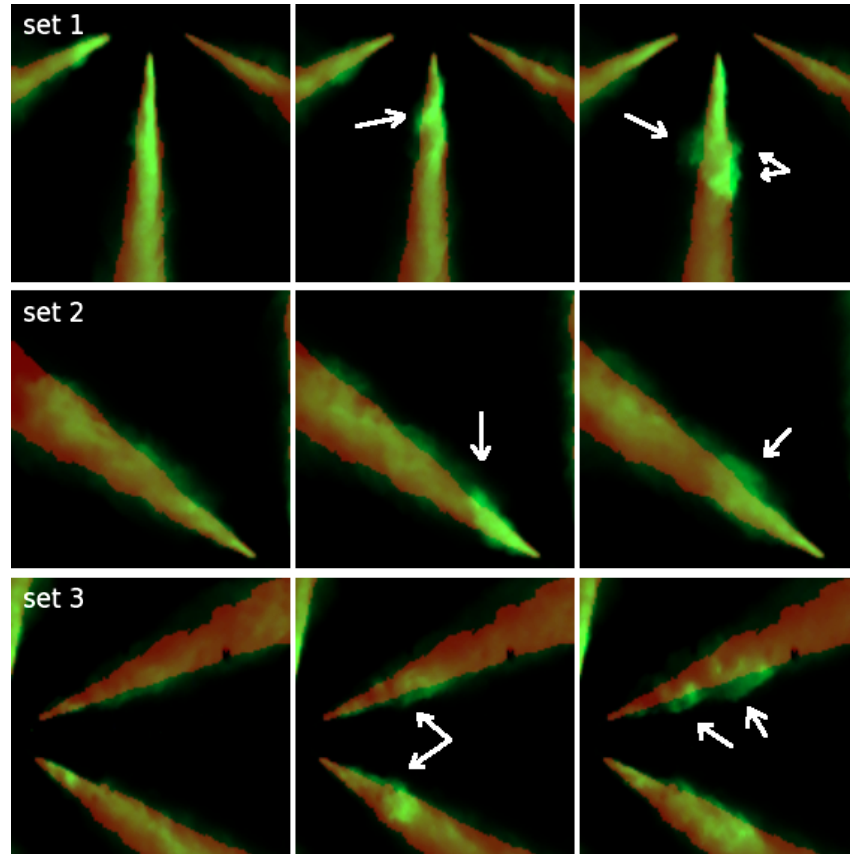


Figure 4.2.10: Comparison of the width of a transient anomaly occurring just before the injection reached the stable regime, to the spray shape in the stable regime. Images provide a magnified view of the anomalies in the middle three columns of Figure 4.2.9. An image overlay generated from the spray shape in the stable phase of the same injections has been added, i.e. the last column of Figure 4.2.9 has been binarized and bitwise added to the red colour channels of the central three columns in Figure 4.2.9. It can be seen the transient bulges, as observed in Figure 4.2.9, provide a wider spray shape than the spray in the stable regime. White arrows indicate bulges extending beyond the stable spray overlay that are the result of transient expansions *after* the very early SOI transient phase has passed.

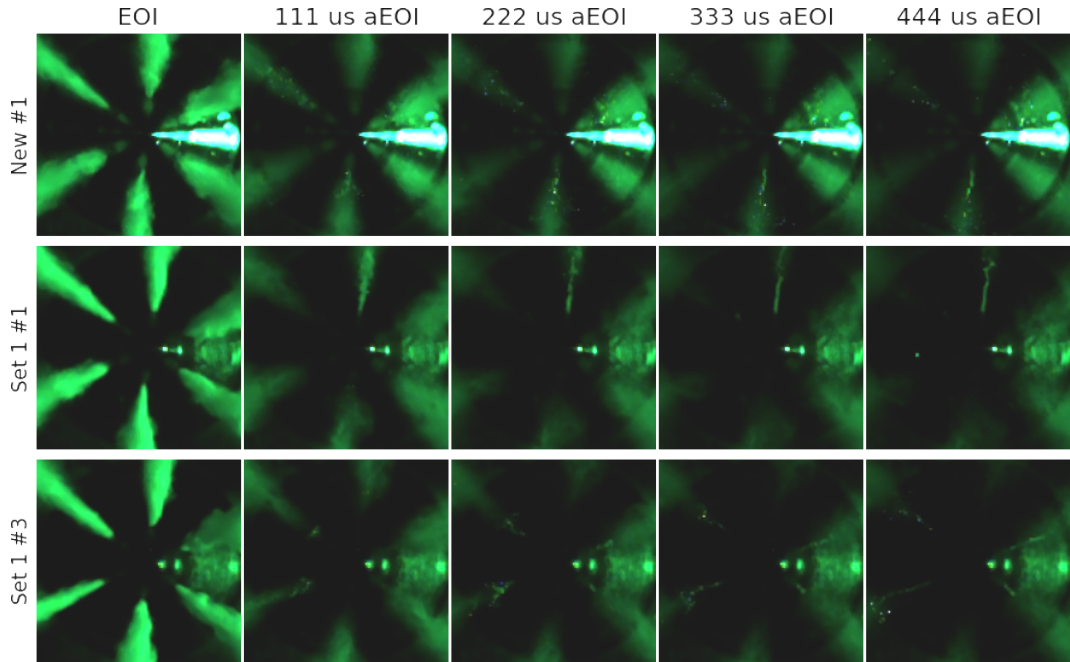


Figure 4.2.11: End of injection fuel expulsion, ligament formation, and breakup, observed from one new and two *Set 1* injectors. Images have not been manipulated or enhanced, apart from an increase in brightness, to show the low contrast between (specular) background, residual atomized cloud, and expelled ligaments and droplets. The saturated horizontal band in the top image row is the result of specular reflections off the tip of the new (clean) injector nozzle. Ligaments and droplets become most apparent when studying image-to-image deformation of the ligaments and displacement of droplets. Images have been magnified to show only the central $7 \times 7 \text{ mm}^2$ of an injection. All injections were recorded at a common rail pressure of 100.0 MPa, time scale provided above the top image row relates to the *observed* end of injection by considering sudden spray widening resulting from needle drop. The reported times are not necessarily equal to the time at which the injection was programmed/expected to end.

4.3 Spray analysis

The improved recording quality of both SIM16 and FASTCAM systems compared to the recordings in the previous chapter made extensive preprocessing, as done in Section 3.3.1, unnecessary. Manual preprocessing *was* applied in order to enhance visibility of images presented in this thesis, but no extensive preprocessing was required for analysis. Image (pre)processing before analysis consisted of background subtraction and intensity rescaling, both done by application of standard functions from the SciPy libraries[79]. Background and image quality were sufficient to allow OTSU threshold determination for most recordings, occasionally a manually determined threshold was applied to focus on specific effects. Extensive threshold analysis as conducted in the previous chapter was not required. The algorithm for OTSU threshold determination as applied in this research was directly imported from the `scikit-image` *SciKit image processing toolbox* [86], designed for use in conjunction with the SciPy libraries.

Based on the split in measurement *series 1* and *series 2*, and the chronology of the fuel spray evolution, this section is divided into the following five subsections.

- *Start of injection penetration rate* - Investigating the fuel evolution and hole to hole penetration variation at the start of injection up to 225 μs *aSOI*. This investigation only considers the *series 1* measurements.
- *Transient regime* - Looking at anomalies at the start of injection during needle lift, up to roughly 500 μs *aSOI*⁴. These anomalies were recorded in the *series 2* measurement series, and excludes hole to hole penetration variations mentioned in the above category.
- *Stable spray regime* - Treating the spray shape and its evolution after the initial transient period has passed, from roughly 500 μs *aSOI* up to the end of injection.

⁴The actual needle lift lasted shorter than the reported 500 μs , however some anomalies were observed shortly following the needle lift time window. It is assumed these additional anomalies are indirectly caused by the needle lift, and may reflect for example flow stabilization in the SAC after the needle has reached the fully opened position.

- *End of injection* - Considering any visible changes in the spray evolution during needle closure.
- *Post-injection* - Analysing the spray and any other visible effects after the injection had ended, up to roughly 1 ms *aEOI*.

The first two categories overlap in time as they are both looking at the early spray evolution. The final three categories all treat *series 2* measurements only, as these domains were recorded outside the time window of the SIM16 system. In the previous chapter, Section 3.3.3, it was shown radial anomalies from used injectors occurred at their earliest 250 μs after the start of injection. The division made in this section is applied to discriminate between SOI effects, occurring *before* the radial expansions (bulges) observed in Section 3.3.3, and those which might correlate to the observations done in Chapter 3. The 225 μs threshold corresponds to the longest recording period of the SIM16 system.

4.3.1 Start of injection penetration rate

The apparent reproducibility shown in Figure 4.2.3 has been analysed by determination of the spray penetration for every individual orifice for all recordings⁵. Ideally (i.e. for an ideal injector) the spray penetration plotted versus time *aSOI* should be identical for every orifice and for every recording, providing six overlapping steep lines, one for every orifice, the inclination corresponding to the spray tip velocity. Assuming a used injector deviates from this ideal picture, the main deviations can be divided into the following three groups.

- *Not all orifices provide an equal initial spray tip velocity* - The spray tip trend lines originate from the same position in the graph, indicating identical start times, but have different inclinations, i.e. the fuel spray penetration rate is reduced for certain orifices.
- *Not all orifices start injecting at the same time* - Penetration trends remain parallel, but have a different time offset, shifting the intersection with the horizontal axis towards the right for a delayed start of injection. This can be indicative for an inhomogeneous fuel flow inside the injector.

⁵In the present section analysis is limited to a comparison of penetration data from new injectors to used injectors studied in this investigation. Comparison of penetration data to literature is provided in Chapter 5.

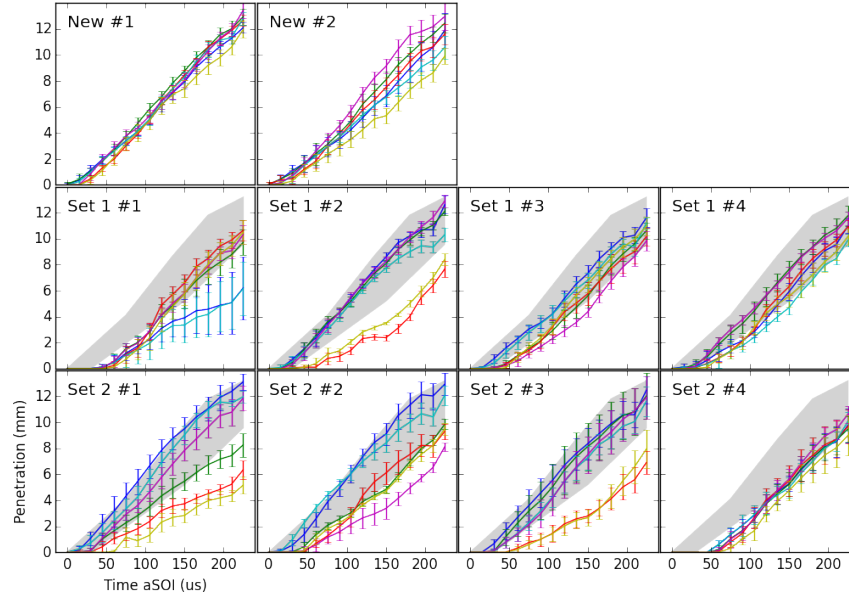


Figure 4.3.1: Spray tip penetrations at the start of injection. Every individual trend line corresponds to the average penetration plotted versus time $aSOI$ for one orifice of the named injector. Grey areas correspond to the penetration envelope measured from the new injectors. All data points were calculated from SIM16 measurement data. Elaborate explanation of characteristics visible in these graphs is treated in the main text.

- *High injection to injection variation of the early spray evolution* - Provides the clearest deviations, as the average spray tip penetrations would be accompanied by large error margins, providing a wide error band within which all sprays become essentially indiscriminable. This is similar to the classical case of increasing the random error of an experiment.

Full analysis of the SOI's recorded with the SIM16 system in *series 1* provided the graphs presented in Figure 4.3.1 for injectors from the *New*, *Set 1* and *Set 2* sets. To qualitatively show deviations from ideal behaviour, when comparing a new and a used injector, only a few recordings would have sufficed. All recorded penetrations measured from all ten injectors are provided to explicitly show not all used injectors suffered from large hole to hole variations, and some used injectors behaved nearly indiscernible from a new injector.

To ease comparison, grey areas have been added to *Set 1* and *Set 2* graphs, corresponding to the spray penetration envelopes of both *New* injectors. Penetrations measured from a used injector that remained within the grey shaded area are statistically indiscernible from penetrations measured from new injectors. For all *Set 1* and *Set 2* graphs some orifices produced a spray penetration retarded with respect to new injectors, the corresponding trend line lying be-

neath the grey area. Most retarded sprays proved highly reproducible from injection to injection, the accompanying error margin being of the same order as observed for a new injector. Injector *Set 1 #1* provided a reduced spray penetration from two orifices (reduced inclination) and additionally showed a large standard deviation, indicating large injection to injection variations in the measured spray penetrations. Injectors *Set 1 #3*, *Set 1 #4*, and *Set 2 #4* provide near-identical penetrations from all orifices (i.e. graphs lie very close to each other), but the trend lines seem to be shifted to the right. This indicates spray velocity, penetration, and symmetry are similar to those measured from a *New* injector, but all injections start approximately 30 to 50 μs later than for a new injector. I.e. if *Set 1 #3*, *Set 1 #4*, and *Set 2 #4* graphs were all translated to the left by 30 to 50 μs , spray penetrations would have been indiscernible from a new injector.

The origin of any hole to hole asymmetry occurring in the transient regime was not researched in this investigation, however some spontaneous improvement of spray penetrations was observed for several of the used injectors over time. The *series 2* data set acquired with the FASTCAM camera was recorded nearly a year after the initial *series 1* measurements, and at a reduced frame rate of 45 kfps. For most injectors there was no significant difference in the determined spray penetrations between the two measurement series, however a few injectors produced different penetrations at the start of injection when measured with the FASTCAM system. For these injectors the hole to hole variations observed with the SIM16 system were greatly reduced, and the overall spray penetration improved. The hole to hole variation in early penetration is therefore not necessarily the result of a fixed, irreversible alteration inside the injector. The spray improvements observed from some of the used injectors is shown in Figure 4.3.2, where spray penetrations from several used injectors as measured with both camera systems are compared in combined graphs. Despite the tremendous improvement for some orifices the overall variation in spray penetration from used injectors remained larger than for new injectors.

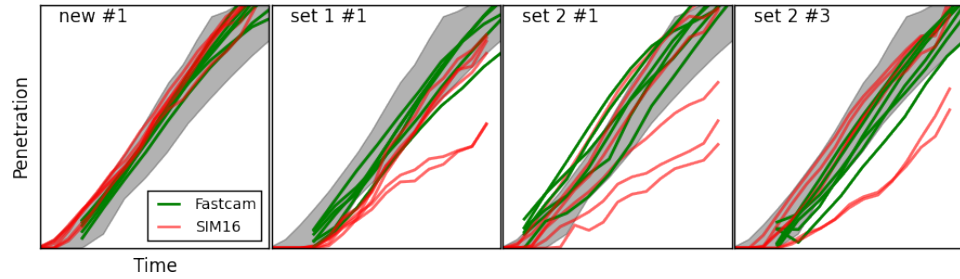


Figure 4.3.2: Improvement of the spray penetration resulting from the use of injectors in an inert environment. Red trend lines provide the spray penetrations measured with the SIM16 system, green trend lines correspond to penetration measurements of the same injectors with the FASTCAM system, nearly a year later. Every trend line corresponds to the spray penetration from one of the six orifices of the named injector. For clarity error bars have been omitted. For the FASTCAM measurements the spread in penetrations is less than for the SIM16 measurements, however spray penetrations are still not as reproducible as for the new (leftmost) injector. The grey band visible in the background of all graphs indicates the envelope of measured spray penetrations from both new injectors. Penetration curves have been corrected for the different injection pressures applied in the SIM16 and FASTCAM measurement series.

4.3.2 Transient regime

Increasing the time window under consideration from the first $225\ \mu\text{s}$ up to the first half millisecond, the injection spans the full transient regime before the steady-state spray shape is attained. Considering the results from the previous chapter, this is the time region in which radial expanding anomalies are expected for used injectors. The reduced spray penetrations treated in the previous section also appeared in this transient regime, however the expansions of fuel sprays were not treated in Section 4.3.1.

Analysing the spray anomalies observed during and after needle lift, three transient-phase anomalies were discriminated:

- SOI *puffs* - Tiny spray widening occurring from both new and used injectors, visible in the first frame of fuel injection.
- *Early radial anomalies* (ERAs) - Transient radial expansions occurring shortly after SOI, strongly coupled to the reduced initial spray penetrations observed in Section 4.3.1. These anomalies proved to be similar to those observed in Section 3.2.2 and occurred only for used injectors.
- *Late radial anomalies* (LRAs) - Radial transients appearing approximately

250 μs to 350 μs *a*SOI occurred in all injector groups, although used injectors produced more pronounced anomalies. These anomalies are expected to be associated with the needle reaching the fully open position.

4.3.2.1 SOI puffs

Upon the first needle opening in the nozzle, the inrush of fuel will expel any residual fuel present in the nozzle from an earlier injection. This expulsion produces a radial expanding puff preceding the main injection, often referred to as a mushroom head or spearhead transient, and has been treated in Section 2.1.1. These initial fuel expulsions represent a minimal fuel mass compared to the total fuel injected and they were not observed for injections into extreme high ambient densities in the previous chapter. The low fuel mass will have insufficient total momentum to noticeably deform the initial spray evolution or provide an ejecting spearhead or mushroom-shaped head when injecting into a liquid backpressure environment. In a gaseous backpressure medium at roughly 30 times lower density than in the previous chapter, these SOI *puffs* will produce small but visible anomalies.

The recording conditions applied with the camera systems used in this research⁶ prevented investigating the evolution of SOI *puffs* in the very early stage of injection. In several cases recordings did show the presence of tiny spray widening at the beginning of an injection. Figure 4.3.3 provides images of several recordings where the SOI *puff* can be seen. For used injectors the SOI *puff* could be followed by a radially expanding anomaly (ERA), although the latter anomalies would start occurring only 200 μs *a*SOI. The SOI *puffs* were not always observed, and the examples provided in Figure 4.3.3 were hand-picked and colour optimized to enhance visibility. A quantitative analysis of SOI *puffs* was not conducted as these effects were too small to properly image and analyse.

⁶The SIM16 system was unsuitable for recording the very early *puffs* due to the low signal to noise ratio. The FASTCAM system provided an insufficient magnification and frame rate to properly determine SOI *puffs*, but in several instances the SOI *puffs* were nonetheless observed.

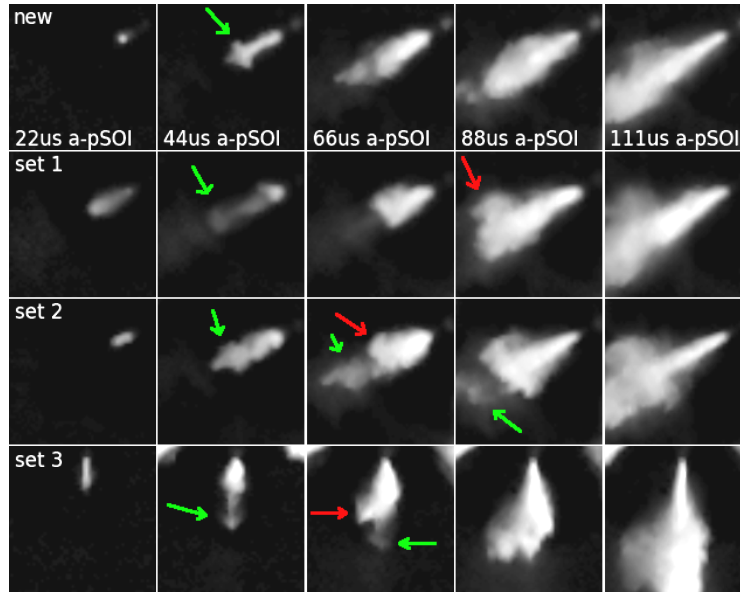


Figure 4.3.3: Discriminating between the pre-injection puffs originating from residual fuel in the nozzle (green arrows) and the anomalous radial expansions (red arrows) observed from used injectors only. For used injectors the tiny SOI *puff* was often followed by an additional ERA. Injection pressure for all recordings 80.0 MPa, images represent an area of roughly 4×4 mm, intensity has been non-linearly rescaled to enhance visibility.

4.3.2.2 Early radial anomalies

Fuel sprays evolving with a reduced initial spray penetration, as treated in Section 4.3.1, nearly always showed additional transient widening of the spray or spray tip. The radial anomalous expansions occurred at the early start of injection, but after the initial SOI *puff* had occurred. The key differences between the *early radial anomalies* (ERAs, red arrows) and the generally observed SOI *puffs* (green arrows) in Figure 4.3.3 are:

- *Puffs* occur *at the start* of injection, essentially being visible in the very first frame of a recording, and are barely visible. The ERAs occur later in time, allowing clear temporal discrimination from SOI *puffs* in most cases.
- *Puffs* represent a much smaller total fuel mass. The tiny SOI *puffs* were barely visible in the applied set-up while ERAs lead to a spray widening clearly visible under nearly all circumstances.
- The ERAs were observed when analysing injections from used injectors only. The SOI *puffs* occurred equally frequent for new and used injectors.

Although ERAs were already visible in images recorded with the SIM16 system⁷, the images acquired with the FASTCAM system provided an increased signal-to-noise ratio, resulting in an improved image quality of these anomalies.

The ERAs observed in this investigation were always coupled to sprays that suffered a reduced early penetration, and it is assumed the two are related through momentum transfer. It was observed in the previous section that retarded spray evolutions were followed by acceleration of the spray at a later stage, the penetration ‘catching up’ with the average penetration of the other orifices. During this acceleration process fuel leaving the orifice back-impinged on the slow moving atomized fuel spray near the nozzle, and this impingement led to a local radial expansion of the fuel spray. Recorded images showed the early spray formation had a broad spray head, but the resolution was insufficient to study the formation of ERAs in high detail. Figure 4.3.4 provides several image series of the evolution of ERAs observed from used injectors. For comparison the last image in each recording row provides the fuel spray in the stable regime, 1 ms *a*SOI. New injectors showed a widened early spray as a result of the transient growth in the early phase, as was treated in Section 2.1.2, however the widened sprays associated with an ERA from used injectors does not maintain a straight spray edge, shows large injection to injection fluctuations, and remains present for a longer period of time.

To quantify the observed spray widening resulting from ERAs the analysis from Section 3.3.3 was slightly modified. The fuel spray cone angle and accompanying variation from used injectors were larger than for new injectors, but ERAs affected the spray shape to a lesser extent than observed in the previous chapter. Studying the temporal evolution of the fuel spray cone angle allowed discrimination between ERAs and ‘common’ early spray widening observed from new injectors. The off-axis expansions resulting from an ERA remained at a nearly stationary position in the early spray evolution for a prolonged period of time, and off-axis transients were discriminated by noting the fuel spray cone angle did not quickly return to the minimal angle observed in the stable regime. Figure 4.3.5 provides the average fuel spray cone angles measured from every individual orifice for every injector, averaged over ten subsequent injections. Most used injectors show a prolonged persistence of an increased fuel spray cone angle. In some cases an increase of the fuel spray cone angle can be observed after the injection had started, the fuel spray cone

⁷See for example the upper right spray, third row, last frame in Figure 4.2.4.

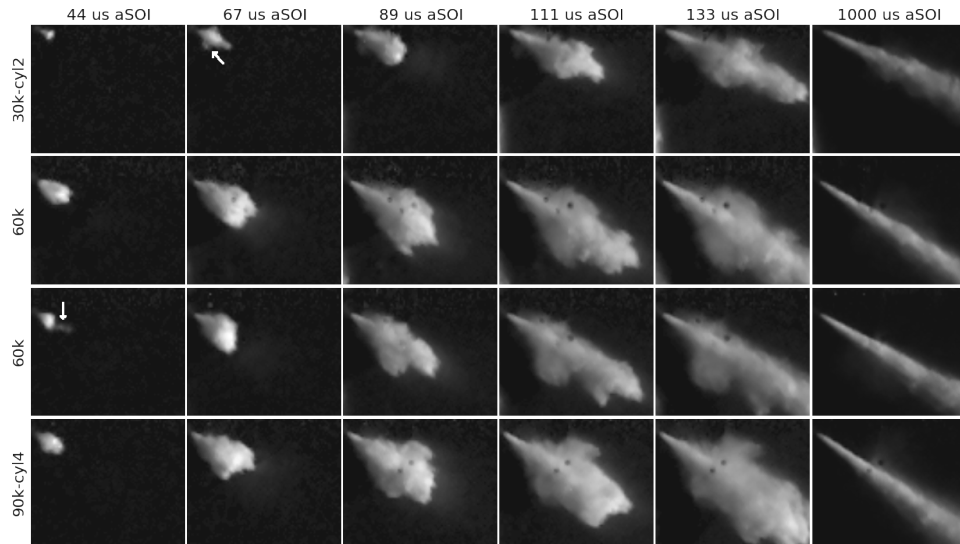


Figure 4.3.4: Evolution of ERAs occurring shortly after the start of injection. For two injections, the SOI *puff* was visible in the first frames, indicated by white arrows. Every row corresponds to the evolution of one injection, images taken at indicated times *aSOI*. The initial spray width during an ERA is significantly increased w.r.t spray width in the stable regime, last image in every row. Images correspond to a $6.6 \times 5.6 \text{ mm}^2$ area.

increasing from roughly $70 \mu\text{s}$ *aSOI* onwards, indicating the radial expansion of an early radial anomaly. For comparison, a small vertical bar has been added at the right of every graph, indicating the average fuel spray cone angle in the stable regime of the given injector.

The *New #2* injector provided more pronounced transient expansions at the early start of injection than *New #1*, but less than used injectors, and the spray cone angles decreased faster than for most used injectors. The increased spread in penetration rates at the start of injection in Section 4.3.1, i.e. the broad band of penetrations for the *New #2* injector in Figure 4.3.1, is consistent with the observed increase in spray cone angle at SOI. Note this increased dispersion from new injectors occurred *at* SOI while the ERAs observed from used injectors occurred *after* injection had started.

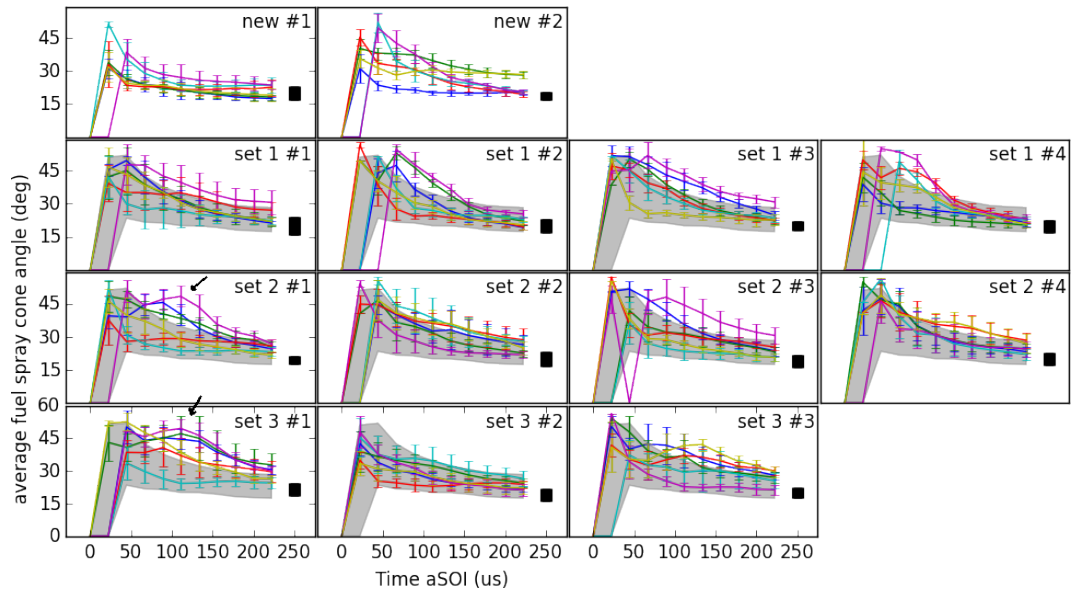


Figure 4.3.5: Spray cone angle evolution at the early start of injection, during needle lift, where spray cone angle is *indicative* for spray widths resulting from ERAs. New injectors show an increased spray cone angle at the start of injection, in agreement with Section 2.1.2, the initial spray widening is however short-lived. For several used injectors a radial expansion at roughly $100\ \mu\text{s}$ aSOI can be observed to grow *after* transients associated with needle lift have passed. For example, the purple trend lines in both *Set 2 #1* and *Set 3 #1* graphs show the average fuel spray cone angle is increasing from roughly $70\ \mu\text{s}$ aSOI up to $120\ \mu\text{s}$ aSOI at which point the maximum fuel spray cone angle, and accompanying fuel spray width, is achieved (black arrows). Black solid bar on the right of every graph indicates spray cone angle and variance in the stable regime.

The average spray width can alternatively be studied versus time $aSOI$ at a fixed distance from the orifice, where the presence of ERAs should lead to a temporal increase of the spray width. The advantage of determining the spray width at a fixed distance, compared to calculating the average spray cone angle is that any local expansions will not be averaged out by the non-transient part of the spray. The effect of any radial expansion will be more pronounced on the overall spray width. There are however several drawbacks to the application of this method as a result of the high variation in the evolution of ERAs:

- ERAs forming further downstream of the spray, past the point of interest, will be invisible.
- Reduced spray penetration rates can distort the graph, as any transient will become visible at a later time and the average spray width at a fixed time $aSOI$ will be reduced by the retarded spray
- As only the total width at a fixed point is considered, large radial transients (i.e. transients that cover a significant surface of the total view screen) are indistinguishable from small, locally expanding, anomalies.

To mitigate the impact of these effects, one should ideally calculate spray widths at a large set of distances from the orifices and correct for retarded sprays by either artificially time-shifting retarded sprays to coincide with non-retarded data, or by creating a separate data set for retarded sprays. Such analysis would however be a disproportionate amount of work for the results attained. All results are interdependent but can not be combined together in a straightforward manner to produce a single ‘figure of merit’, without effectively reducing the data to the average fuel spray cone angles as determined in Figure 4.3.5. Spray width determination at a fixed distance from the orifice is however sensitive to local variations and insensitive to variations downstream of the spray, and it can be a useful tool to study detailed evolutions of ERAs in specific time/space windows. Figure 4.3.6 provides the average spray width evolution from all orifices and all injectors, determined at a fixed distance of 2.3 mm from the individual orifices.

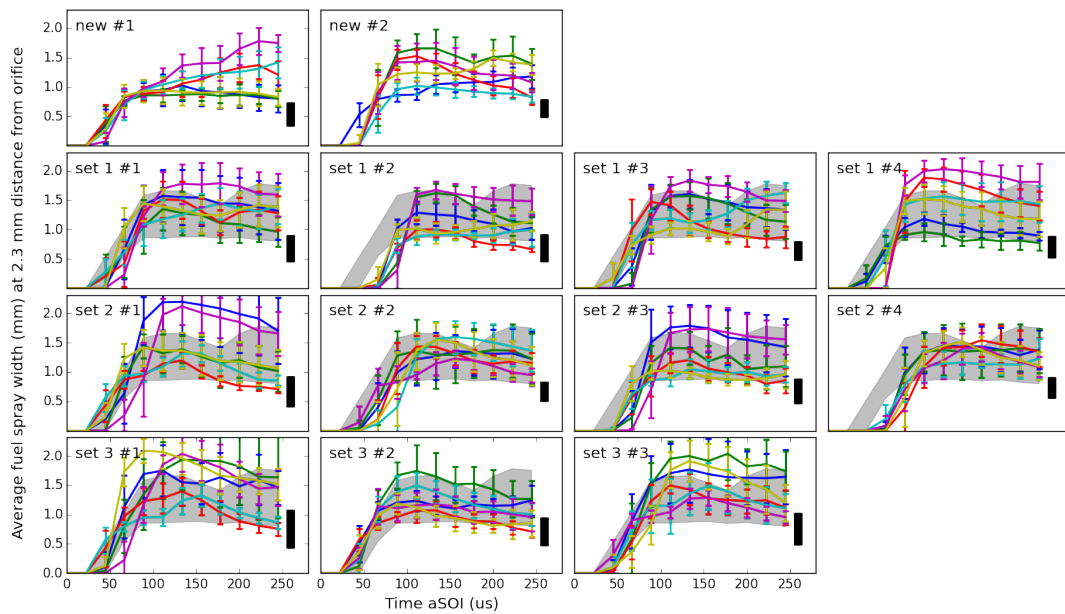


Figure 4.3.6: Average spray width of the emerging fuel spray, measured at a fixed distance of 2.3 mm from the nozzle tip, and plotted versus time. This graph should be considered *in combination* with the average spray cone angle graph, Figure 4.3.5. Most used injectors that show a minimal change in the average fuel spray cone angle w.r.t. new injectors in Figure 4.3.5, also show only a minimal difference in fuel spray width. Black bar on the far right indicates the spray width at 2.3 mm from the nozzle tip when the spray has stabilized, at 1 ms *aSOI*. Gray background indicates the spray width envelope of the new injectors, and has been added to all *Set 1 – Set 3* graphs to ease comparison.

At a first glance Figure 4.3.6 seems to provide similar information as Figure 4.3.5. Nearly every trend line appearing above the grey envelope in Figure 4.3.5 correspond to an observed increased maximum spray width in Figure 4.3.6. Additional details become visible when considering the evolution of the spray width at a fixed distance from the orifice, compared to the time evolution of the average fuel spray cone angle:

- *Retarded fuel sprays become visible* - For example two out of six orifices for injector *Set 2 #4* produce spray cone angles deviating from *New* injectors in Figure 4.3.5, however *all* spray penetrations from *Set 2 #4* are retarded, as the spray width evolution clearly lags with respect to the spray width from the *New* injectors.
- *Transient evolutions can be extrapolated* - Comparing the average spray cone angles with the average spray widths at 2.3 mm from the orifices for injector *Set 3 #1* indicates three transients are at their *largest* roughly 100 μs to 130 μs *aSOI*, as the spray cone angles in Figure 4.3.5 are greatest at that time. One of the sprays shows a maximum spray width 2.3 mm from the orifices at 80 μs to 100 μs *aSOI* in Figure 4.3.6, indicating the transient is not stationary, and continues to radially expand downstream of the measurement point.

Although these extrapolations are not full proof, they do allow a first screening to determine which (set of) measurements might provide additional interesting characteristics. Quantitative determinations of spray widths at fixed distances from the orifices should therefore not be used for the quantitative results, but rather as a first *qualitative* determination which data sets should receive further attention.

Average fuel spray cone angles proved to be the best indicator for transient radial anomalies. Both used and new injectors show an increased early fuel spray cone angle, and the high injection to injection variation of ERA morphology decreased overall impact of early radial anomalies on the average fuel spray cone angle. Nonetheless, the severe impact of some of these anomalies on the spray shape is sufficient to use the fuel spray cone angle for determining whether anomalous spray behaviour occurred. Based on the results treated in Section 3.2.2, radial expanding bulges were expected to occur from roughly 250 μs *aSOI* onwards for used injectors. ERAs often started well within the first 200 μs , as shown in Figure 4.3.4. Although the time of occurrence of the

formation of anomalies treated here and in the previous chapter do not coincide, based on morphology and appearance they are expected to be the same anomalies.

4.3.2.3 Late radial anomalies

In a subset of the data a second, smaller, bulge was observed that started as early as $200\ \mu\text{s}$ or as late as $350\ \mu\text{s}$ *aSOI*, and appeared from both new and used injectors. These late radial anomalies (LRAs) remained within the envelope of the earlier spray, or in the case of a used injector, within the circumference of the ERAs. Low contrast and lack of information required to do a full 3D reconstruction made analysis of these LRAs impractical. Qualitative observations of LRAs are provided, as contrast variations can be indicative of changes in flow velocities. Care should be taken conclusions based on these qualitative observations can not be confirmed.

Non-linear intensity rescaling, followed by posterizing the images, increased contrast of LRA transients, allowing anomalies as observed in Figure 4.2.9 to be studied closer. Figure 4.3.7 provides the occurrence and evolution of nearly coincidentally occurring LRAs from two opposing orifices of a used injector, shortly followed by a third anomaly from another orifice, all occurring within a single injection. This rather extreme case was hand-picked, and although the size of the LRAs were representative for these transients, three of them occurring within such a short time was not. Directly in front of the heads of the evolving transients it can be seen the intensity of the atomized cloud is less than the intensity of the LRA head⁸. As the spray is illuminated nearly perpendicular, this darkening can not be the result of a shadow cast on the spray plume, and it is assumed the reduced image intensity is the result of a reduction in atomized spray density. This *can* be indicative for a reduction in fuel flow velocity preceding the LRAs. Without a full 3D reconstruction of the whole injection this can however not be confirmed.

LRAs occurred equally well from both new and used injectors. Considering the time at which these transients occur, and the small width of the LRAs, it is assumed these anomalies are related to the needle reaching the upper seat.

⁸In the top row of Figure 4.3.7 this can also be seen in the original recordings, although contrast is lower than in the bottom image row.

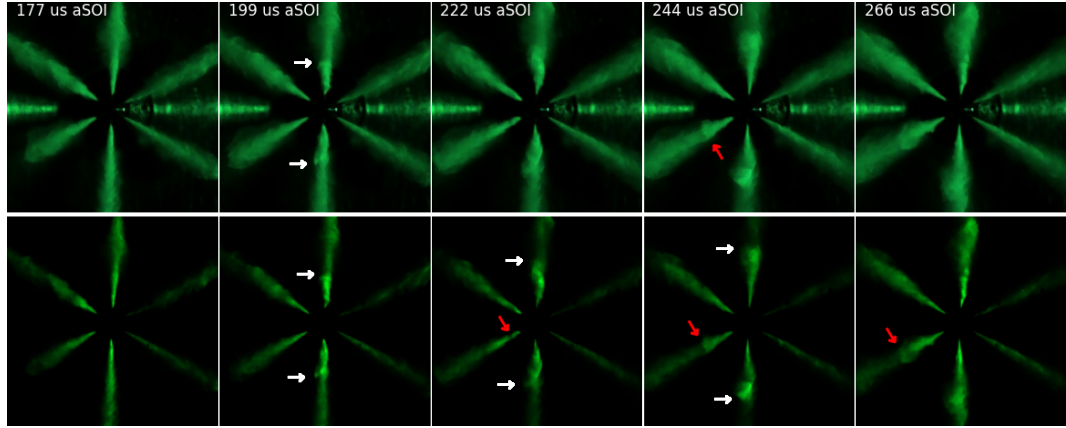


Figure 4.3.7: Occurrence of late radial anomalies (LRAs). Top image row provides the original recording of a LRA from a *Set 1* injector. Second row shows the same images after background subtraction and posterization to enhance visibility. White arrows in the top row indicate the first clear appearance of two LRAs. The red arrow indicates the start of a third LRA in this injection event. Arrows in the bottom row indicate the locations of the heads of the three LRAs.

4.3.2.4 Overview of transients treated in this Section

Considering the bulges observed in the previous chapter, and after having investigated the reduced spray penetrations in the previous section, the following conclusions can be drawn with respect to the three types of anomalies observed here:

- SOI *puffs* occur from both new and used injectors and are related to residual fuel in the orifices when an injection starts. These are not influenced by injector age.
- *Early radial anomalies* occur from used injectors, and are expected to be caused by internal flow alteration related to injector usage (deposits, wear). It is expected these ERAs correspond to the bulges observed in the previous chapter, despite ERAs observed in this chapter occurring at an earlier time. The high ambient density applied in the previous chapter is expected to be the cause for the observed delay.
- *Late radial anomalies* seem to correspond to the bulges observed in the previous chapter when considering the *time* of occurrence. The LRAs presented here occur for both new and used injectors, and the size of the anomalies are *much* smaller than observed in the previous chapter. It is therefore considered a coincidence the timings are of similar magnitude.

Origins of the observed small LRAs are expected to lie in internal injector mechanics unrelated to injector age/mileage (i.e. needle lift), as LRAs are observed equally well for both new and used injectors.

4.3.3 Stable spray regime

After the transient-rich start of injection the fuel spray enters the stable injection regime, where the majority of the fuel would be injected inside a firing engine. In this investigation the stable regime lasted for 0.3 ms to 1 ms, depending on the measurement series. The prime focus of this research was aimed at monitoring transient early spray evolution behaviour, and not all measurement series were suitable for analysis of the stable regime. The fuel injection period ranging from roughly half a millisecond after SOI up to EOI could be used to study the stable regime for the longest total injection durations of 1.5 ms. In this time window the fuel spray cone from a new injector is expected to be quasi steady-state, and remains unchanged until EOI, as injectors are designed and manufactured to inject a constant, unchanging, spray in the quasi steady-state regime. Analysis of this region is expected to produce clean and predictable results, where deviations and error margins are expected to reflect accepted manufacturing and operation tolerances, rather than being a measure for injector performance. For the deposit rich injectors, this is an interesting regime as it may shed light on the effects deposits and wear can have on the main part of the fuel injection.

The analysis and results treated in this section are based on the measurement *series 2* only, in *series 1* the stable regime was not recorded. The stable regime was visible in the time window from 555 μs to 1330 μs after the start of injection. Comparing this time window to the reported injection duration of 1.5 ms in Table 4.3, it can be seen the window does not extent up to the end of injection. The remaining 110 μs , corresponding to 5 recorded frames, the fuel spray evolution sometimes showed the presence of needle drop transients, and the injection was no longer in the stable regime. These anomalies will be treated in the next section.

At the beginning of the steady-state regime, roughly from 555 μs to 760 μs a_{SOI} , residual atomized clouds from anomalies that occurred in the initial transient-rich regime were often still present, and degraded analysis results of sprays in the stable regime. To minimize this degradation, an increased binarization threshold could be applied before determining quantitative results

in this region, mitigating distortion. It was however decided to reject the early data, as discontinuities resulting from suddenly changing thresholds would be unavoidable. Figure 4.3.8 provides sets of images recorded from several different injectors at two fixed times after the start of injection. Since the fuel spray shape was highly stable, the two time instances $aSOI$ that correspond to the beginning and the end of the stable spray regime were selected to maximize visibility of any spray change in the stable regime. The third row shows a binarized combination of the two upper rows, indicating in red the spray shape at the start and in green at the end of the stable regime. The white region provides the average spray shape, averaged over the complete stable regime. In the differentiating (third) image row, a residual background fog from early spray widening can be observed, visible by the red cloud extending beyond the white, averaged, spray circumference. The effect of this residual background fog has been eliminated in subsequent calculations by analysing only the time window from 760 μs onwards.

To quantify spray constancy, fuel spray cone angles have been determined for all injections and all injectors in the stable regime. Ideally the fuel spray cone angle in the stable regime provides a single number, as all orifices are identical and all injections were done at similar conditions. Both error margins of determined fuel spray cone angles, and structural differences in fuel spray cone angles for different orifices will provide an insight in system reproducibility in the stable regime. An additional advantage of determining fuel spray cone angle was the possibility of comparison to literature values of fuel spray cone angles at similar injection conditions. It is expected the determined spray cone angles in this investigation can deviate somewhat as evaporation is inhibited, resulting in wider sprays than would be measured in a high temperature environment. Figure 4.3.9 shows for all thirteen injectors the determined fuel spray cone angles in the stable regime, plotted versus time $aSOI$. Every graph contains six trend lines, corresponding to the six sprays from the individual orifices. For some used injectors different orifices produced different spray cone angles, i.e. the *Set 1 #1* injector in Figure 4.3.9 shows an empty band in between two groups of trend lines, indicating there is a structural change in the fuel spray cone angles from different holes. In a similar fashion, *Set 1 #4* shows there is a temporal transient widening for some sprays, as the upper trend lines show a local maximum in the determined spray cone angle at roughly 950 μs $aSOI$.

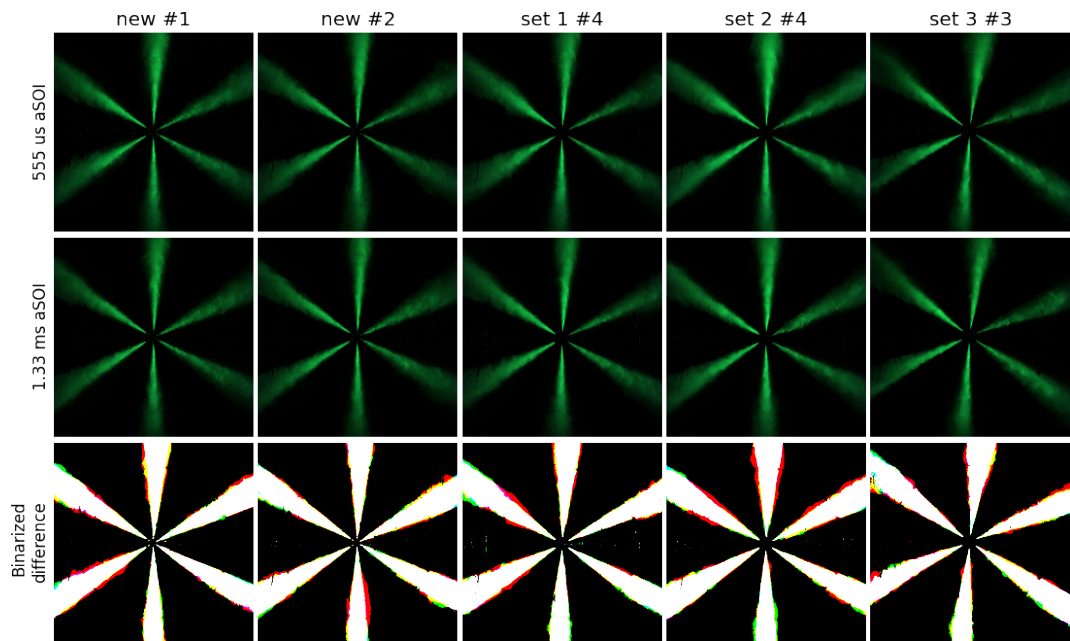


Figure 4.3.8: Image sets of the fuel spray in the stable regime. Top row provides images recorded from indicated injectors at $555 \mu\text{s}$ aSOI, second row same injections near the end of injection. Third row provides a binarized version of the top two rows, using *red* to indicate spray shape at $555 \mu\text{s}$ and *green* for 1.3 ms aSOI. White spray indicates the average spray shape, averaged over the complete quasi steady-state regime. Red overspill is expected to be the result of leftover transient expansions from the start of injection, which has been rejected for subsequent analysis. For the used injectors, injections *not* containing excessive radial anomalies at SOI have been deliberately selected. Image corresponds to an area of $3.9 \times 3.9 \text{ mm}^2$.

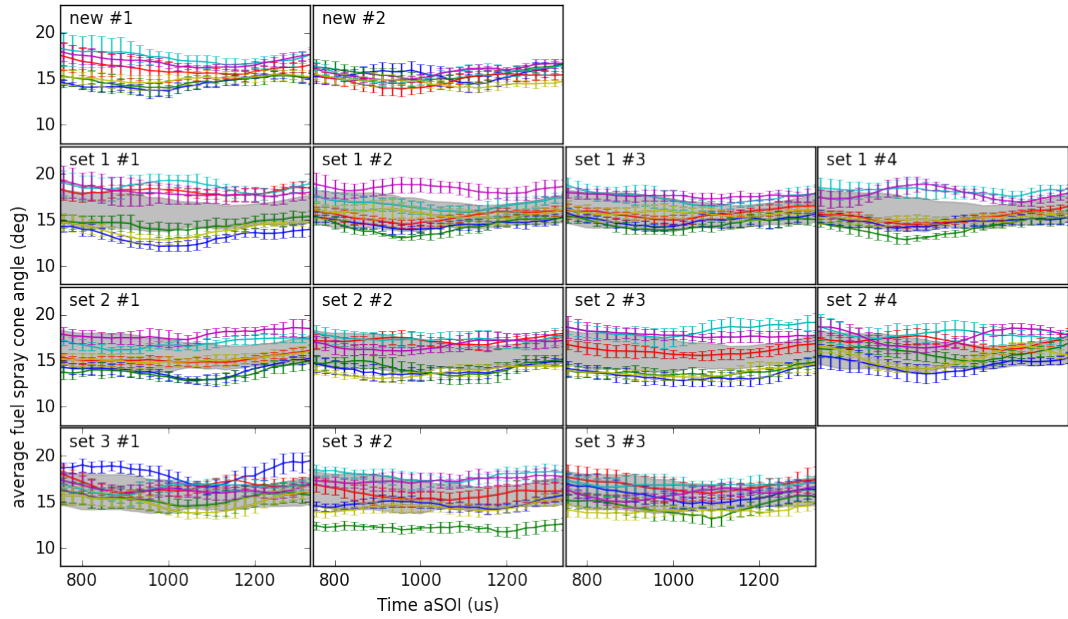


Figure 4.3.9: Fuel spray cone angle evolution in the stable regime for all thirteen injectors. The horizontal axis starts at $750 \mu\text{s}$ to eliminate residual cloud artefacts present before $750 \mu\text{s}$. Every data point provides the mean, with accompanying standard deviation, of at least ten angles determined from different recordings. Every trend line corresponds to the fuel spray cone angle measured from one of the six nozzle holes.

When the complete fuel spray is imaged under reactive or evaporative conditions, the definition of a fuel spray cone angle can be complicated, as the fuel spray will not have a straight spray edge up to the spray tip. The visible part of a typical fuel spray in the quasi steady-state regime would resemble the solid orange part of the spray depicted in Figure 2.1.2, and depending on the exact conditions, the part of the spray that produces a straight spray edge can vary in length. Measuring a spray cone angle therefore requires defining selection criteria for the part of the spray one takes into consideration for the analysis. In the present investigation this ambiguity does not occur, as the limited field of view serves as a natural cut off, i.e. in the stable regime the spray tip lies outside the field of view, and the recorded sprays provide a straight spray edge up to the point where the spray leaves the field of view. A less well-known parameter that can impact the measured spray cone angle is the detection algorithms applied for the analysis, and a different binarization algorithm can lead to a significant change of the spray cone angle. For example, [87] provides a comparison of two commonly used algorithms, and shows changing the algorithm can lead to a change of 25% in the measured spray cone angle. In the present investigation no image segmentation was applied, i.e. the complete

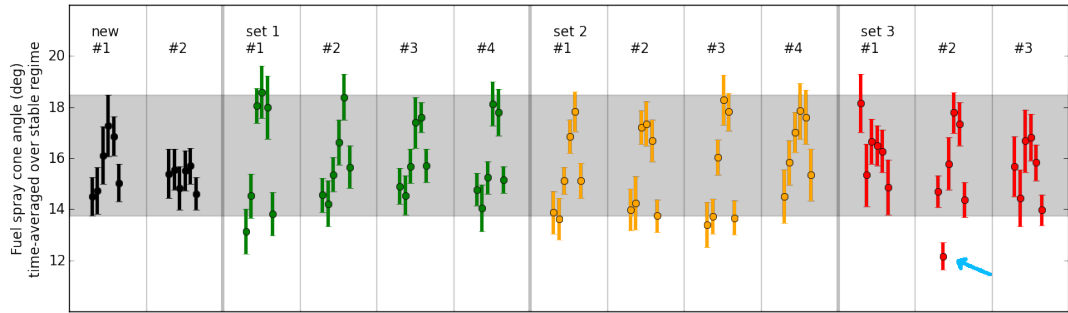


Figure 4.3.10: Spray cone angles for the individual orifices of all injectors, averaged over the full stable region and the complete measurement series. The horizontal axis is divided into thirteen sections, one for each injector, each section containing the average spray cone angles measured for all six orifices of the indicated injector. (black) Two *New* injectors, (green, orange, red) *Set 1 – Set 3* injectors. Gray horizontal band shows maximum and minimum spray angles (plus standard deviations) from the two new injectors. There is only *one* orifice from *one* injector, indicated by the blue arrow, that clearly deviates from the average fuel spray cone angle determined from the new injectors. Note the vertical axis does not start at zero.

visible spray was analysed, and for binarization the standard OTSU method was applied.

As can be seen in Figure 4.3.9, all spray cone angles from all orifices are nearly constant in the stable regime, and an average spray cone angle can be determined for all orifices and injectors, averaged over the full stable regime. This allows for easy graphical comparison of all average spray cone angles as the time evolution is averaged out. Figure 4.3.10 shows the combined results for all thirteen injectors investigated in this research, where the time-averaged spray cone angle from every orifice of every injector is plotted versus orifice number for every injector.

Figures 4.3.9 and 4.3.10 indicate the stable regime is indeed providing a stable fuel spray, even for the 90k-mile *Set 3* injectors. For the used injectors the averages show a higher spread compared to new injectors, i.e. the measurement points for the averaged spray cone angles in Figure 4.3.10 show a larger spread than for the new injectors. There is no severe fuel spray cone angle deviation observed for used injectors compared to new injectors, with the one exception indicated by the blue arrow in Figure 4.3.10.

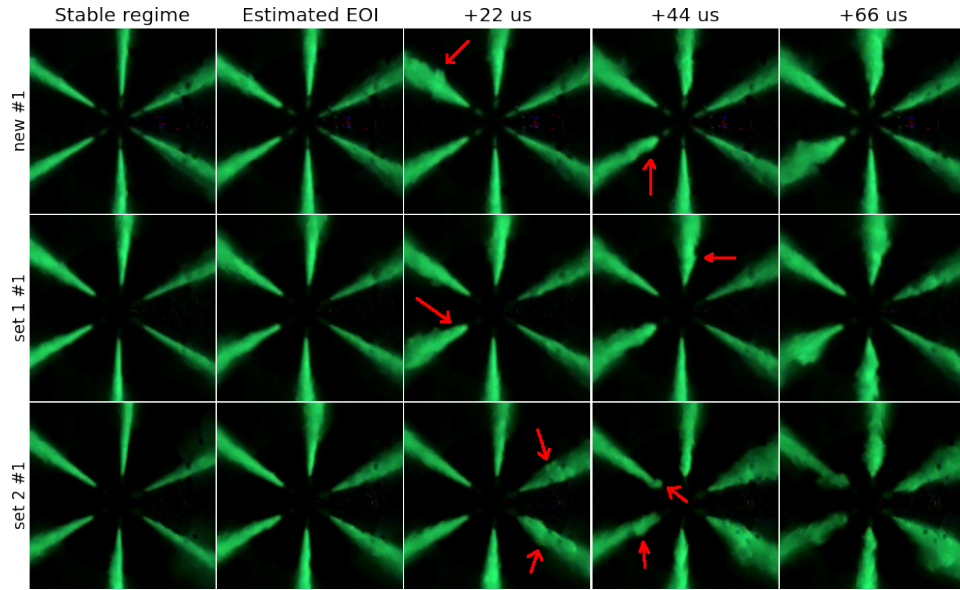


Figure 4.3.11: Transients occurring shortly before the fuel injection terminates. These transients are expected to be caused by changes in the internal geometry during needle drop, leading to an altered internal fuel flow. Every row represents a single EOI event, red arrows have been inserted to emphasize the occurrence of transients in the subsequent spray evolution. First image column corresponds to the spray in the stable region, roughly 0.5 ms *bEOI*. Estimated EOI is based on the visible presence of EOI puffs. Images correspond to a $10 \times 10 \text{ mm}^2$ area.

4.3.4 End of injection

The closing of the valve at the end of injection, the drop of the needle, produces anomalous EOI effects. These effects are extremely short lived, due to the short closing time of the valve, and are visible as slight puffs near EOI. These puffs were observed in a time window $130 \mu\text{s}$ to $65 \mu\text{s}$ before the visible liquid flow out of the orifice ceased, depending on the injector and injection conditions. Although these EOI transients could be subject of an extensive study on anomalous EOI behaviours, they were not considered in this research. Here, they were noted as being present, and care was taken to prevent these effects from accidentally being included in the data used in the previous section. The observed effects have been included in the thesis, and examples are provided in Figure 4.3.11, to discriminate between EOI transients occurring during needle closure, and post-injection expulsions treated in the subsequent section. From a practical point of view, the occurrence of EOI puffs provided a clearly visible spray change suitable for determining the end of an injection.

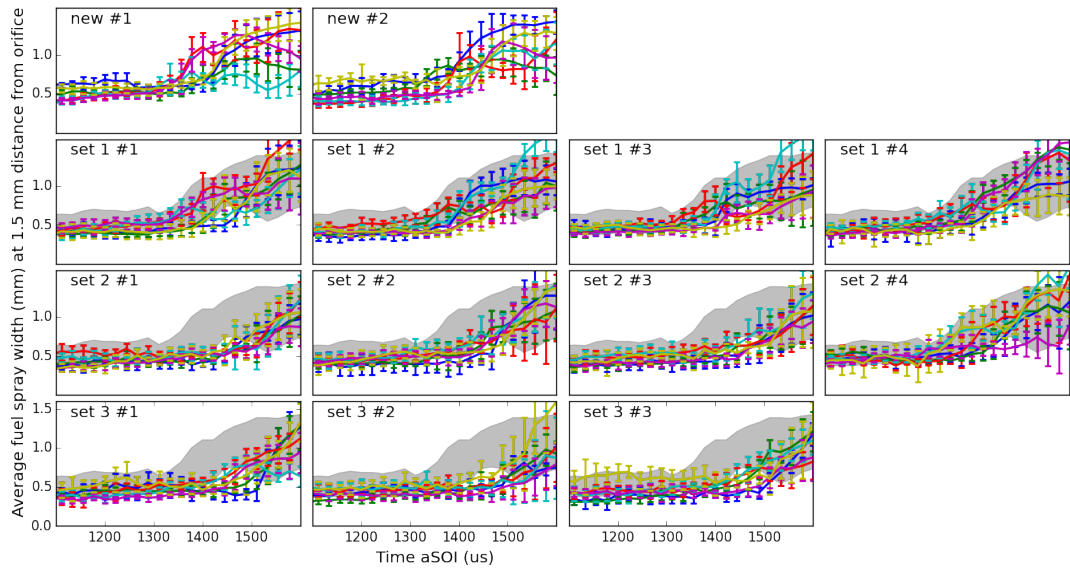


Figure 4.3.12: Spray width of the fuel spray 1.5 mm downstream of the orifice, measured at the end of injection. Horizontal axis provides time $aSOI$, vertical axis provides the spray width. Every graph indicates the average spray width for every individual orifice, averaged over at least ten recordings. The grey background present in the graphs on rows 2, 3, and 4 provide the spray width envelope from both new injectors as a reference. No discrimination is possible between spray widening resulting from radial diffusion of the main fuel spray, and spray widening resulting from needle closure puffs.

The observed radial expanding transients shortly before EOI led to local spray widening. As a rudimentary analysis of EOI spray widening, the spray widths for every injection and every individual orifice was determined at 1.5 mm distance from the orifice at the end of injection, and the determined spray widths are provided in Figure 4.3.12. Not every injection showed the presence of EOI puffs resulting from needle drop, however all sprays from every orifice in every injection did show post-injection spray widening of the main fuel spray. The spray widening depicted in Figure 4.3.12 provides no obvious insight in the EOI puffs and their morphology. The spray widening is however showing an interesting additional characteristic. All injections showed spray widening, but the retarding of the onset of $aEOI$ spray widening for a subset of injectors (injectors *Set 2 #1,2,3* and *Set 3 #1,2,3*) shows these injectors all had the EOI *structurally* delayed by $50\ \mu s$ to $100\ \mu s$.

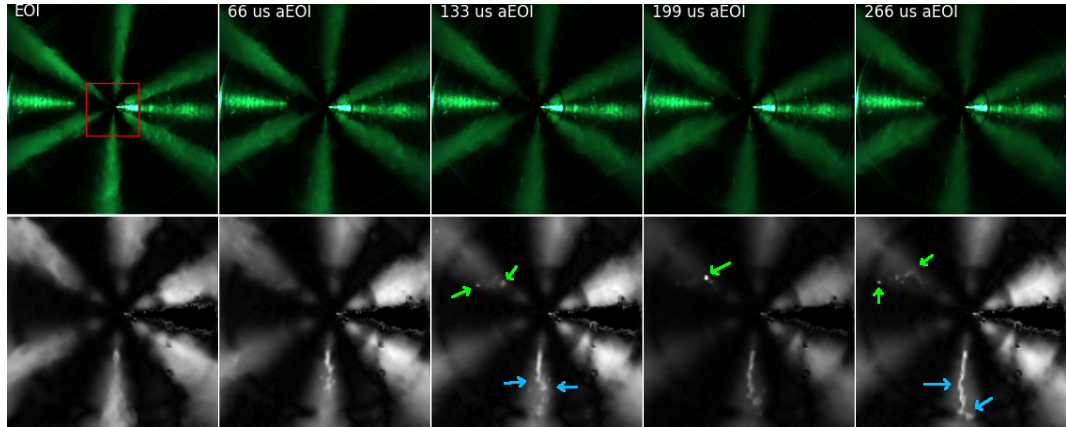


Figure 4.3.13: Image set of post-injection ligament expulsion. Leftmost image provides the end of the (atomized) main injection. Subsequent images are recorded at the indicated time $aEOI$. Top row provides the original recording without any filters or corrections, showing ligament and droplet visibility is poor due to low contrast compared to the atomized stage. Bottom row provides an enlarged view of the central part of the corresponding image in the top row (red square) after contrast optimisation. Note how the ligament evolves in a wiggling way (bottom orifice, blue arrows), and how another orifice (top left, green arrows) shows droplet expulsions. Injection was from a new injector at a common rail pressure of 100.0 MPa into a 3.3 MPa non-reactive background at 114 °C. Image scale top row $30 \times 30 \text{ mm}^2$, bottom row $7.5 \times 7.5 \text{ mm}^2$.

4.3.5 Post-injection expulsions

After needle closure at the end of injection, and after any transients as treated in Section 4.3.4, fuel injection into the ambient environment has ceased completely. Residual fuel will however still be present inside the SAC and nozzle holes after needle drop. This residual fuel in the nozzle can be ejected post-injection, as was shown in Section 2.1.4. In the current investigation, post-injection expulsions of liquid fuel was clearly and unmistakably observed for all injections, and from all injectors, for all recordings in the CVC. An example of a liquid expulsion is provided in Figure 4.3.13 where post-injection recordings clearly show the simultaneous expulsion of ligaments and droplets from several orifices. These ligaments and droplets have been investigated to determine whether $aEOI$ expulsions can be used as an indicator for injector quality, i.e. if the amount of ligaments and droplets, or their morphologies, can be correlated to the injector state.

Ligaments and droplets were quantified by determining the total observed surface covered by ligaments and droplets after the end of injection. A rigorous filtering algorithm pipeline was applied to extract droplet surface pixel count. An example of the different stages of the analysis is provided in Figure 4.3.14, the main components of the algorithm consisted of:

- *Basic image enhancement* - Subtracting specular backgrounds, renormalizing the intensity histogram, and applying a non-linear rescaling of the intensity histogram greatly enhanced contrast of the liquid features under investigation (second row in Figure 4.3.14).
- *Sector masking* - Based on the full evolution of the spray, parts of the image that lie outside the regions of interest were masked out. Areas in the recorded images where sprays never occurred, i.e. the central tip of the injector within the ring of nozzles, and the regions in between adjacent sprays, were blanked out to reduce the amount of false-positives in the subsequent steps.
- *First droplet and ligament candidate screening* - An edge-detect algorithm marked all locations where (relatively) sharp transitions in intensity occurred over a distance of a few pixels. These edges corresponded to either droplets and ligaments or to specular artefacts. All *closed* areas of thus-detected edges were considered potential candidates (third row in Figure 4.3.14).
- *False-positive screening* - Detected droplets and ligaments that remained stationary during the full post-injection time, or that were already present before the main injection had ended, were considered specular artefacts. These were rejected as false-positives, since droplets and ligaments should not occur before the end of injection and should not remain stationary.
- *Summation of all detected droplets and ligaments* - After having determined all pixels that were covered by liquid expulsions, direct counting of the amount of covered pixels resulted in a quantified pixel area for every post-injection frame of every recording (bottom row in Figure 4.3.14).

It is apparent that the application of such a multitude of steps can lead to data loss, most notably the erroneous division of ligaments into individual droplets. The bottom right image in Figure 4.3.14 shows the liquid ligament ejected

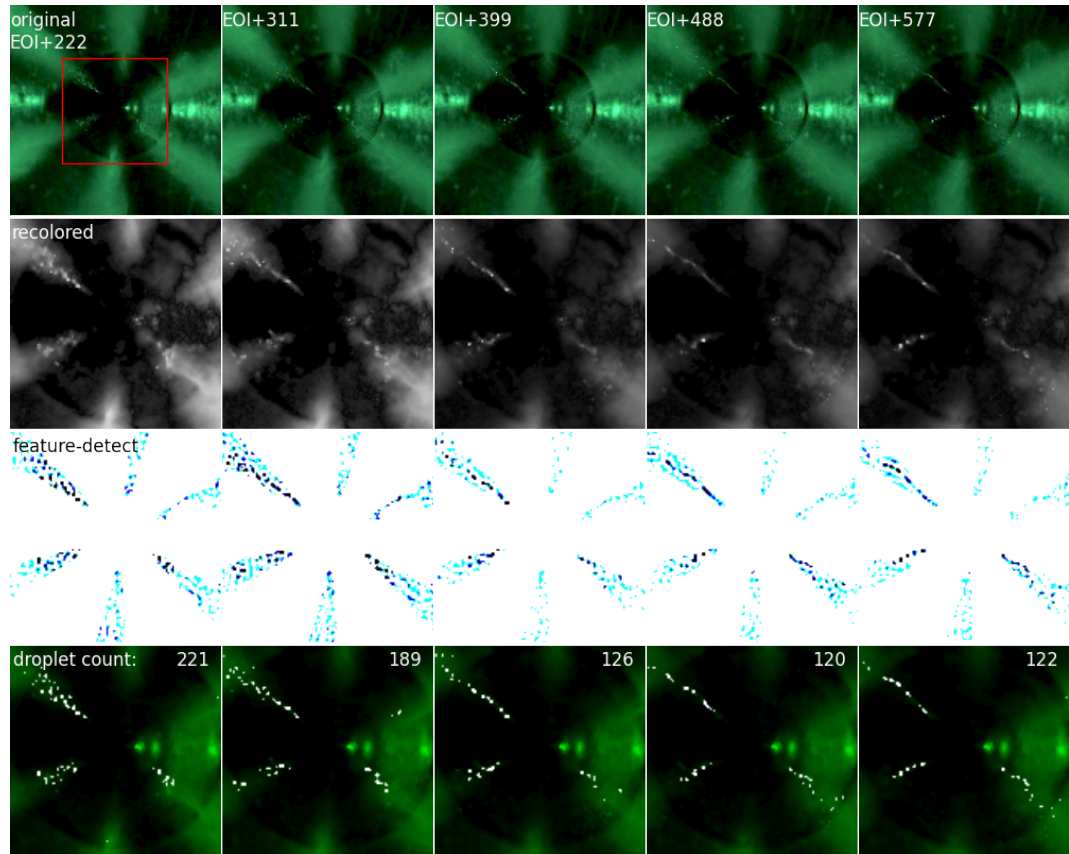


Figure 4.3.14: Image manipulations applied to extract droplet surface counts. From left to right every column provides a different time instance in the expulsion process of a single injection event. Top row provides the original recording, second row shows a background-corrected and non-linear re-intensified image, where the visibility of ligaments and droplets has improved. Third row shows ‘liquid candidates’ after application of a detection algorithm. Fourth row provides a combined view of the original recording (green) with detected ligaments and droplets reinserted as white pixels. The images in the second to fourth row provide a magnified view of the area indicated by the red square in the top left image.

from the top left orifice was interpreted as a stream of independent droplets by the algorithm. Comparison of algorithm results to manual counting in a subset of the data showed the algorithm underestimated ligament and droplet surfaces by up to 15%. Subsequent frames from a single recording, where changes in ligament and droplet morphology led to a significant change in the effectiveness of the algorithm, were co-analysed to improve accuracy of the results. The 15% surface underestimate was thus reduced to a typical error of approximately 6%. This frame combination strategy must be applied with care, as the total amount of ligaments and droplets changes during the post-injection expulsion. Ligaments tended to grow, providing a larger surface count at later times *aEOI*, while high velocity droplets left the view screen as time advanced. To prevent stacked uncertainties from this process, all analyses were conducted on a fixed subset of recorded post-injection frames. The time window selected for this subset of frames was determined by full analysis of several post-injection expulsion recordings, and determining when the *average* amount of ligaments and droplets was nearly constant.

Averaging the determined covered pixel surface in this time window provided an average surface estimate with accompanying error margin suitable for subsequent comparisons. Although the detailed dynamic processes of post-injection ligament and droplet expulsions were lost by time averaging, every single injection was characterized by a single number (plus error margin) suitable for further analysis. Comparison of total numbers of droplets ejected for every recorded injection showed there was no consistency in the amount of ejected ligaments and droplets for injections from a given injector. Total covered pixel areas, i.e. the calculated droplet surfaces, varied from injection to injection for every injector, and participating orifices changed in a non-repeatable sense from injection to injection. Figure 4.3.15 provides the determined surface counts for ten chronologically subsequent measurements from four injectors. The determined droplet surfaces changes in a non-predictable way for every subsequent injection, and based on the trendlines there is no difference between new and used injectors.

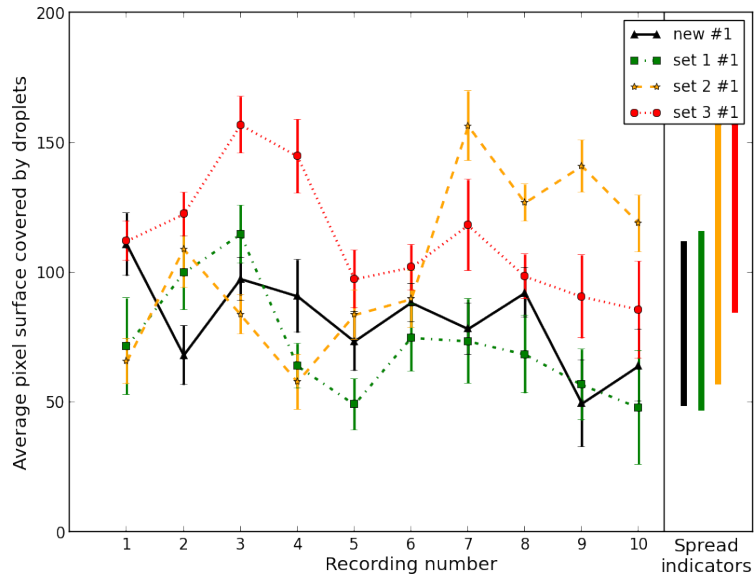


Figure 4.3.15: Trend lines for the total amount of ejected ligament and droplet surfaces. Every graph corresponds to a different injector, where horizontally the chronological recording number is plotted, and vertically the average post-injection droplet expulsion surface, expressed in pixels. Four solid bars on the far right indicate the spread in the plotted graphs, i.e. the bars extend from the lowest to the highest observed pixel surface count for any injector, and serve as an indication for the inconsistency in the amount of ejected ligaments and droplets.

By reducing all injections from one injector to a single *spread interval*, as depicted on the far right in Figure 4.3.15, comparison of expelled ligaments and droplets from different injectors became possible. Figure 4.3.16 provides a comparison of the ligament and droplet expulsions, where every bar corresponds to the range of measurement results of the given injector. For example, the very first vertical bar ranges from 68 to 117 on the vertical scale. This indicates that from all measurements of the *New #1* injector, the *lowest* determined pixel surface of any post-injection expulsion covered 68 pixels, while the *highest* observed surface count covered 117 pixels. All other measurements from this one injector provided surface counts somewhere in between these two values. Figure 4.3.16 provides results from two datasets, one dataset recorded from six injectors at a common rail pressure of 100.0 MPa and a dataset of all thirteen injectors recorded at a common rail pressure of 80.0 MPa.

As stated at the beginning of this chapter, results presented here have been published in a conference paper [83] and a journal article [84], and the two datasets in Figure 4.3.16 correspond to the two data sets used for the two publications. The numerical results of the analysis however slightly differ

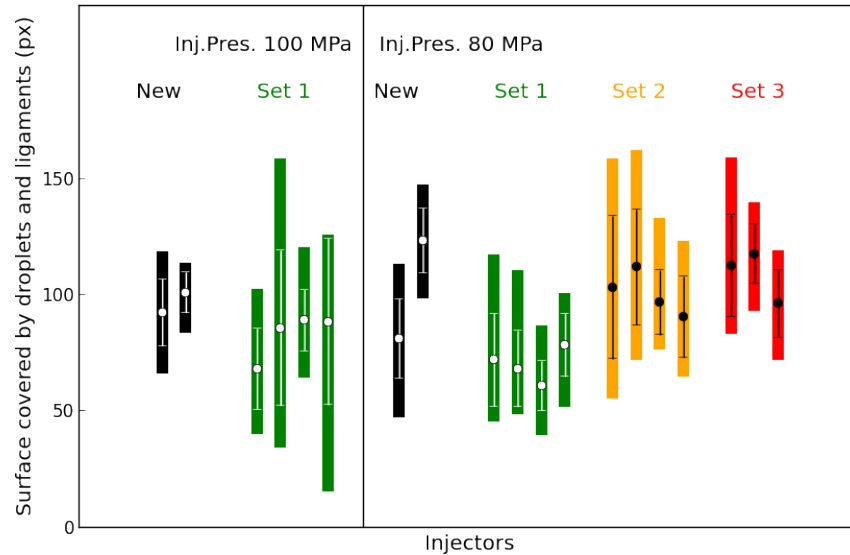


Figure 4.3.16: Post-injection expulsions reduced to a single indicator per injector. Every data bar provides the spread in determined $aEOI$ expulsion surface for that specific injector. First six bars indicate determined expelled pixel surfaces from *New* and *Set 1* injectors, injecting at a pressure of 100.0 MPa. Subsequent thirteen bars provide results measured at an injection pressure of 80.0 MPa. The means and standard deviations have been included within the spread indicators.

between the results published in the two references and published here. The general trend and overall conclusions remain the same, but graphs containing numerical results differ as optimized algorithms extracted higher numbers from the data. This also reduced algorithm-induced noise and provided higher overall surface counts. The high level of injection to injection variations remained present, and comparison of results from different injectors still provided the same conclusion: There is no observable difference between injectors of different mileage.

4.4 Discussion

Based on the measurements treated in this chapter, it is clear fuel sprays show several transient characteristics during injection. Table 4.4 provides a short overview of the most relevant transients, their main characteristics, and expected causes.

The first, fourth, and sixth entry in Table 4.4 regards minor puffs which are expected to be related to needle motion, and occur for both new and used injectors. At the fifth point, in the stable regime, no significant difference in spray shape between used and new injectors was observed. The last entry,

Time window	Observed effect	Possible underlying mechanics	Comments
SOI up to 88 μs <i>a</i> SOI	Pre-injection <i>puff</i> SOI	Residual fuel from an earlier injection is expelled at start of a new injection.	Very hard to discriminate in the current setup, occurred for all injectors.
44 μs to 200 μs <i>a</i> SOI	Reduced early spray penetration	Internal flow alterations resulting from wear or deposits.	Observed only for used injectors. Highly repeatable hole to hole variation in early spray penetration.
70 μs to 300 μs <i>a</i> SOI	Radial expanding anomalies (ERA)	Coupled directly to reduced early penetration; momentum transfer from axial to radial.	Occurred from orifices that showed a reduced early spray penetration. Injection to injection variation w.r.t. shape and size is large.
250 μs to 350 μs <i>a</i> SOI	Puff at end of transient period (LRA)	Needle reaching upper seat position produces flow instabilities.	Observed from all injectors, used injectors seem slightly worse. Only very tiny alteration visible, not always present.
500 μs <i>a</i> SOI up to EOI	Stable region	-	Highly stable spray shape. Some used injectors show structural difference in spray width. High reproducibility of spray cone angle.
At EOI	EOI puff	Needle drop closes valve, alters injection pattern due to sudden change in pressure difference SAC-cylinder.	Slight widening of atomized stage, sometimes observed from all orifices simultaneously. Occurs for all injectors.
EOI to 1 ms <i>a</i> EOI	Post-injection droplet expulsion and ligament formation	Momentum conservation or ingestion of gas into the SAC forces liquid fuel out at low velocity after valve closed.	Not related to injector dribble originating from travelling pressure waves or other 'cracking pressure'-related causes.

Table 4.4: Overview of different spray anomalies and injection regimes treated in this chapter.

post-injection expulsions, is expected to have a noticeable effect on engine-out soot. These a EOI expulsions occur equally well for new and used injectors. The two remaining points, entries two and three in Table 4.4, are strongly coupled and indicate injector age/mileage can impact early spray evolution. The listed effects in points two and three of Table 4.4 were not observed for new injectors.

It is unclear how the observed reduced fuel spray penetration, and accompanying radial expansion, affect combustion. These effects are short lasting transients occurring in the very early start of injection, before the main fuel flow (stable regime) has fully developed. The reduced penetration is resolved generally within roughly $250\ \mu\text{s}$ a SOI, and hole to hole comparison of spray lengths provide a symmetrical injection pattern before the stable regime commences. The accompanying radial expansions are short lived, and are expected to contain only a small amount of fuel. These arguments would favour the conclusion that early spray anomalies from used injectors will have no significant effect on combustion.

However, considering the injectors under investigation were designed for a total injection period of 1 ms to 3 ms (depending on load) in a running engine, transients lasting for 0.25 ms can cover a significant part of the total injection duration. For operating conditions implementing multiple injections, or split pilot-main injections where individual injections last shorter than 1 ms, the relative importance of reduced early spray penetrations will increase. In addition, fuel from the radial expansions remain present close to the orifice for the full injection period, and diffusion-mixing with air can lead to the formation of fuel-air mixtures within the combustible limit, several millimetres from the nozzle tip. These fuel-air mixtures may self-ignite, and continued air entrainment into the main fuel spray will entrain combustion products instead of 'fresh' air. This can impact downstream ignition, flame lift-off length and possibly soot formation.

Subsequent study of combustion characteristics, most notably the effect of local fuel vapour pockets on the early combustion, is paramount in understanding the relevance of the observed anomalies. Studies have started at Brunel University London on these aspects, and early ignition near the nozzle is investigated both for new and used injectors. This additional work is however not the sole work of the Ph.D. candidate, and inclusion of preliminary results in this thesis would not be appropriate.

Injectors	Average fuel spray cone angle	
	Early spray, 65 μ s to 240 μ s	Stable regime, 750 μ s to 1330 μ s
<i>New</i>	$25^\circ \pm 5^\circ$	$15.5^\circ \pm 0.8^\circ$
<i>Set 1</i>	$30^\circ \pm 8^\circ$	$15.9^\circ \pm 1.6^\circ$
<i>Set 2</i>	$31^\circ \pm 7^\circ$	$15.7^\circ \pm 1.6^\circ$
<i>Set 3</i>	$31^\circ \pm 7^\circ$	$15.7^\circ \pm 1.4^\circ$

Table 4.5: Average fuel spray cone angles measured in the CVC.

Table 4.5 provides an overview of the determined fuel spray cone angles calculated in this chapter. Comparison of results in these tables to literature values is treated in Chapter 5. The standard deviations (SDs) reported in Table 4.5 reflect a combination of uncertainties, as was discussed in Section 3.4.3. Due to the increased resolution of the FASTCAM camera with respect to the MIRO4 camera system, the uncertainty resulting from image resolution was strongly reduced. A slight mismatch between injection and focal plane was still present, but due to the fixed position of the injector, this uncertainty had become a known systematic error, and spray cone angles and penetrations have been corrected for the mismatch. Analysis of the data showed the uncertainty in spray cone angle resulting from limited camera resolution was on the order of 0.2° for an individual fuel spray, and on the order of 0.08° for the combined averaged set. The reported SDs for the spray cone angles in the initial transient regime in Table 4.5, are for more than 95% the result of injection to injection variations. For sprays in the quasi steady-state regime, injection to injection variation was the dominant factor influencing the SD for new injectors. Considering Figure 4.3.10, it is expected that for used injectors the hole to hole variations in the mean spray cone angles had the highest impact on determined SDs.

At the end of Section 4.1.2 it was noted the *Set 2* injectors had received an after market cleaning agent at approximately 30,000 miles. Although the effectiveness of the cleaning agent on removing deposits was not known, two extreme possibilities (perfectly clean vs. no effect at all) were provided. Considering the spray images in Figure 4.2.4 and the results provided in Figures 4.3.1, 4.3.10, and 4.3.12, it is clear *Set 2* injectors are not performing as good as the best-performing *Set 1* injectors. It is however equally clear from all data generated in this investigation that injector to injector variation *within every group* is high. Taking the variations within each injector group into account, it would be inappropriate to make a claim about the effectiveness or quality

of the cleaning agent. Note in this respect that only statements about the impact of the cleaning agent on the *injectors* could be made. If, for example, the cleaning agent was aimed at removing deposits in the fuel system upstream of the injector, the impact of the cleaning agent could not be determined in the present investigation, as only spray characteristics from these injectors were studied.

4.5 Conclusion

The datasets and injectors treated in this chapter show spray characteristics of used injectors can deviate from the spray characteristics of a new injector. The start of injection can show a highly asymmetric hole to hole spray penetration for used injectors, and radial expanding anomalies were observed as well. These effects indicate spray tip velocities are reduced, or fuel momentum is redirected from axial to radial, for some of the orifices during the transient start of injection. In the quasi steady-state spray regime there is little difference between injectors at different stages of their lifetimes. Transient effects observed in the early stage of spray formation for used injectors, show a high repeatability for some spray deformations, most notably the reduced early fuel spray penetration seems highly repeatable in participating orifice, penetration reduction, and subsequent evolution. Radial expansions of the evolving fuel spray at SOI, occurring only for orifices showing a reduced penetration rate, are nearly always present and show large injection to injection variations in size and shape. These transients indicate axial momentum is temporarily transferred to radial momentum at SOI, influencing penetration rate.

In general higher mileage injectors produced more pronounced and stronger deviating transients at the start of injection. Nonetheless, for all sets of injectors *not all* injectors suffered spray degradations, and at least one injector from every group of the used injector sets occasionally showed spray behaviour similar to the injection pattern from a new injector.

In the stable regime used injectors provided spray shapes comparable to new injectors, but several used injectors could provide an increased spread in spray cone angles from different orifices. The fuel spray cone angles were highly constant from injection to injection, and with a few exceptions the fuel spray cone angles remained constant in the stable regime.

All injectors, under all injection conditions into a gaseous backpressure

medium, showed the expulsion of ligaments and droplets after the injection had ended and the needle was in the closed position. There was no quantitative difference between different injectors and their expulsions, i.e. injector mileage and/or deposits seemed to have no effect on the post-injection expulsions. The total fuel volume released by these post-injection expulsions is low compared to the total amount of fuel injected. The expected impact on combustion inside a real engine is expected to be minimal, however the fuel is injected at the end of the injection cycle, and the ejected ligaments and droplets are expected to lead to (increased) in-cylinder soot formation.

Chapter 5

Discussion of results

In Chapter 2 empirical mathematical models for determining key parameters during spray formation and breakup were treated. In addition a qualitative, conceptual model of the complete injection–combustion process was provided, which included recent investigations on transient aspects of spray formation and evolution. The shape and evolution of a fuel spray from a diesel injector can be predicted qualitatively based on injection conditions, and when sufficient details of the system are available several parameters can be calculated quantitatively a priori. There is a high level of agreement of both conceptual and quantitative models to experiments.

This chapter compares qualitatively the similarities and differences between spray shapes imaged in Chapter 4 to those treated in Section 2.1. In addition, key spray characteristics have been calculated to determine if measured spray parameters correspond to expectations based on the empirical models treated in Chapter 2. Thus, it will be determined to what extent the spray shapes imaged in this research are comparable to those one would observe inside a real-world, firing engine. Results from Chapter 3 are not treated in the present chapter, as the ambient conditions applied in Chapter 3 are not representative for real world engines, and the models treated in Chapter 2 do not apply.

5.1 Qualitative comparison of spray evolutions

Measurements and analysis conducted in Chapter 4 provided insights into the impact of injector age (mileage) on the evolution of high pressure diesel sprays. The effect of injector usage on the spray shape was studied by comparison of spray characteristics from used injectors to those of new injectors. All

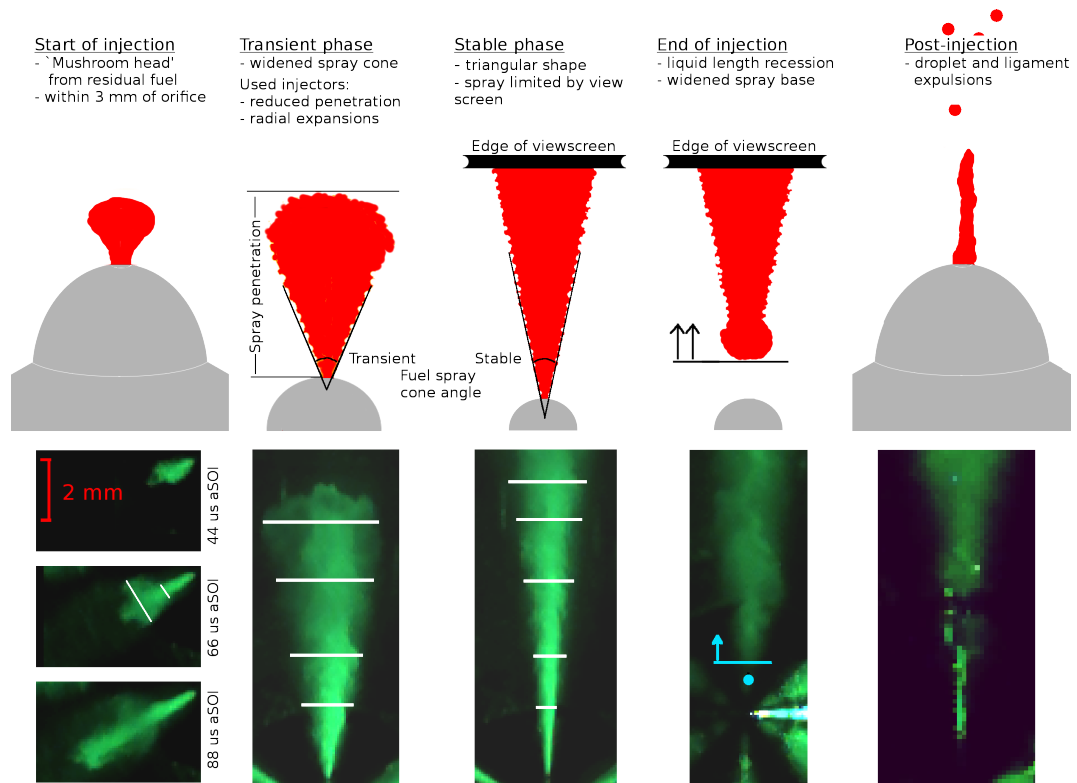


Figure 5.1.1: Qualitative treatment of different stages in the injection process, in combination with the characteristics observed in this work. The second row contains images recorded in this work and showing the indicated behaviour in the cartoon in the top row. White lines in bottom images indicate spray widths at different positions in the spray. Blue dot and horizontal line in fourth image column provides the position of the orifice and the edge of the spray. Brightness of images has been increased to enhance visibility, the last image shows pixellation due to an increase in magnification and contrast enhancement.

transient characteristics treated in Sections 2.1.1, 2.1.2, and 2.1.4 were observed in measurements conducted in the CVC, and have been treated in Chapter 4. In addition, for used injectors two more anomalies were observed during the transient, needle opening phase; A reduced early penetration rate, and radially expanding bulges. The reduction of early spray penetration has been shortly mentioned in Section 2.3, and has been observed by other groups [72][73][74] during the time this investigation was conducted. The radial bulges observed in this work have not been discussed in the investigations treated in Section 2.3, although an alteration of the average fuel spray cone angle was observed in the investigations treated in Section 2.3.

The spray shape at different stages of injection as recorded in this work can be compared to those treated in Section 2.1. Figure 5.1.1 contains a modified overview of the different stages of diesel injection, similar to Figure 2.1.12,

mimicking the recording conditions applied in the current investigation for a new injector. The combustion phase has been removed, the spray tip has been cut off by the edge of the view screen, only the atomized spray phase is visible, and the injector is opaque. Underneath the cartoons in Figure 5.1.1, images as recorded in this work have been provided that show the same spray evolution stage.

From a qualitative point of view, images recorded from the new injector show no deviation compared to what would be expected inside a quiescent diesel engine, apart from the lack of evaporation and combustion. It was shown in Chapter 4 that the used injectors produced essentially indiscriminate spray shapes from the new injector, with the two exceptions mentioned above: A reduced spray penetration, and accompanying radial expansions within the first 0.5 ms of the injection. The images of reduced spray penetrations in this work are similar to those in [72], and a side-by-side comparison of the recorded penetrations from [72] to sprays measured in this work is provided in Figure 5.1.2. It can be seen that the observed spray penetration reduction behaves in a qualitatively similar way. The fouled injectors show hole to hole variations in penetration during the initial stage of injection, but the reduced penetration has been resolved by its own at the end of the transient phase.

The observed radial expanding anomalies have not been treated in literature to date, and no material is available to compare the anomalies to. Considering the radial expansions occurred for most of the used injectors and under varying injection pressures, the radial bulges are assumed to be characteristic for used injectors that show reduced early penetrations. A possible cause for the anomalous penetration reduction, and subsequent transient widening of the spray, may be found in an altered fuel flow inside the SAC nozzle, caused by the presence of deposits. Without investigation under reactive conditions, the impact of these bulges on combustion can not be confirmed. A comparison of the fuel spray shape near the end of injection of a deposit rich injector to the spray shape from a new injector does provide some insights on the possible significance of these radial expansions. Although the radial expanding anomalies occur early in the transient regime, and quickly diffuse into the surrounding environment, the low temperature inside the CVC prevented rapid evaporation of the anomalies. By application of a low binarize threshold, residual atomized fuel from the radial expansion at SOI can be made visible close to the injector tip, nearing the end of injection.

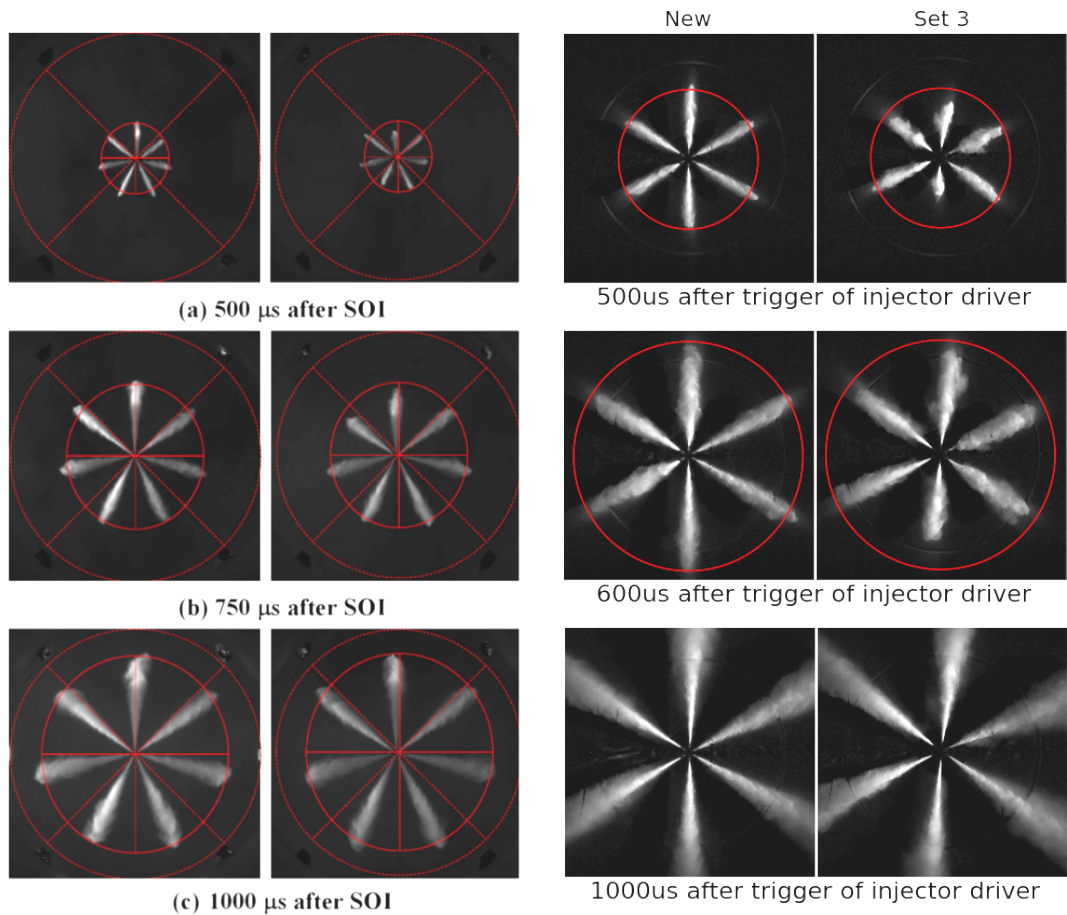


Figure 5.1.2: Comparison of the reduction in early penetration observed in this work to [72]. Image scales differ, and the number of orifices in [72] was seven. Left two columns provide the spray penetration for a new and a fouled injector imaged in [72]. Right two image columns provide the penetration recorded in this work for a *New* and a *Set 3* injector. The time of recording of the middle row in the right image set was slightly earlier compared to the left images, as at $t = 750 \mu\text{s}$ the sprays had reached the end of the view screen in the present work. Times stated *aSOI* for the left image sets correspond to the time after the solenoid current was applied, reported in the right set of images.

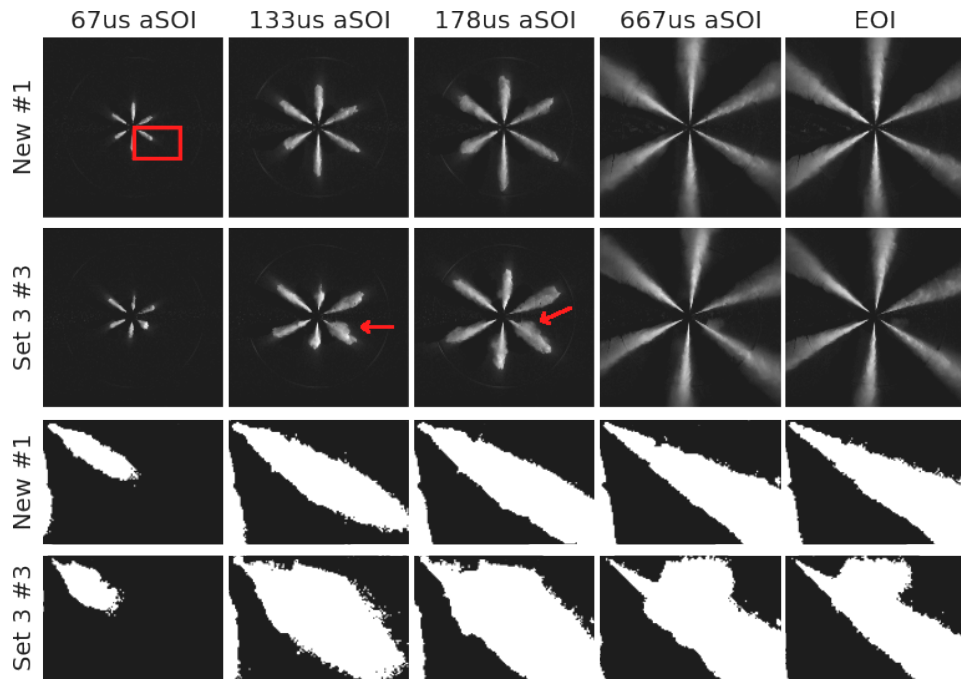


Figure 5.1.3: Persistence of an off-axis anomaly. First two image rows show the injection of diesel into the CVC at indicated time *aSOI* for a *New* and a *Set 3* injector. Bottom two image rows provide a magnified view of the rectangular area indicated in the top left image. The bottom two rows have been binarized by application of a two times noise-level threshold. The red arrows indicate the location of a radial expansion from the *Set 3* injector. Bottom image row clearly shows the presence of a residual atomized fuel pocket at *EOI*, present at the same location as the initial bulge.

Figure 5.1.3 provides a set of images recorded from both a *New* and a *Set 3* injector. The spray evolution at *SOI* is provided, along with a single frame recorded during the stable regime, and one frame at *EOI*. In addition, Figure 5.1.3 provides magnified and binarized images of the bottom-right spray, with the binarize threshold set at two times noise-level of the camera. It is clear the radial bulge from the start of injection has produced a pocket of residual atomized fuel near the nozzle, still present at the end of injection. Under reactive conditions this fuel pocket will have evaporated and possibly combusted long before *EOI*. The possible impact of combustion of such a fuel pocket on the downstream equivalence ratio, and combustion of the main fuel spray, is unknown.

5.2 Fuel spray cone angle and penetration

The analyses in Chapter 4 relied for a significant part on the comparison of the fuel spray cone angles, and the evolution of these angles, for new and used injectors. Radial anomalies were determined through analysing changes in spray width in the early phase of injection, and the injection quality in the stable regime was judged by the quality of the spray cone angle. The penetration at the start of injection was investigated in Chapter 4, and a clear change in penetration rate was observed for part of the orifices of several used injectors. In this section, the spray cone angles and penetrations measured in Chapter 4 are compared to the angles and penetrations expected based on the empirical models treated in Chapter 2.

5.2.1 Fuel spray cone angles

Equation 2.8 provided the empirical relation between injection parameters and the fuel spray cone angle,

$$\theta = 2 \arctan \left(\frac{4\pi\sqrt{3}}{6A} \sqrt{\frac{\rho_a}{\rho_l}} \right) \quad (2.8 \text{ revisited})$$

where A is a constant dependant on nozzle geometry, ρ_a is the density of the ambient environment and ρ_l is the density of the injected fuel. The fuel density was constant in all experiments, $\rho_l=830 \text{ kg m}^{-3}$, as the same mineral diesel was used in all investigations. The ambient medium consisted of compressed nitrogen at a pressure ranging from 3.0 MPa to 3.4 MPa and temperature ranging from 104 °C to 119 °C, depending on the experiment. The constant A was approximately 5 for the nozzles investigated in this work. Based on these parameters, the expected spray cone angle can be calculated and directly compared to the values provided in Table 4.5. The combined calculated and measured values are provided in Table 5.1.

Measurements conducted in the CVC were done under engine-like ambient densities, and the fuel spray cone angle was expected to comply to the empirical model. Table 5.1 shows, within the error margin of the measured spray cone angle, the measurements overlap with the theoretically predicted angle. Considering Figure 4.3.10, it is clear the calculated spray angle interval from 14.9° to 15.5° fits within the error margins of the combined data sets of all

Measurement series	Measured angle (deg)	Model calculated expected angle (deg)
- New inj.	$15.5^\circ \pm 0.8^\circ$	14.9° to 15.5°
- Set 1	$15.9^\circ \pm 1.6^\circ$	14.9° to 15.5°
- Set 2	$15.7^\circ \pm 1.6^\circ$	14.9° to 15.5°
- Set 3	$15.7^\circ \pm 1.4^\circ$	14.9° to 15.5°

Table 5.1: Spray cone angles measured in the present investigation, compared to the expected angles based on empirical models.

injectors. It is therefore concluded that the fuel spray cone angles measured in the CVC from a new injector agrees to the empirical model found in literature, treated in Section 2.1.5.

The fuel spray cone angles determined in the stable regime for used injectors can not be quantitatively compared to existing models, as there are no models available for such injectors. The two recent studies treated in Section 2.3, conducted during the same time as this investigation, observed *both* an increase [74] and a decrease [72] in the fuel spray cone angle from deposit rich injectors. In the present investigation, the most notable effect was an increase in the standard deviation of the fuel spray cone angle, while the angle itself changed only marginally. Closer inspection of the graphs provided in the cited articles revealed that:

- The decrease in fuel spray cone angle reported in [72] is visible in the provided graph in the article, reproduced in Figure 2.3.1. Without error margins it is however not possible to properly compare the reported difference in [72] to the observations in this work.
- The increase in fuel spray cone angle reported in [74] is accompanied by a two- to fourfold increase in standard deviation. In some cases the fuel spray cone angle from the deposit rich injector is comparable to, or even smaller than, the clean injector.

The average fuel spray cone angles from deposit rich injectors measured in this work, and the accompanying error margins, indicate the deposit rich injectors did not produce a significantly altered fuel spray cone angle in the quasi steady-state regime. The average angles are slightly larger than for the new injector, but the increased SDs makes the difference insignificant. Throughout this thesis, error margins have been studied in order to analyse results from used injectors. It is hoped future models, either empirical or theoretical,

will be able to provide an estimate on the expected uncertainty of determined fuel spray cone angles, as the variation in the spray cone angle seems to be impacted most for a deposit rich injector in the stable regime.

5.2.2 Spray penetration

In the initial needle opening phase, the fuel spray tip and corresponding spray length were measured in the CVC until the spray tip left the field of view. Although data acquired in this time window is limited, there was sufficient data available to determine fuel spray penetration in the early stage of injection. In Section 4.3.1 the spray penetration was used to compare spray behaviour of new and deposit rich injectors, and a reduction of initial spray penetration was observed from several orifices of some used injectors. In this section the average fuel spray penetrations, measured from new injectors, will be compared to the theoretical penetrations treated in Chapter 2, and calculated with equations¹ 2.4, 2.5 and 2.6:

$$0 < t < t_b : \quad S = C_v \left(\frac{2\Delta P}{\rho_l} \right)^{0.5} t \quad (2.4 \text{ revisited})$$

$$t > t_b : \quad S = \left(\frac{C_v \sqrt{2C_a}}{a \cdot \tan \frac{1}{2}\theta} \right)^{0.5} \left(\frac{\Delta P}{\rho_a} \right)^{0.25} (Dt)^{0.5} \quad (2.5 \text{ revisited})$$

$$0 < t < t_b : \quad S = \alpha \cdot t^{3/2} \quad (2.6 \text{ revisited})$$

Penetration analysis of the used injectors would not provide any additional insights; Figure 4.3.1 indicated sprays from most orifices of the used injectors did not significantly differ from new injectors. Main differences in penetration between new and used injectors were either an overall delayed start of injection, or a temporal reduction in early penetration from several orifices. The delayed start of the injection however did not lead to a change in penetration rate. A strong reduction in penetration velocity *would* be interesting for analysis, if the reduced penetration rate would persist throughout the full injection. In the present investigation the reduced early penetration rates were resolved within roughly 250 μ s. The models provided by equations 2.4, 2.5 and 2.6 are unsuitable for analysis of such transient behaviour in the penetration.

Figure 5.2.1 provides the spray tip penetration from the *New #1* injector in combination with the expected penetrations based on equations 2.4, 2.5 and

¹The first and last equation provide the expected spray penetration in the same time window, and correspond to two different models, 2.4 from [20] and 2.6 from [27].

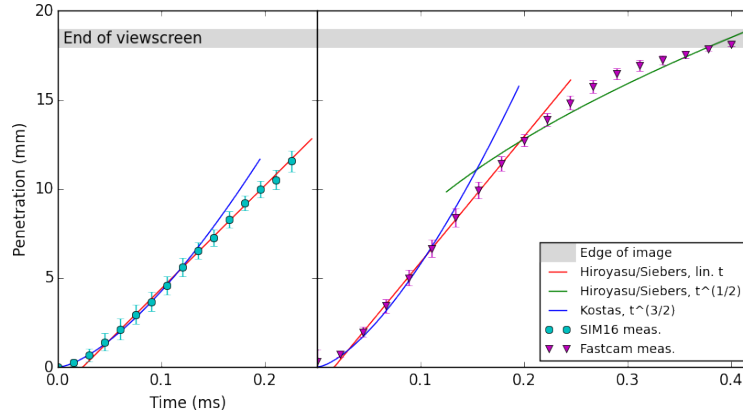


Figure 5.2.1: Measured fuel spray tip penetration for both measurement *series 1* (left graph) and *series 2* (right graph) treated in Chapter 4, combined with theoretical predictions. Note *series 1* and *series 2* were recorded at different injection pressures. Three solid curves (two for left graph) correspond to predicted penetrations based on equations 2.4 (red), 2.5 (green) and 2.6 (blue). See text for notes on the provided error margins.

2.6. Averaging of the spray tip penetration was done over the full recording set *and* all six orifices of the injector. The two data sets presented in Figure 5.2.1 correspond to penetration measurements from the SIM16 *series 1* and FASTCAM *series 2* measurement series. These two measurement series were recorded at different injection pressures, and a difference in penetration rate can be observed in Figure 5.2.1. The error margins provided in Figure 5.2.1 correspond to the arithmetic standard deviations of the averaged penetrations, and do not take systematic variations into account. The error margins plotted in Figure 5.2.1 underestimate the actual errors by an unknown factor, but with an upper limit of $\times 3.1$. There is good agreement between measurements and Equation 2.6 (blue) for the early spray evolution, up to $100 \mu\text{s}$ *aSOI*. Fair agreement with Equation 2.4 (red), describing spray penetration at the earliest time window, can be observed after roughly $75 \mu\text{s}$. This was to be expected, as Equation 2.6 was specifically developed to correct for observed discrepancies between measurements and estimates based on Equation 2.4 at the very early spray stage. The underestimate of penetration indicated by the green graph in the right graph of Figure 5.2.1, corresponding to Equation 2.5, has been widely observed for contemporary common rail injection systems, see for example Figure 2.1.5 taken from [29]. This discrepancy is, therefore, of no major concern.

5.3 Deposit rich injectors

For deposit rich injectors a quantitative comparison to literature was not possible. Section 5.1 indicated the overall (qualitative) spray evolution from a used injector is comparable to that of a new injector, apart from the additional anomalies observed in the transient regime, during needle lift. The available models for calculating expected spray cone angles and penetration rates, based on injection conditions, do not provide the possibility to correct for the presence of deposits. A quantitative model that couples changes in the internal SAC fuel flow to alterations of the external spray evolution, is required to further analyse the observed anomalies from used injectors. The impact of an alteration of the internal fuel flow on the external spray evolution can currently not be estimated, and it is therefore not possible to determine whether the observed anomalies are consistent with what would be expected for a fouled nozzle. Nonetheless, as can be seen in Table 5.1, in the quasi steady-state regime the spray cone angle is comparable to what would be expected for a new injector, although the corresponding spread in the fuel spray cone angle increases for used injectors.

Chapter 6

Conclusions

A group of 20 common rail diesel fuel injectors have been studied to determine the impact of injector usage on the evolution of the fuel spray. Injectors taken from real-world engines at different stages of their lifetime provided a wide variety of injector conditions. It was shown the fuel spray shape at the start of injection, up to roughly 0.5 ms *a*SOI, often suffered a reduced spray penetration from several orifices for used injectors. These reductions in spray penetrations were highly repeatable from injection to injection, and were often accompanied by radially expanding transients. Eight out of eleven used injectors suffered from these retarded spray penetrations, older injectors (i.e. injectors taken from higher mileage vehicles) produced more frequent, and worse, spray retardations than newer ones. Brand new injectors showed no reduced early spray penetration in the transient regime. Transient radial dispersions accompanying reduced spray penetrations at the start of injection, appeared to remain stationary close to the nozzle. In several cases these radially dispersed plumes remained present near the tip of the injector, even after injection had ended.

These transient effects are not related to the increased dispersion often observed during the initial needle-opening phase, as treated in Section 2.1.2. The additional reduced penetration and increased dispersion observed in this work occurred *after* the initial needle-opening transients, and were only visible from used, deposit rich, injectors. The additional transients have not been observed in earlier investigations by others, and the impact of the temporal increase in dispersion on the early phase of combustion is not known.

The spray shape in the quasi steady-state regime, and spray dynamics at the end of injection, were nearly indiscriminate for new and used injectors. Minor differences in calculated fuel spray cone angles in the stable regime were

not significant, except for the spray cone angle from *one* orifice of a single high-mileage injector. The accompanying standard deviations in the measured spray cone angles were twice as large for the used injectors than for the new injectors. Expulsions of ligaments and droplets post-injection were recorded for both new and used injectors, and analysis showed there was no significant difference in expulsions of ligaments and droplets between used and new injectors.

Fuel injections were imaged from new, same type injectors to serve as a benchmark for sprays recorded from used injectors. The fuel spray evolution imaged from new injectors showed spray shape evolutions, spray tip penetrations, and transient characteristics were in agreement with current literature. The sprays recorded in this work were therefore representative for injections into quiescent diesel engines, except for the inhibited evaporation and combustion.

Although not a key research target of this study, the experimental set-up applied in the initial investigation (Chapter 3) exceeded expectations. The set-up was easy to use, flexible, and well-suited for qualitative measurements of spray evolutions under extreme back pressure conditions.

Chapter 7

Directions for future work

Based on the results presented in this thesis, future research on the impact of deposits on fuel spray evolution and combustion can focus on several aspects revealed in this work. A continuation of the investigation presented in this thesis by expanding the parameter space, to create more knowledge on the effect of deposits on the overall fuel spray evolution, should however be conducted with care. In Section 1.3 it was noted several other groups with renowned experts in the field, have started to investigate the impact of deposits on the spray shape and penetration rate. It is expected more research will be conducted on this subject in the near future, and a general understanding of the relevant parameters on spray degradation from deposit rich injectors may subsequently be available. For example, the impact of the observed spray changes on the combustion quality could be studied by continuing along the lines of this thesis, replacing the inert environment with a reactive ambient medium. The CVC used in this work was designed for high pressure, high temperature, reactive conditions, and by charging the system with an oxygen rich and high temperature medium, the combustion of fuel sprays can be studied. A systematic comparison of combustion characteristics from new injectors to used, deposit rich injectors may show a structural change in the combustion dynamics. If such a change could be observed, it might open the way to explaining how, fundamentally, the presence of deposits degrade combustion quality. Recent work in [73] shows there is already an increased interest in the combustion characteristics from deposit rich injectors. An in-depth investigation on combustion characteristics in the CVC will definitely provide new insights, and will produce useful data that could be combined with other investigations. The strength of the CVC set-up lies in the possibility to research a large number of injectors in

a relatively short timespan, providing the possibility to produce large amounts of data, in turn allowing extensive analyses. An aspiring researcher should however be thoroughly aware this field is evolving, and (s)he should carefully investigate current research subjects of other groups on sprays and combustion from deposit rich injectors to prevent duplicating existing studies.

A research focussed on more practical applications, and that continues roughly along the lines of this investigation can be conducted on the removal of deposits. Figure 4.3.2 indicated the degradation of the early spray shape is not necessarily a permanent effect. A study on the effectiveness of fuel additives, or possibly on diesel–biodiesel blends, for removing deposits could be conducted in the current set-up provided the researcher would have access to a sufficiently large pool of used injectors. This will require the use of a reactive environment, as in the current configuration deposits are partly removed during injection, while growth of new deposits is prevented by maintaining an inert environment. As stated earlier the CVC was designed for combustion research, making this a viable research opportunity.

Although the appearance of post-injection expulsions of ligaments and droplets was only touched upon in this thesis, a cooperative study with a colleague at Brunel showed expelled ligaments remain present close to the injector nozzle after injection. In a combusting environment these ligaments will continue to evaporate and burn long after the main fuel injection has ended. A study on the impact these post-injection expulsions can have on in-cylinder soot formation and UBHC emissions might lead to future developments on reducing engine-out emissions for diesel engines.

From a more fundamental point of view, the CVC can be used to study, with a high level of detail, general spray evolution and/or combustion under highly reproducible conditions. By varying the ambient environment and injection conditions, fundamental characteristics of sprays can be studied over a wide range of parameters. The maximum peak pressure of 12 MPa and safe continuous working pressure of 8 MPa in combination with the heating system, allows studying the spray evolution under supercritical conditions of both the ambient environment and the fuel. Minor alterations to the injection system would allow the CVC to be used for injection of different fuels, for example liquefied natural gas, compressed gas, or pure alcohols. This is however indicative of the capabilities of the CVC system applied in this research, and is not directly related to the investigation treated in this thesis.

Bibliography

- [1] J.B. Heywood. *Internal Combustion Engine Fundamentals*. McGraw-Hill, 1989.
- [2] R.D. Reitz. Modeling atomization processes in high-pressure vaporizing sprays. *Atomisation and Spray Technology*, 3:309–337, 1987.
- [3] A. Lefebvre. *Atomization and Sprays (Combustion,)*. CRC Press, 1989.
- [4] W.S. Chiu, S.M. Shahed, and W.T. Lyn. A transient spray mixing model for diesel combustion. *SAE Transactions*, 85(760128):502–512, 1976.
- [5] T. Kamimoto and M.H. Bae. High combustion temperature for the reduction of particulate in diesel engines. *SAE International*, 880423, 1988.
- [6] Y.-H. Won, T. Kamimoto, and H. Kosaka. A study on soot formation in unsteady spray flames via 2-d soot imaging. *SAE International*, 920114, 1992.
- [7] T.E. Parker, J.R. Morency, R.R. Foutter, and W.T. Rawlins. Infrared measurements of soot formation in diesel sprays. *Combustion and Flame*, 107:271–290, 1996.
- [8] J.E. Dec. A conceptual model of di diesel combustion based on laser-sheet imaging. *SAE Technical Paper*, 970873, 1997.
- [9] M.P.B. Musculus, P.C. Miles, and L.M. Pickett. Conceptual models for partially premixed low-temperature diesel combustion. *Progress in Energy and Combustion Science*, 39:246–283, 2013.
- [10] R.D. Reitz and F.B. Bracco. On the dependence of spray angle and other spray parameters on nozzle design and operating conditions. *SAE International*, 790494, 1979.
- [11] C. Heimgartner and A. Leipertz. Investigation of the primary spray breakup close to the nozzle of a common – rail high pressure diesel injection system. *SAE International*, 2000-01-1799, 2000.
- [12] Y. Ren and X. Li. Assessment and validation of liquid breakup models for high-pressure dense diesel sprays. *Front. Energy*, 10(2):164–175, 2016.
- [13] M. Linne. Analysis of x-ray phase contrast imaging in atomizing sprays. *Exp Fluids*, 52:1201–1218, 2012.

- [14] M. Linne, M. Paciaroni, T. Hall, and T. Parker. Ballistic imaging of the near field in a diesel spray. *Exp. in Fluids*, 40:836–846, 2006.
- [15] S. Bae and J. Kang. The structure of a break-up zone in the transient diesel spray of a valve-covered orifice nozzle. *Int. J. Engine Res.*, 7:319–334, 2006.
- [16] H. Hillamo, T. Sarjovaara, O. Kaario, V. Vuorinen, and M. Larmi. Diesel spray visualization and shockwaves. *Atomization Sprays*, 20(3):177–189, 2010.
- [17] Z. Wang, H. Ding, X. Ma, H. Xu, and M.L. Wyszynski. Ultra-high speed imaging study of the diesel spray close to the injector tip at the initial opening stage with single injection. *Applied Energy*, 165:335–344, 2016.
- [18] C. Crua, T. Shoba, M. Heikal, M. Gold, and C. Higham. High-speed microscopic imaging of the initial stage of diesel spray formation and primary breakup. *SAE Technical Paper*, 2010-01-2247, 2010.
- [19] H. Hiroyasu and M. Arai. Structures of fuel sprays in diesel engines. *SAE International*, 900475, 1990.
- [20] J.D. Naber and D.L. Siebers. Effects of gas density and vaporization on penetration and dispersion of diesel sprays. *SAE International*, 960034, 1996.
- [21] L.C. Ganippa, S. Andersson, and J. Chomiak. Transient measurements of discharge coefficients of diesel nozzles. *SAE Technical Paper*, 2000-01-2788, 2000.
- [22] L.-Y. Zhou, S.-F. Dong, H.-F. Cui, X.-W. Wu, F.-Y. Xue, and F.-Q. Luo. Measurements and analyses on the transient discharge coefficient of each nozzle hole of multi-hole diesel injector. *Sens. Actuators A*, 244:198–205, 2016.
- [23] S.S. Sazhin, C. Crua, D. Kennaird, and M. Heikal. The initial stage of fuel spray penetration. *Fuel*, 82:875–885, 2003.
- [24] M.R. Turner, S.S. Sazhin, J.J. Healey, C. Crua, and S.B. Martynov. A breakup model for transient diesel fuel sprays. *Fuel*, 97:288–305, 2012.
- [25] J. Arrègle, J.V. Pastor, and S. Ruiz. The influence of injection parameters on diesel spray characteristics. *SAE International*, 1999-01-0200, 1999.
- [26] S. Gupta, R. Poola, and R. Sekar. Injection parameter effects on diesel spray characteristics. *SAE International*, 2000-01-2787, 2000.
- [27] J. Kostas, D. Honnery, and J. Soria. Time resolved measurements of the initial stages of fuel spray penetration. *Fuel*, 88:2225–2237, 2009.

- [28] Ö.O. Taşkıran and M. Ergeneman. Experimental study on diesel spray characteristics and autoignition process. *J. of Combustion*, 2011:528126, 2011.
- [29] E.W. Eagle, S.B. Morris, and M.S. Wooldridge. High-speed imaging of transient diesel spray behavior during high pressure injection of a multi-hole fuel injector. *Fuel*, 116:299–309, 2014.
- [30] Y. Li and H. Xu. Experimental study of temporal evolution of initial stage diesel spray under varied conditions. *Fuel*, 171:44–53, 2016.
- [31] R.J.H. Klein-Douwel, P.J.M. Frijters, L.M.T. Somers, W.A. de Boer, and R.S.G. Baert. Macroscopic diesel fuel spray shadowgraphy using high speed digital imaging in a high pressure cell. *Fuel*, 86:1994–2007, 2007.
- [32] S. Som and S.K. Aggarwal. Effects of primary breakup modeling on spray and combustion characteristics of compression ignition engines. *Combustion and Flame*, 157:1179–1193, 2010.
- [33] K. Kitaguchi, T. Fujii, S. Hatori, T. Hori, and J. Senda. Effect of breakup model on large-eddy simulation of diesel spray evolution under high back pressures. *Int. J. Engine Res.*, 15(5):522–538, 2014.
- [34] A.J. Yule and D.G. Salters. On the distance required to atomize diesel sprays injected from orifice-type nozzles. *J. of Automobile Eng.*, 209(3):217–226, 1995.
- [35] D.L. Siebers. Liquid-phase fuel penetration in diesel sprays. *SAE International*, 980809, 1998.
- [36] A. Montanaro, L. Allocca, J. Johnson, S.-Y. Lee, J. Naber, and A. Zhang. Influence of the nozzle geometry of a diesel single-hole injector on liquid and vapor phase distributions at engine-like conditions. *SAE International*, 2013-24-0038, 2013.
- [37] A.I. Ramírez, S. Som, S.K. Aggarwal, A.L. Kastengren, E.M. El-Hannouny, D.E. Longman, and C.F. Powell. Quantitative x-ray measurements of high-pressure fuel sprays from a production heavy duty diesel injector. *Exp. Fluids*, 47:119–134, 2009.
- [38] S. Moon, Y. Gao, J. Wang, K. Fezzaa, and T. Tsujimura. Near-field dynamics of high-speed diesel sprays: Effects of orifice inlet geometry and injection pressure. *Fuel*, 133:299–309, 2014.
- [39] S. Moon, Y. Gao, S. Park, J. Wang, N. Kurimoto, and Y. Nishijima. Effect of the number and position of nozzle holes on in- and near-nozzle dynamic characteristics of diesel injection. *Fuel*, 150:112–122, 2015.
- [40] M. Linne. Imaging in the optically dense regions of a spray: A review of developing techniques. *Progress in Energy and Combustion Science*, 39:403–440, 2013.

- [41] S.P. Duran, J.M. Porter, and T.E. Parker. Picosecond ballistic imaging of diesel injection in hightemperature and highpressure air. *Exp. Fluids*, 56:84, 2015.
- [42] S. Moon, Y. Matsumoto, and K. Nishida. Entrainment, evaporation and mixing characteristics of diesel sprays around end-of-injection. *SAE International*, 2009-01-0849, 2009.
- [43] J. Manin, M. Bardi, L.M. Pickett, R.N. Dahms, and J.C. Oefelein. Microscopic investigation of the atomization and mixing processes of diesel sprays injected into high pressure and temperature environments. *Fuel*, 134:531–543, 2014.
- [44] S. Kook, L.M. Pickett, and M.P.B. Musculus. Influence of diesel injection parameters on end-of-injection liquid length recession. *SAE Int. J. Engines*, 2(1):1194–1210, 2009.
- [45] C. Koci, G. Martin, T. Bazyn, W. Morrison, K. Svensson, and C. Gehrke. The influence of diesel end-of-injection rate shape on combustion recession. *SAE International*, 2015-01-0795, 2015.
- [46] B. Knox and C. Genzale. Effects of end-of-injection transients on combustion recession in diesel sprays. *SAE International*, 2016-01-0745, 2016.
- [47] M.P.B. Musculus, T. Lachaux, L.M. Pickett, and C.A. Idicheria. End-of-injection over-mixing and unburned hydrocarbon emissions in low-temperature-combustion diesel engines. *SAE International*, 2007-01-0907, 2007.
- [48] A.B. Swantek, D. Duke, F.Z. Tilocco, N. Sovis, C.F. Powell, and A.L. Kastengren. End of injection, mass expulsion behaviors in single hole diesel fuel injectors. *ILASS Americas annual conference*, 2014.
- [49] G.E. Irish and R.W. Mattson. Cleaner injectors and less smoke with hydrogen-treated diesel fuel. *SAE International*, 640459, 1964.
- [50] E.G. Reynolds. A procedure for the assessment of pintle injector nozzle blockage (nozzle coking) in indirect injection diesel engine. *SAE International*, 861409, 1986.
- [51] K.G. Claar, G.H. Blythe, and S.B. Pocinki. Diesel fuel properties and additive effects on di injector deposit formation. *SAE International*, 932738, 1993.
- [52] J. Barker, P. Richards, C. Snape, and W. Meredith. Diesel injector deposits - an issue that has evolved with engine technology. *SAE of Japan*, 20119126, 2011.
- [53] R. Caprotti, N. Bhatti, and G. Balfour. Deposit control in modern diesel fuel injection systems. *SAE International*, 2010-01-2250, 2010.

- [54] S.A. Basha, K.R. Gopal, and S. Jebaraj. A review on biodiesel production, combustion, emissions and performance. *Renewable and Sustainable Energy Reviews*, 13:1628–1634, 2009.
- [55] E.M. Shahid and Younis Jamal. A review of biodiesel as vehicular fuel. *Renewable and Sustainable Energy Reviews*, 12:2484–2494, 2008.
- [56] A. Leedham, R. Caprotti, O. Graupner, and T. Klaua. Impact of fuel additives on diesel injector deposits. *SAE International*, 2004-01-2935, 2004.
- [57] R. Caprotti, A. Breakspear, O. Graupner, and T. Klaua. Detergency requirements of future diesel injection systems. *SAE International*, 2005-01-3901, 2005.
- [58] R. Caprotti, A. Breakspear, O. Graupner, T. Klaua, and O. Kohnen. Diesel injector deposits potential in future fueling systems. *SAE International*, 2006-01-3359, 2006.
- [59] J. Tang, S. Pischinger, M. Lamping, T. Körfer, M. Tatur, and D. Tomazic. Coking phenomena in nozzle orifices of di-diesel engines. *SAE Int. J. Fuels Lubr.*, 2(1):259–272, 2009.
- [60] R. Barbour, R. Quigley, D. Browne, and A. Panesar. A comparison of peugeot dw10 dynamometer and vehicle engine performance. *TAE Esslingen*, 2011.
- [61] P. Risberg and S. Alfredsson. The effect of zinc and other metal carboxylates on nozzle fouling. *SAE Technical Paper*, 2016-01-0837, 2016.
- [62] M. Arondel, H. Rodeschini, M. Lopes, and B. Dequenne. Fuel additives for reduction of internal diesel injectors deposits (idid, lacquering): A critical and priority route. *SAE International*, 2012-01-1687, 2012.
- [63] M.D.C. Almena, O.L. Esperilla, F.M. Manzanero, Y.M. Duarte, L.C.Q. Toscano, and G. Wolff. Internal diesel injector deposits: Sodium carboxylates of c12 succinic acids and c16 and c18 fatty acids. *SAE International*, 2012-01-1689, 2012.
- [64] P. Lacey, S. Gail, J.M. Kientz, G. Benoist, P. Downes, and C. Daveau. Fuel quality and diesel injector deposits. *SAE Int. J. Fuels Lubr.*, 3(3):1187–1198, 2012.
- [65] P. Lacey, S. Gail, J.M. Kientz, N. Milovanovic, and C. Gris. Internal fuel injector deposits. *SAE Int. J. Fuels Lubr.*, 5(1):132–145, 2011.
- [66] R. Quigley, R. Barbour, E. Fahey, D.C. Arters, W. Wetzel, and J. Ray. A study of the internal diesel injector deposit phenomenon. *TAE Esslingen*, 2011.
- [67] R. Dallanegra and R. Caprotti. Chemical composition of ashless polymeric internal diesel injector deposits. *SAE International*, 2014-01-2728, 2014.

- [68] D. Tziourtzioumis and A. Stamatelos. Effects of a 70% biodiesel blend on the fuel injection system operation during steady-state and transient performance of a common rail diesel engine. *Energy Conversion and Management*, 60:56–67, 2012.
- [69] R. Uitz, M. Brewer, and R. Williams. Impact of fame quality on injector nozzle fouling in a common rail diesel engine. *SAE International*, 2009-01-2640, 2009.
- [70] D.E. Winterbone, E. Clough, K.K. Rao, P. Richards, and D. Williams. The effect of dl nozzle fouling on fuel spray characteristics. *SAE International*, 922232, 1992.
- [71] P. Richards, R.D. Walker, and D. Williams. Fouling of two stage injectors - an investigation into some causes and effects. *SAE International*, 971619, 1997.
- [72] S. d’Ambrosio and A. Ferrari. Diesel injector coking: Optical-chemical analysis of deposits and influence on injected flow-rate, fuel spray and engine performance. *J. Eng. Gas Turbines Power*, 134:062801, 2012.
- [73] A. Magno, E. Mancaruso, and B.M. Vaglieco. Optical investigation of injection and combustion phases of a fouled piezoelectric injector in a transparent cr diesel engine. *SAE International*, 2013-01-1591, 2013.
- [74] A. Magno, E. Mancaruso, and B.M. Vaglieco. Experimental investigation in an optically accessible diesel engine of a fouled piezoelectric injector. *Energy*, 64:842–852, 2014.
- [75] R. Pos, R. Cracknell, and L. Ganippa. Transient characteristics of diesel sprays from a deposit rich injector. *Fuel*, 153:183–191, 2015.
- [76] R. Pos and L. Ganippa. Comparison of spray characteristics from different nozzles and fuels in an non-reactive medium. *FISITA*, F2014-CET-164, 2014.
- [77] C. Willert, B. Stasicki, J. Klinner, and S. Moessner. Pulsed operation of high-power light emitting diodes for imaging flow velocimetry. *Meas. Sci. Technol.*, 21:075402, 2010.
- [78] S.M. Hagsäter, C.H. Westergaard, H. Bruus, and J.P. Kutter. Investigations on led illumination for micro-piv including a novel front-lit configuration. *Exp. Fluids*, 44:211–219, 2008.
- [79] Eric Jones, Travis Oliphant, Pearu Peterson, et al. Scipy: Open source scientific tools for python, 2001.
- [80] P.T. Boggs, R.H. Byrd, J.E. Rogers, and R.B. Schnabel. Users reference guide for odrpack version 2.01, 1992.
- [81] The Scipy community. Multi-dimensional image processing (scipy.ndimage documentation pages), 2015.

- [82] R. Pos, R. Wardle, R. Cracknell, and L. Ganippa. Spatio-temporal evolution of diesel sprays at the early start of injection. *Applied Energy, under review*, 2017.
- [83] R. Pos, R. Cracknell, and L. Ganippa. Characteristics of high pressure diesel sprays at the end of injection. *ICE 2015, Conference Proceedings*, 2015.
- [84] R. Pos, M. Avulapati, R. Wardle, R. Cracknell, T. Megaritis, and L. Ganippa. Combustion of ligaments and droplets expelled after the end of injection in a multi-hole diesel injector. *Fuel*, 197:459–466, 2017.
- [85] S. Howard, N. Manak, B. Olateju, J. Wood, and L. Ganippa. Design & fabrication of a constant volume high pressure combustion chamber to study diesel spray mixing. Master’s thesis, Brunel University London, SED, 2010.
- [86] The Scipy community. scikit-image: Image processing in python, 2015.
- [87] V. Macian, R. Payri, A. Garcia, and M. Bardi. Experimental evaluation of the best approach for diesel spray images segmentation. *Experimental Techniques*, 36(6):26–34, 2012.